

MILKY WAY RED DWARFS IN THE BORG SURVEY; GALACTIC SCALE-HEIGHT AND THE DISTRIBUTION OF DWARFS STARS IN WFC3 IMAGING

B. W.HOLWERDA^{1,2}, M. TRENTI³, W. CLARKSON⁴, K. SAHU⁵, L. BRADLEY⁵, M. STIAVELLI⁵, N. PIRZKAL⁵,
 G. DE MARCHI², M. ANDERSEN⁶, R. BOUWENS¹, R. RYAN⁵ I. VAN VLEDDER¹, D. VAN DER VLUGT¹

ApJ accepted + ERRATUM

ABSTRACT

We present a tally of Milky Way late-type dwarf stars in 68 WFC3 pure-parallel fields (227 arcmin²) from the Brightest of Reionizing Galaxies (BoRG) survey for high-redshift galaxies. Using spectroscopically identified M-dwarfs in two public surveys, the CANDELS and the ERS mosaics, we identify a morphological selection criterion using the half-light radius (r_{50}), a near-infrared J-H, G-J color region where M-dwarfs are found, and a V-J relation with M-dwarf subtype.

We apply this morphological selection of stellar objects, color-color selection of M-dwarfs and optical-near-infrared color subtyping to compile a catalog of 274 M-dwarfs belonging to the disk of the Milky Way with a limiting magnitude of $m_{F125W} < 24(AB)$. Based on the M-dwarfs statistics, we conclude that (a) the previously identified North/South discrepancy in M-dwarf numbers persists in our sample; there are more M-dwarfs in the Northern fields on average than in Southern ones, (b) the Milky Way's single disk scale-height for M-dwarfs is 0.3-4 kpc, depending on sub-type, (c) the scale-height depends on M-dwarf subtype with early type (M0-4) high scale-height ($z_0 = 3 - 4$ kpc) and later types M5 and above in the thin disk ($z_0 = 0.3 - 0.5$ kpc). (d) a second component is visible in the vertical distribution, with a different, much higher scale-height in the Southern Fields compared to the Northern ones. We report the M-dwarf component of the Sagittarius stream in one of our fields with 11 confirmed M-dwarfs, 7 of which are at the stream's distance. In addition to the M-dwarf catalog, we report the discovery of 1 T-dwarf and 30 L-dwarfs from their near-infrared colors. The dwarf scale-height and the relative low incidence in our fields of L- and T-dwarfs in these fields makes it unlikely that these stars will be interlopers in great numbers in color-selected samples go high-redshift galaxies. The relative ubiquity of M-dwarfs however will make them ideal tracers of Galactic Halo substructure with EUCLID and reference stars for JWST observations.

1. INTRODUCTION

Counting stars to infer the shape and size of our Milky Way Galaxy is a classic experiment in Astronomy. However, it is also among the most prone to insufficient data as well as conceptual shortfalls (e.g., Herschel 1785; Kapteyn 1922). Over time, it was established that the Milky Way's scale height is inversely proportional to the masses of stars sampled (Gilmore & Reid 1983; Gilmore 1984; Siegel et al. 2002). Initially, many of the Galactic models were focused on relatively luminous giant stars and rarely addressed (sub)stellar objects due to completeness issues (see for reviews of star counts and Galactic structure; Bahcall 1986; Gilmore et al. 1989; King et al. 1990; Majewski 1993).

Interest has now shifted to the spatial distribution of (sub)stellar objects, in part because they are possibly the most significant interlopers in studies of extremely high redshift objects (see e.g., Caballero et al. 2008), but also because these are physically some of the longest lived objects. Consequently, any deep high-redshift survey, espe-

cially in the near-infrared, undertaken with the Hubble Space Telescope automatically becomes a census of the smallest Milky Way stars. More importantly, these objects constitute the most numerous and oldest population of stars in the Galactic disk. For instance, Pirzkal et al. (2005) determined the scale-height of different types of dwarfs from the Hubble Ultra Deep Field (HUDF, Beckwith et al. 2006). Ryan et al. (2005) found L and T dwarfs in a small set of ACS parallel observations. Stansaway et al. (2008) and Pirzkal et al. (2009) determined the Galactic scale-height of M-dwarfs from the Great Observatories Origins Deep Survey fields (GOODS, Giavalisco et al. 2004). Ryan et al. (2011) added a search of early WFC3 pure-parallel fields for L and T dwarfs. These studies gradually improved statistics on L, T and M-dwarfs to several dozens of objects.

The identification of these Galactic dwarfs in images is difficult as one needs both high-quality data to distinguish from extragalactic sources and a good understanding of the initial mass function or the local density of these objects as a class. Two of the above studies (Pirzkal et al. 2005, 2009) benefited from spectroscopic identification of the dwarf subtype in the HST/ACS grism spectra of the HUDF and GOODS fields (the GRAPES⁶ and PEARS⁷ projects respectively). Combined with an in-

¹ Leiden Observatory, Leiden University, P.O. Box 9513, 2300 RA Leiden, The Netherlands benneholwerda@rssd.esa.int, twitter: benneholwerda

² Research Fellow, European Space Agency, ESA-ESTEC, Keplerlaan 1, 2200 AG Noordwijk, the Netherlands

³ University of Melbourne?

⁴ Department of Natural Sciences College of Arts, Sciences and Letters, University of Michigan-Dearborn 4901 Evergreen Road, Dearborn, MI 48128, USA

⁵ Space Telescope Science Institute, Baltimore, MD 21218, USA

⁶ Grism ACS Program for Extragalactic Science, see Pirzkal et al. (2004)

⁷ Probing Evolution And Reionization Spectroscopically, see Pirzkal et al. (2009).

dex of stellarity in the direct image, this made identification of the dwarfs near certain. Alternatively, Kilic et al. (2005) used high-precision proper motion to identify the Galactic objects. Once an object has been identified as a candidate dwarf, its luminosity distance must be estimated, which requires accurate (sub)typing. Without direct spectra, we will show that this can be readily achieved with sufficient color coverage from the optical to the near-infrared. A dwarf census including subtype and distance, can answer several outstanding issues regarding the shape of the Milky Way traced by its most numerous stellar members.

Pirzkal et al. (2009) found, like Stanway et al. (2008), an odd discrepancy in the numbers of M-dwarfs: there are 24% more M-dwarfs in the Northern than in the Southern GOODS field. Since our vantage point in the Milky Way is above the plane of the disk, one would expect the Southern GOODS fields to have more M-dwarfs. However, as present, this discrepancy has only been determined from two sight-lines out of the Galaxy, so it is still possible this may be source count field-to-field variance. By studying the older stellar population content of our Galaxy along many sight-lines down to the faintest possible magnitude, we can directly observe and measure the shape of the thin Galactic disk as traced by the old stellar population.

In order to improve our understanding of the contribution of faint dwarfs to Galactic structure, we will need much improved statistics to compare against Milky Way structure models. We use the recent *HST/WFC3* Pure Parallel searches for bright high-redshift galaxies to find Milky Way dwarfs and determine the parameters of their distribution in the Milky Way disk (Trenti et al. 2011; Yan et al. 2010; Bradley et al. 2012). Thus far, based on *HST* imaging, the disk scale height for dwarfs has been found to be: 300 pc (Table 1). (Zheng et al. 2001), 400 ± 100 pc (Pirzkal et al. 2005), 350 ± 50 pc, (L, T dwarfs Ryan et al. 2005), 370 ± 65 pc (for M4–M9 dwarfs) and 300 ± 70 pc (for M0–M9 dwarfs, Pirzkal et al. 2009) and 300 ± 25 (± 31 systematic) pc. (>M8, Ryan et al. 2011).

The goal of this paper is to explore the reality of the North-South difference in M-dwarf counts and to accurately determine the scale-height of our Milky Way as traced by M-dwarfs. Previously, Ryan et al. (2011) investigated the L and T dwarf content, here we focus our analysis on the M dwarfs.

The paper is organized as follows, §2 reports the properties of the *HST/WFC3* observations we use, §3 discusses how we generate the relevant SExtractor catalogs, §4 presents our observational calibration of morphological identification of stars, M-dwarfs specifically, and subsequent sub-typing of the M-dwarfs. §5 presents our catalog of dwarfs in the BoRG fields and briefly discusses the validity of our morphological selection. In §6 we discuss the North/South difference, the Galactic scale-height as a function of dwarf subtype. §10 lists our conclusions and outlines future work.

2. WFC3 OBSERVATIONS

We use three WFC3 data-sets for this project: the CANDELS public v0.5 data-release, and the Early Release Science mosaic, both in the GOODS-South field for calibration and characterization of known M-dwarfs, and the BoRG pure-parallel observations for the detection of

Table 1
The scale-heights for the thin disk of dwarf stars from the literature.

Milky Way Scale Height (z_0) (pc.)	Reference	type stars
300	Zheng et al. (2001)	
400 ± 100	Pirzkal et al. (2005)	
350 ± 50	Ryan et al. (2005)	L, T dwarfs
370 ± 65	Pirzkal et al. (2009)	M4–M9 dwarfs
300 ± 70	Pirzkal et al. (2009)	M0–M9 dwarfs
$300 \pm 25 \pm 31$	Ryan et al. (2011)	>M8

new Galactic M-dwarfs.

Table 2
Summary of the WFC3 observations of BoRG, CANDELS (v0.5) and ERS on GOODS-S.

	BoRG	CANDELS	ERS
Filters	<i>F125W</i> , <i>F160W</i> , <i>F098M</i> , <i>F606W</i> (<i>F600L</i>)	<i>F125W</i> <i>F160W</i>	<i>F125W</i> <i>F160W</i> <i>F098M</i>
pixelscale	0''.08	0''.06 (resampled to 0''.08)	0''.08
PSF	0''.12	0''.12	0''.12
Exposure times (seconds)			
<i>F125W</i>	700–5100	1000	5017.61
<i>F160W</i>	500–3900	1050	5017.61

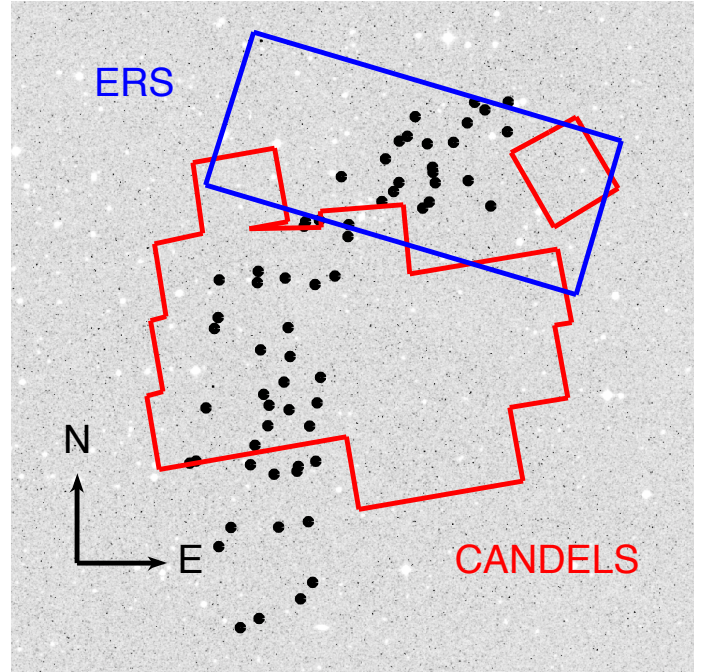


Figure 1. The GOODS South field with the The CANDELS v0.5 data-release of the deep part of the survey (red) and the Early Release Science mosaics (blue) overlaid on a digital sky survey image. The black circles mark the PEARS-identified stars.

2.1. CANDELS GOODS-S observations

The Cosmic Assembly Near-IR Deep Extragalactic Legacy Survey (CANDELS, Grogan et al. 2011; Koekemoer et al. 2011) is designed to explore galaxy evolution, from redshift $z = 1.5$ to ~ 8 . The survey is designed to cover approximately 800 arcmin 2 and is divided into two parts; CANDELS/Deep survey on both GOODS-N and GOODS-S and CANDELS/Wide covering GOODS as well as the EGS, COSMOS, and UDS fields. Data from the survey are non-proprietary and are published in a series of data-releases as soon as reduced to scientific quality (see <http://candels.ucolick.org>). In this paper we use the v0.5 data-release of the GOODS-South field, the first epoch of the CANDELS/Deep survey. Exposure times and sensitivity are very similar for this initial mosaic to the BoRG pure-parallel observations (Table 2) in the two near-infrared channels ($F125W$ and $F160W$). We resampled the CANDELS $F125W$ and $F160W$ mosaics to a pixel scale of 0. $'08$ using DRIZZLE (Fruchter & Hook 2002) to conform to the BoRG standard. For subsequent analysis, we only use a sub-section of this field (Figure 1), where PEARS and CANDELS coverage overlap.

2.2. Early Release Science WFC3 mosaic in Goods-South

The WFC3 imaging of the GOODS-S field is from the Early Science Release (ERS Windhorst et al. 2011) (see the footprint information at http://candels.ucolick.org/survey/tile_maps/GOODS-S.html and Figure 1). The 10 WFC3 fields in the ERS program were also imaged with the $F125W$, $F160W$ and $F098M$ filters, the reason it was included in the Ryan et al. (2011) sample. We retrieve the data from the Hubble Legacy Archive (www.hla.stsci.edu), and combined these into a mosaic using SWARP (<http://www.astromatic.net/software/swarp>) to the same pixel scale as the BoRG fields. Figure 1 shows the overlap of this mosaic with the PEARS-S survey (Pirzkal et al. 2009).

2.3. BoRG

Our principal data-set is the WFC3 data from the BoRG (Brightest of Reionizing Galaxies, HST GO/PAR-11700, Trenti et al. 2011; Bradley et al. 2012) survey to identify Milky Way dwarf stars from their morphology and color. The BoRG observations are undithered HST/WFC3 conducted in pure-parallel with the telescope pointing to a primary spectroscopic target with the Cosmic Origin Spectrograph (typically a high- z QSO at high Galactic latitude). The limitations for such observations are primarily that no dithering strategy can be used (final images are at WFC3 native pixel scale) and total exposure times are dictated by the primary program.

The program's initial aims were to obtain 176 arcmin 2 of sky in 38 pointings, using four WFC3 filters ($F606W$, $F098M$, $F125W$, and $F160W$). An extension of the BoRG program in Cycle-19 brought more parallel observations and the full reproduced set of 68 images is presented in Bradley et al. (2012). Because lines of sight are independent and well separated on the sky mostly at high Galactic latitudes ($|b| > 20^\circ$, see Figure 2), the BoRG survey samples the Milky Way disk away from the plane better than single sight-lines (e.g., the GOODS or H(U)DF

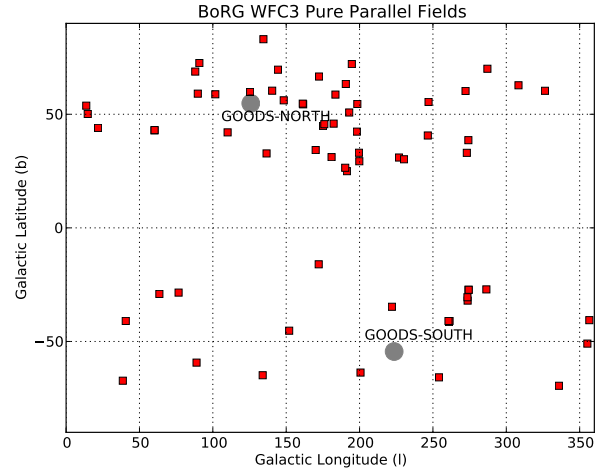


Figure 2. The position of the 68 unique WFC3 Pure Parallel Fields in Galactic coordinates (red squares). The sampling of the Milky Way disk structure of substellar objects is much better than the two lines-of-sight by the GOODS/PEARS fields (black circles). We discard one field (borg_1815-3244) for its low latitudes and line-of-sight through the plane of the disk and close of the center of the bulge.

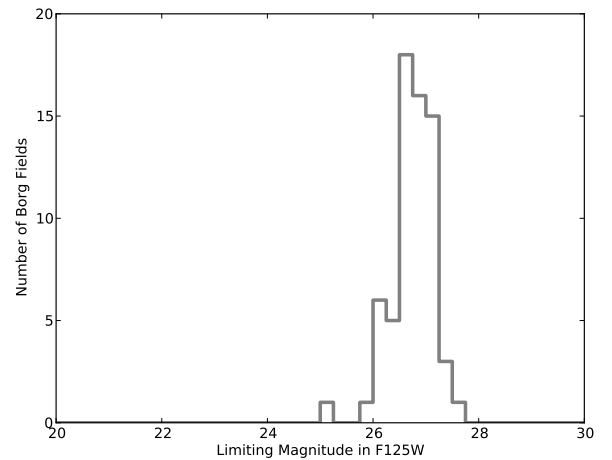


Figure 3. The distribution of limiting magnitude in the $F125W$ filter from Bradley et al. (2012). Photometric detections are reliable down to 26 magnitude.

fields). The BoRG data-set used here is the second data-release of 68 WFC3 fields (Table ??) for a total of approximately 209.9 arcmin 2 as described in detail by Trenti et al. (2011) and Bradley et al. (2012), including some reprocessed fields from another pure-parallel program with similar science goals (Hubble Infrared Pure Parallel Imaging Extragalactic Survey, HIPPIES, HST GO/PAR-11702, Yan et al. 2010). We use the WFC3 data-products generated by the BoRG team (see for details Bradley et al. 2012). This is a standard multi-drizzle reduction of these undithered WFC3 data with Laplacian edge detection (van Dokkum 2001) to the individual FLT files to mitigate detector hot pixels and cosmic rays. Stellar objects are not affected by this filtering.

The BoRG survey is designed to identify relatively

bright ($m_{F125W} \leq 27$) high-redshift galaxies from their broad-band colors using the Lyman-Break technique (Steidel et al. 1996). The primary aim of the survey is to select redshift $z \sim 7.5$ galaxies as $F098M$ dropouts. Two near-infrared filters ($F125W$ and $F160W$) are used for source detection and characterization down to 26 mag (Figure 3). One optical filter ($F606W$ or $F600LP$ in the case of the HIPPIES survey) is used to control contamination from lower redshift sources; $z \sim 1.5$ compact galaxies, AGNs, and cool Milky Way stars. Our interest here now goes to the latter of these interlopers. Given the near-random pointing nature of the pure-parallel HST program (higher Galactic Latitude objects are preferred for COS targets), the BoRG fields are minimally affected by field-to-field (cosmic) variance (Trenti & Stiavelli 2008). Therefore, this catalog is uniquely positioned to set constraints on the number density of unresolved sources, either Milky Way stars or $z \sim 8$ galaxies.

A recent BoRG observing campaign (BoRG13) is presented by Schmidt et al. (*in preparation*), which includes approximately 50 arcmin² of new data (13 fields) and deeper observations of two previous BoRG pointings. This brings the total J-band area of the BoRG survey to ~ 350 arcmin² makes BoRG the largest existing near-infrared survey with HST, e.g., compare with CANDELS wide (260 arcmin²) or deep (120 arcmin²). We include nine BoRG13 fields as additional lines-of-sight in our sample (see Table ??).

3. CATALOG GENERATION

To construct the catalogs for the BoRG Fields, we ran SExtractor (Bertin & Arnouts 1996; Holwerda 2005) with similar settings as Trenti et al. (2011) but set to include MU_MAX, r_50 and other morphological information. Source detection was done in the $F125W$ image, with the other filters run in dual-image mode. The multi-drizzle weight files were used as RMS maps (once normalized, following the prescription in Casertano et al. 2000, WEIGHT_TYPE=MAP_RMS), but scales appropriately to reflect the noise correlation introduced. The photometric zero-points are from Dressel et al. (2010); Windhorst et al. (2011): $F606W$: 26.08, $F600LP$: 25.85, $F098W$: 25.68, $F125W$: 26.25, and $F160W$: 25.96 respectively with A_V corrections derived for each individual field (Table ??). These settings resulted in 93106 objects in the BoRG survey.

4. CANDELS AND ERS CALIBRATION CATALOGS

We generated SExtractor v2.8 catalogs with the same settings as above for the section of the resampled CANDELS mosaic, which includes the PEARS-S coverage (Figure 1) to obtain $F125W$ and $F160W$ luminosities and morphological information for the spectroscopically identified M-dwarfs. Optical magnitudes for these are from ACS photometry presented in Pirzkal et al. (2009). The overlap between the PEARS-S survey and CANDELS mosaic is a sample of 24 M-dwarfs (Table 5). We will use their morphology to select bona-fide stars in the $F125W$ images and their colors to select and sub-type the M-dwarfs.

A second calibration catalog of 22 bona-fide PEARS-identified M-dwarfs is constructed based on the ERS mosaics (Table 6). The ERS mosaic pixel scale was set to be identical to the BoRG fields and all the SExtractor

parameters are kept identical to the BoRG ones. Similar to the CANDELS and BoRG catalog, detection was done in $F125W$ with the catalogs in $F160W$, $F098M$ and $F606W$ or $F600LP$ in dual mode for the respective photometry. Cross-correlation with the PEARS identified sources used the published right ascension and declination from Pirzkal et al. (2009) converted to pixels but due to some lingering issues with the wcs coordinates in the ERS data, we are less certain about the cross-identification than in the CANDELS data ($\sim 0.1''$ uncertainty in position). Because of these issues and the uncertainty in the flux calibration between CANDELS and the ERS mosaics (Figure 4), we adopt the CANDELS mosaic as our primary calibrator for morphological selection and sub-typing and the ERS to calibrate the color-color selection and as a check of the CANDELS data.

4.1. CANDELS and ERS photometry

We used the same zeropoints for all the filters as those used for the BoRG survey (Trenti et al. 2011; Bradley et al. 2012) and ERS (Windhorst et al. 2011). However, the ERS data was taken when the WFC3 instrument was still cooling down and hence one could expect slightly different WFC3 performance between the CANDELS and ERS photometry catalog. To check, we identified stars (using the r_{50} criterion below) in the full ERS mosaic and cross-correlated these with the full CANDELS catalog (derived from the $0.06''$ mosaic). The overlap is 13 point-sources. Figure 4 shows the difference SExtractor magnitudes for these stars between the CANDELS and ERS mosaics in the $F125W$ and $F160W$ filters.

Discarding the faintest objects as their stellarity becomes uncertain (Figure 5), the mean difference between the overlap stars for different apertures ($m_{F125W} < 24$, $m_{F160W} < 23.5$) are listed in Table 3. We take the differences in the MAG_APER as the most reliable as these were computed for identical-size apertures. Because we used the ASSOC option in SExtractor, the placement of these apertures could conceivably be slightly different (typically less than a pixel difference) but this is not enough to explain the offset in photometry.

Thus, for the following, we correct the ERS photometry by subtracting 0.43 and 0.39 for the $F125W$ and $F160W$ respectively. However, we lack a similar information for the $F098M$ filter and adopt a correction of 0.4 magnitude, the mean of the correction for the $F125W$ and $F160W$ correction.

Table 3
The difference and rms between the CANDELS and ERS magnitudes for the $F125W$ and $F160W$ filters. The aperture for MAG_APER is $0.48''$ (8 and 6 pixels respectively).

Filter	MAG_ISO	MAG_AUTO	MAG_APER
$F125W$	-0.34 (0.23)	-0.40 (0.26)	-0.43 (0.19)
$F160W$	-0.26 (0.11)	-0.28 (0.10)	-0.39 (0.10)

4.2. Morphological Identification of Stars

To identify the low-mass dwarfs in our catalogs, we opt for a strict morphological selection to allow the color information to be used for identification of the stellar type

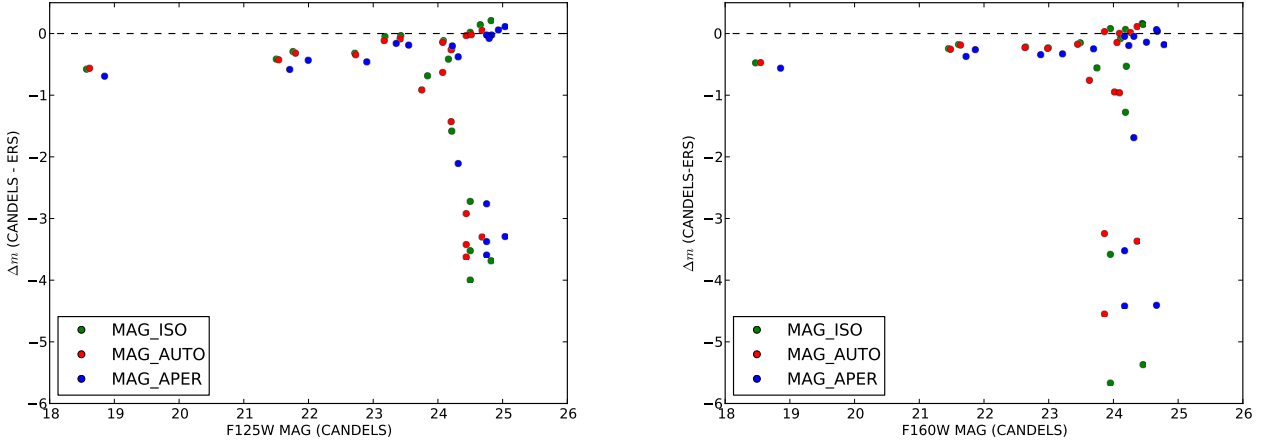


Figure 4. The difference in magnitude between the CANDELS and ERS mosaics. The CANDELS SExtractor catalog was generated from the 0''.06 pixel scale, full mosaic. Cross-correlation with the ERS mosaic yielded 13 stellar objects. There is an offset in both filters between the mosaics.

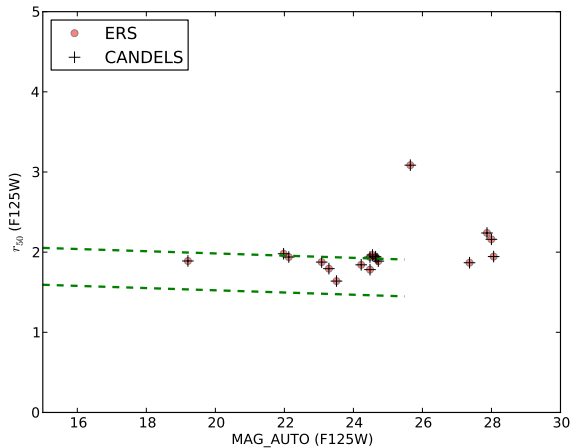


Figure 5. The relation between MAG_AUTO and half-light radius (r_{50}) for the common objects between the CANDELS v0.5 field and the ERS (see Figure 1). The green lines are the stellarity criterion for the half-light radius. Beyond $MAG_AUTO \sim 24$, the stellarity of these objects is doubtful.

and subtype. There are several SExtractor parameters cuts in use to identify unresolved sources, all of them a variation on a concentration index; the CLASS_STAR, native to SExtractor, the half-light or effective radius (r_{50}) used by Ryan et al. (2011), the flux ratio between two pre-defined apertures, e.g., the stellarity index $S_2 = MAG_aper(1pix)/MAG_ISO(F125W)$ in Pirzkal et al. (2009), and the relation between the brightest pixel surface brightness and total source luminosity (MU_MAX/MAG_AUTO , Holwerda 2005; Holwerda et al. 2005; Leauthaud et al. 2007, who used it to discard stars.).

Using the M-dwarf catalog for CANDELS, we define three morphological criteria: one based on the stellarity index (S_2), one on the MU_MAX/MAG_AUTO ratio, and one for the half-light radius (r_{50}) for $F125W$ catalog. If we fit the relation between S_2 , MU_MAX/MAG_AUTO and r_{50} with MAG_AUTO for

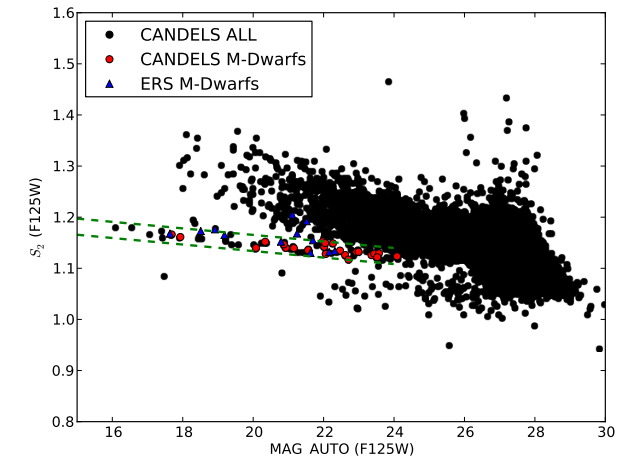


Figure 6. The S_2 parameter for the CANDELS subfield of Figure 1, (crosses) and the bona-fide M-dwarfs identified in this field by PEARs (red points). The green dashed lines indicate our S_2 selection criterion.

these M-dwarf we get:

$$|S_2 + 0.0065 \times MAG_AUTO - 1.18| < 0.016 \quad (0.018), \quad (1)$$

the relation between MU_MAX and the luminosity (MAG_AUTO),

$$|\frac{MU_MAX}{MAG_AUTO} - 0.0085 \times MAG_AUTO - 0.65| < 0.019 \quad (2)$$

and the half-light radius (r_{50}),

$$|r_{50} - 0.014 \times MAG_AUTO - 2.03| < 0.23. \quad (3)$$

with the variance in the relation determined from the scatter of the M-dwarfs around the fit. Thus, by definition these criteria will typically select all 24 M-dwarfs in the CANDELS field. Figure 6, 7, and 8 show these three criteria for objects in the CANDELS sub-field catalog with the PEARs M-dwarfs highlighted. For comparison,

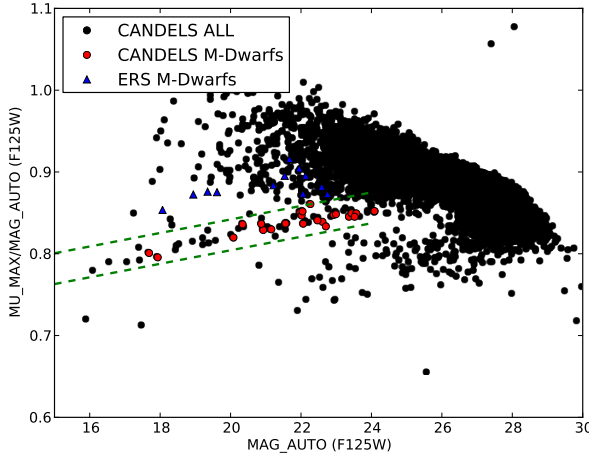


Figure 7. The MU_MAX/MAG_AUTO parameter for the CANDELS subfield of Figure 1, (crosses) and the bona-fide M-dwarfs identified in this field by PEARS (red circles). The green dashed lines indicate our MU_MAX/MAG_AUTO selection criterion.

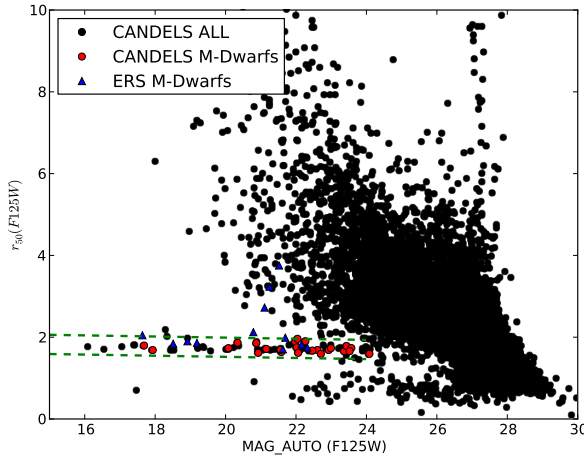


Figure 8. The r_{50} parameter (half-light radius) for the CANDELS subfield of Figure 1, (crosses) and the bona-fide M-dwarfs identified in this field by PEARS (circles). The green dashed lines indicate our r_{50} selection criterion.

the ERS M-dwarfs are also marked. Table 4 shows how many stars they select in the CANDELS field.

Our goal is to define criteria that would successfully select the PEARS stars. We note that our calibrators are the confirmed M-dwarfs and that some of those objects selected as stars in the CANDELS field are still Galactic stars, just not M-dwarfs. All three criteria work remarkably better than CLASS_STAR, selecting stars with little contamination for objects brighter than $m_{F125W} < 24$ (Figures 6–9). However, there is a marked difference in efficiency between the S_2 and MU_MAX/MAG_AUTO criteria and the r_{50} criterion in the 24–25.5 mag range. The half-light radius criterion is much stricter than the other two (Table 4), i.e., it includes most of the PEARS identified M-dwarfs but includes much fewer objects from CANDELS than the other two criteria.

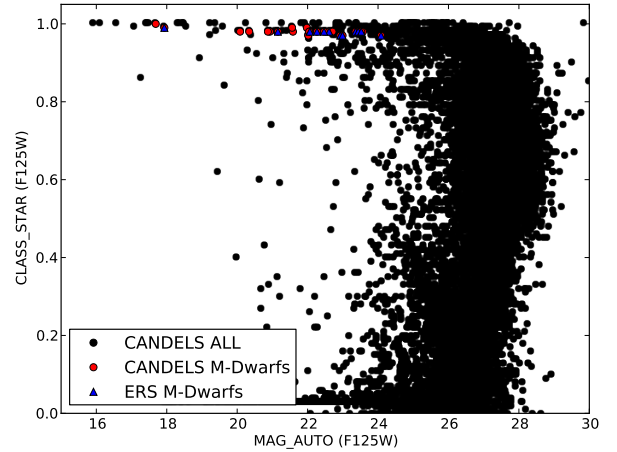


Figure 9. The CLASS_STAR parameter from SExtractor for the CANDELS subfield of Figure 1, (crosses) and the bona-fide M-dwarfs identified in this field by PEARS (circles).

Table 4

The number of selected objects in the CANDELS/GOODS-S mosaic section (Figure 1) for the three different criteria separately and in combinations. The mosaic contains 24 bona-fide M-dwarfs and we note their selected number as well. Stricter limits resulted in some of those not being selected.

criterion	CANDELS	PEARS	M-dwarfs
< 25.5	216	24	
S_2	331	23	
MU_{MAX}/MAG_{AUTO}	120	23	
r_{50}			

The half-light parameter was used by Ryan et al. (2011) in some of these fields to select faint dwarf stars ($1.2 \leq r_{50} \leq 1.8$ pixels with their pixelscale set to $0.^{\prime\prime}09$). Our calibration here shows that this selection criterion is even a little lenient (the selection range can even be narrower), allowing for the different pixel scales, but works very well for the M-dwarfs in these fields.

4.2.1. ERS catalog check

The 22 M-dwarfs in the ERS catalog are also plotted in Figures 6–9 to serve as a check for the morphological selection. Their positions in these figures reveal a sensitivity in both the S_2 and the MU_MAX-MAG_AUTO relations for unresolved objects to the pixel scale. The r_{50} criterion is less sensitive to the scale of the pixels. Most likely, this is because it is computed from the growth curve of an object, i.e., the ordered list of pixels. The other two criteria both depend on an aperture of a single pixel and hence are more sensitive to the pixelscale. Several of the identified objects in the ERS catalog are well away ($r_{50} > 2$ pixels) from those values expected for stars, i.e., unresolved objects. These are likely either mis-identifications in the ERS field or blends with other objects or artifacts.

The comparison shows that both the r_{50} and the MU_MAX/MAG_AUTO work well for stellar selection brighter than 24 mag and the r_{50} includes much less

interlopers down to 25.5 mag. The practical limit of 24 mag for PEARS identified M-dwarfs in $F124W$ would limit identifications to distances from 3.2 to 36.3 kpc depending on M-dwarf subtype (M9-M0 respectively), or some 10-100 thin disk scale-heights. We treat our sample as uncontaminated, photometrically accurate, and calibrated with the CANDELS M-dwarfs up to this conservative limit, which is still two magnitudes above the BoRG photometric detection limit (Figure 3).

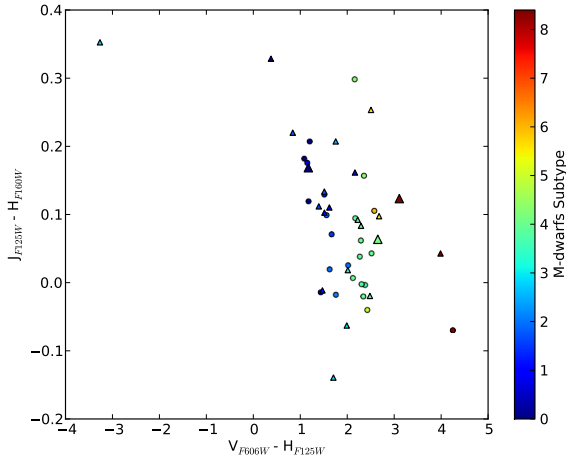


Figure 10. The relation between the $F606W$ - $F125W$ and $F125W$ - $F160W$ colors for the M-dwarf sub-type (0-8) determined from the GOODS, CANDELS and ERS data for the PEARS spectroscopically identified M-dwarfs.

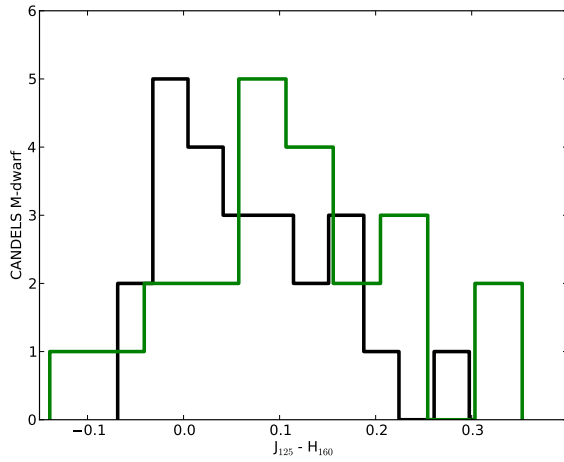


Figure 11. The histogram of the $F125W$ - $F160W$ colors from CANDELS and ERS of the PEARS spectroscopically identified M-dwarfs.

4.3. M-Dwarf NIR color-color selection

The second part of the calibration is an empirical color-color selection for the M-dwarfs in the GOODS-S field. We base the M-dwarf selection in near-infrared colors

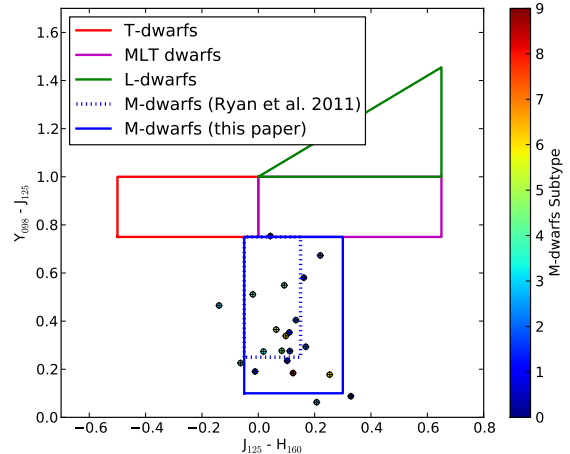


Figure 12. A plot of the $F125W$ - $F160W$ and $F098M$ - $F125W$ colors from the ERS of the 22 PEARS spectroscopically identified M-dwarfs.

because of the wide range in optical-near-infrared colors M-dwarf subtypes can display (Figure 10). To identify M-dwarfs, we require their $J_{F125W} - H_{F160W}$ and $Y_{F098M} - J_{F125W}$ color to be similar to the distribution of the PEARS-identified M-dwarfs. To find the J-H color range, we can use both the CANDELS as the ERS catalog but for the Y-J color, we must rely on the ERS catalog alone.

Figure 11 shows the distribution of $J_{F125W} - H_{F160W}$ color for the PEARS M-dwarfs in the CANDELS and ERS fields. These are not in the range one would infer from Ryan et al. (2011), in their Figures 3 and 4 but wider by a few tenths of magnitudes. The ERS and CANDELS J-H colors are still different by ~ 0.1 magnitude (Figure 11). We suspect that the PEARS M-dwarf $F125W$ - $F160W$ color distribution in CANDELS in Figure 11 is different than the distribution in Ryan et al. (2011) because their colors were derived from spectra convolved with appropriate filter response functions. There is however an under-reported drop in WFC3 detector sensitivity on the red side of the $F160W$ filter (Andersen et al. *in preparation, private communication*). The $F098M$ and $F125W$ filters however, do not suffer from the detector sensitivity degradation at the red side. This could in part account for the small difference in J-H color of the CANDELS M-dwarfs, whose photometry we trust, with the position of M-dwarfs in Figure 3 in Ryan et al. (2011) or the difference in $F125W$ - $F160W$ color with the ERS as the detector was still cooling down (Figure 11)

The ERS mosaics is in the same NIR filters as the BoRG fields ($F125W$, $F160W$ and $F098M$) and Figure 12 shows the position of the 22 objects matched to PEARS M-dwarfs in a J-H, Y-J color-color plot. We show the same color criteria as Figures 3 and 4 in Ryan et al. (2011). The width and position of the Y-J color criterion is close to what one would infer from Figure 3 in Ryan et al. (2011).

Based on both Figure 11 and 12, we define a near-infrared color-color criterion to select M-dwarfs in the BoRG survey; $-0.05 < J - H < 0.3$ and $0.1 < G - J < 0.75$ (the solid blue boxes in Figure 12 and 19 in addition

Table 5

The M-dwarfs identified by PEARS in the CANDELS field. The optical magnitudes are from Pirzkal et al. (2009) and the $F125W$ and $F160W$ magnitudes from our SExtractor catalog of the CANDELS field.

ID	Type	ra	dec	m_{F435W}	m_{F606W}	m_{F775W}	m_{F850W}	m_{F125W}	m_{F160W}
48173	4.0	53.220073	-27.854046	25.22	24.96	23.73	23.15	22.61	22.63
53237	4.0	53.194890	-27.848121	25.19	25.45	24.14	23.49	22.93	22.88
58796	1.5	53.173782	-27.841699	25.70	25.04	24.17	23.85	23.36	23.29
58826	4.3	53.189870	-27.841487	24.76	24.34	23.04	22.39	21.98	21.82
63079	1.0	53.181657	-27.836074	25.49	24.44	23.76	23.47	22.99	23.00
63028	3.7	53.213644	-27.835281	24.29	23.97	22.78	22.15	21.58	21.59
63752	3.9	53.189345	-27.834509	23.80	23.43	22.37	21.74	21.16	21.12
63993	2.0	53.170843	-27.833788	23.81	23.13	22.27	21.91	21.56	21.46
66572	8.4	53.191395	-27.830774	24.60	26.71	24.80	23.58	22.47	22.53
69522	6.0	53.183514	-27.826627	24.89	24.60	23.41	22.64	22.02	21.91
70032	3.9	53.169502	-27.825087	22.88	22.52	21.40	20.77	20.34	20.25
74670	1.0	53.181116	-27.817942	25.79	24.96	24.20	23.97	23.44	23.31
74928	4.0	53.192508	-27.815594	20.55	20.06	19.10	18.51	17.93	17.92
79699	4.0	53.210190	-27.808231	22.75	22.38	21.29	20.66	20.08	20.02
80618	2.0	53.181804	-27.808089	26.31	25.72	24.88	24.48	24.08	24.06
82885	0.2	53.208736	-27.804499	25.77	24.76	24.13	23.83	23.57	23.45
91263	0.9	53.171308	-27.793465	24.35	23.43	22.76	22.49	22.27	22.09
92395	2.1	53.193512	-27.792703	24.44	23.83	22.93	22.54	22.06	22.08
93532	2.0	53.208197	-27.791671	26.19	25.55	24.52	24.07	23.52	23.50
93841	4.9	53.182786	-27.791200	25.10	25.14	23.97	23.34	22.71	22.74
94206	4.3	53.163637	-27.790605	24.71	24.21	23.00	22.37	22.04	21.75
95752	3.8	53.193173	-27.788834	23.42	23.24	22.12	21.53	20.93	20.93
104030	0.0	53.158515	-27.777252	22.95	21.97	21.34	21.16	20.87	20.69
104673	0.0	53.158184	-27.773143	19.76	18.90	18.48	18.04	17.69	17.48

Table 6

The M-dwarfs identified by PEARS in the ERS mosaic. The optical magnitudes are from Pirzkal et al. (2009) and the $F125W$ and $F160W$ magnitudes from our SExtractor catalog of the ERS mosaic.

ID	Type	ra	dec	m_{F435W}	m_{F606W}	m_{F775W}	m_{F850W}	m_{F125W}	m_{F160W}
108497	1.7	53.093027	-27.735838	21.39	20.58	19.78	19.42	19.19	19.07
108014	2.0	53.057966	-27.735053	19.76	18.81	18.37	17.80	17.64	17.47
110839	2.0	53.089621	-27.733082	23.02	22.36	21.48	21.06	21.52	21.30
111269	3.0	53.113985	-27.732740	24.68	23.98	23.05	22.58	21.99	22.05
111982	6.0	53.107958	-27.728253	21.63	21.19	19.94	19.11	18.51	18.41
114688	0.0	53.086462	-27.724381	24.06	23.11	22.49	22.22	22.73	22.41
115223	4.0	53.105121	-27.724124	25.11	24.64	23.51	22.90	22.16	22.18
114563	6.0	53.069511	-27.723391	22.27	21.88	20.69	19.90	19.37	19.12
116612	4.0	53.134575	-27.721317	24.55	23.85	22.70	22.24	21.63	21.53
117391	1.3	53.087638	-27.719656	23.01	22.13	21.42	21.04	20.66	20.67
119050	2.7	53.087816	-27.717329	26.03	24.77	23.84	23.42	23.02	22.81
120814	4.2	53.111938	-27.713369	24.19	23.99	22.87	22.19	21.70	21.61
123686	5.3	53.090399	-27.706629	23.60	23.44	22.25	21.52	20.79	20.72
124539	8.7	53.076943	-27.706018	25.28	25.75	24.27	23.22	22.64	22.52
124624	1.0	53.104778	-27.705292	23.78	23.41	22.76	22.42	21.25	21.08
125478	9.0	53.100622	-27.703149	24.03	24.37	22.53	21.29	20.38	20.34
126754	1.0	53.049225	-27.701327	24.91	23.94	23.19	22.88	22.32	22.21
128173	3.3	53.069739	-27.697205	23.69	23.12	22.11	21.57	21.11	21.09
128247	2.0	53.096541	-27.694200	21.16	20.43	19.62	19.24	18.92	18.78
130804	1.0	53.060606	-27.691367	24.23	23.33	22.66	22.35	21.82	21.71
132690	3.0	53.066145	-27.687565	24.21	23.86	22.91	22.44	27.13	26.77
132690	3.0	53.065896	-27.687864	24.21	23.86	22.91	22.44	22.15	22.29

to the L, T and MLT boxes from Ryan et al. (2011).

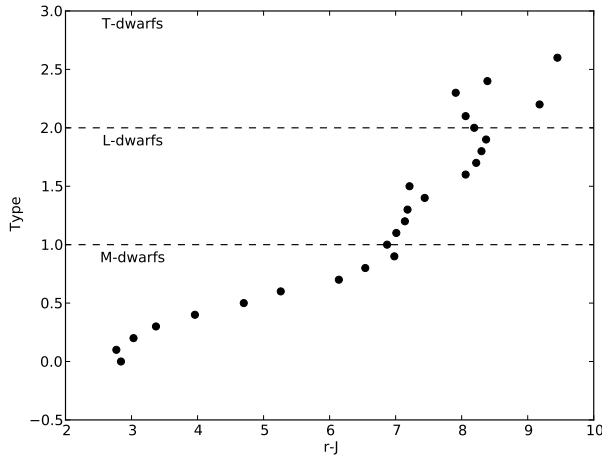


Figure 13. The relation between *sdss-r-J* color and spectral type from Hawley et al. (2002). M-dwarfs are 0-1 with subtype as the decimal. L-dwarfs are 1-2 with the subtypes as the decimal and T dwarfs are type 3 with the decimal assigned subtype as molecular lines start to dominate the spectrum. The later type dwarfs do not show a good linear relation between a wide optical-near-infrared color and sub-type. However, they do show a redder color than all the M-dwarf subtypes and hence we can exclude all most stellar objects based on color.

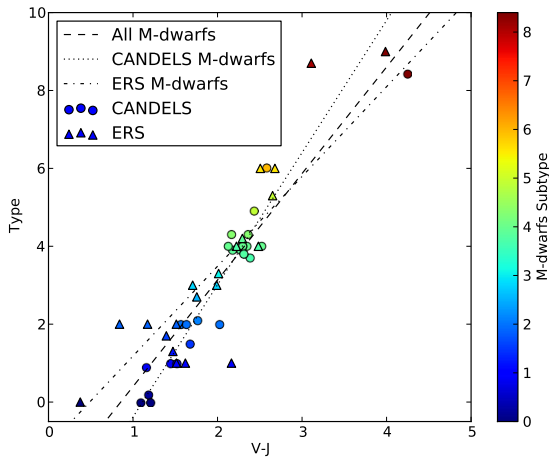


Figure 14. The relation between M-dwarf sub-type (0-8) and the $V_{F606W} - J_{F125W}$ color relation as determined from the GOODS, CANDELS and ERS data for the PEARS spectroscopically identified M-dwarfs. There is a linear relation between this color and the subtype which we use to type the dwarfs in the BoRG WFC3 parallel fields. We show three fits; one based on all M-dwarfs ($t < 6$), only the CANDELS M-dwarfs ($t < 6$) and only the ERS M-dwarfs. We adopt the CANDELS relation as this sample is the cleanest with accurate photometry and similar exposure times as the BoRG fields.

4.4. Sub-typing M-dwarfs

Our last calibration involving the PEARS identified M-dwarfs in the CANDELS and ERS mosaics of the

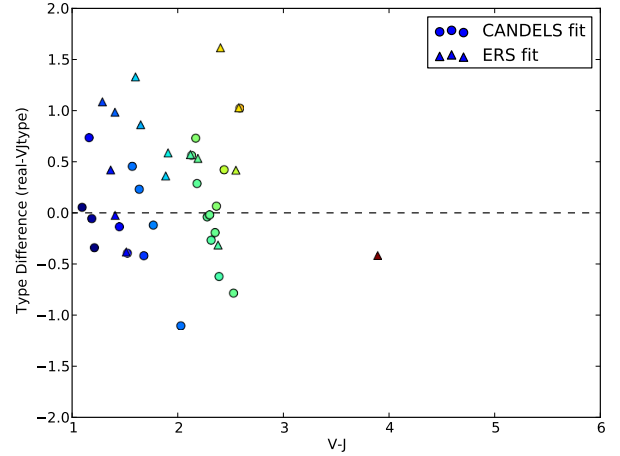


Figure 15. The residual between V-J inferred subtype and the spectroscopic subtype from PEARS for the M-dwarfs in the ERS and CANDELS data. The ERS $F125W$ photometry may be shifted slightly still with respect to the CANDELS's (Figure 11) and this may account for the higher scatter for this subset.

GOODS-S field is to derive a color-subtype relation. Figure 13 shows the relation between $r-J$ color and dwarf type from Hawley et al. (2002). M-dwarfs show a linear relation with a color, provided the baseline is long enough, i.e. optical to infrared. The later L and T dwarfs do not have such a clear relation.

Figure 14 shows the relation between the $V_{F606W} - J_{F125W}$ color and the spectroscopic sub-type as determined by Pirzkal et al. (2009) for the 24 PEARS M-dwarfs in CANDELS and the 22 PEARS M-dwarfs in the ERS. They obtain a type from template fits to each ACS grism spectrum obtained for these objects. Because of design of the PEARS observations, there are oftentimes several spectra taken at different roll-angles. Cross-comparison between the spectral fits show that the uncertainty in the PEARS type classification is less than an M-dwarf subtype. We therefore take these spectral types as our gold standard for the classification of the stellar objects in the WFC3 parallel fields.

Figure 14 shows the relation between the V-J color and spectroscopic type from PEARS. We fit a linear relation to the CANDELS sample because it is the cleanest selection and photometry. The linear relation in the PEARS-identified CANDELS M-dwarfs can be expressed as:

$$M_type = 3.39 \times [V_{F606W} - J_{F125W}] - 3.78 \quad (4)$$

The M-dwarfs identified by PEARS in the ERS mosaic display more scatter than the CANDELS M-dwarfs but after correction of the $F125W$ magnitudes (see above), the V-J colors and their PEARS subtype generally agree well with the relation derived from the CANDELS M-dwarfs, although some difference may remain (Figure 11).

Figure 15 shows the residual between the V-J color type and PEARS spectroscopic type. The PEARS M-dwarfs cover mostly subtype 0-5 and only a few M ($t > 6$) are in this sample. Consequently, the color-subtype relation is most reliably for the earlier subtypes. Based in Figure 15, we take that our subtype based on V-J color

is accurate within a subtype. We adopt this relation to type M-dwarfs in the BoRG fields and compute type uncertainties as a result of the photometric uncertainty in the $F606W$ and $F125W$ magnitudes. We use the absolute magnitudes from Hawley et al. (2002) to compute distance moduli (Table 7) and infer distances.

Table 7

Absolute 2MASS J-band ($F125W$) magnitudes of M-dwarfs from Hawley et al. (2002).

Subtype	M_J
0	6.45
1	6.72
2	6.98
3	7.24
4	8.34
5	9.44
6	10.18
7	10.92
8	11.14
9	11.43
10	11.43

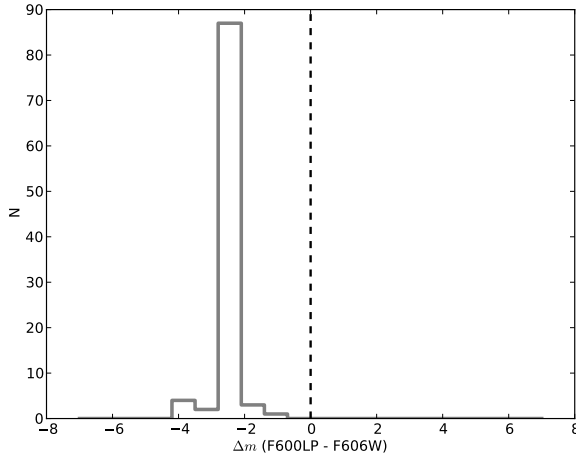


Figure 16. A histogram of the difference in $F600W$ and $F600LP$ MAGAUTO values for those stars in the M-dwarf near-infrared criteria for the three fields in the BoRG survey that have data in both filters.

4.5. Substituting $F600LP$ for $F606W$ photometry

In the case of 24 fields in the BoRG survey, $F606W$ photometry is not available. These fields come from the HIPPIES or COS-GTO parallel observations which opted for $F600LP$ rather than $F606W$. The $F600LP$ filter has a slightly different width compared to the $F606W$ and a different central wavelength (closer to Johnson-I). Fortunately, there are three fields for which both $F606W$ and $F600LP$ data is available. We compared the $F606W$ - $F600LP$ colors for those objects already pre-selected by their near-infrared color and morphology as likely M-dwarf to assess the impact of the change of filters. Figure 16 shows the histogram of the color difference between

the two bandpasses for M-dwarfs. The difference is substantial: $F600LP - F606W = -2.65$ mag with a spread of 0.88 mag. Therefore we correct our $F600LP$ photometry with this difference and increase the uncertainty in the photometry accordingly as well (which should be reflected in the subsequent automated typing).

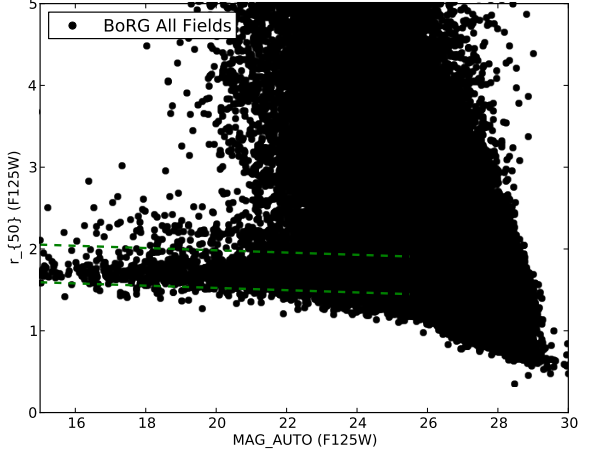


Figure 17. The $F125W$ half-light radius as a function of magnitude for all the BoRG fields. The green dashed lines are the selection criterion from equation 3 to identify stars in these fields. Objects below the bottom green line are more likely to be defects (e.g. remaining hot pixels etc.).

5. STARS IN THE BORG WFC3 PURE-PARALLEL FIELDS

With the morphological and near-infrared color-color selection in hand, we now search the BoRG fields for M-dwarfs as well as other substellar types. Figure 17 shows the same parameter space as Figure 8 but with all the BoRG objects. Based on the r_{50} selection criterion, we find 1308 stars to 24 mag in $F125W$ in the 59 WFC3 parallel fields. For comparison, Figure 18 shows the other morphology criteria. The r_{50} selection criterion seems the most appropriate for the BoRG fields as the locus of stellar points is within the criterion lines. S_2 appears equally applicable but the MU_{MAX}/MAG_{AUTO} criterion shows a discrepancy compared to Figure 7. We suspect this is because the CANDELS data was originally at a different pixel size and this criterion is sensitive to the exact pixel scale of the image. Figure 17 validates therefore our adoption of the r_{50} criterion for the morphological selection of stars.

To identify the various subtypes of stars, we construct a NIR color-color diagram similar to Figure 3 in Ryan et al. (2011), as discussed above. Figure 19 shows this plot with the limits for our selection criteria for approximate types. In the BoRG SExtractor catalog, we identify 30 L-dwarfs, 1 T-dwarfs, 274 M-dwarfs and 29 M, L or T-dwarfs based on the color cuts. The M-dwarf sample is the one of interest here. Tables ??, ?? and ?? list the properties of the identified stars which conform to the M, T and L-dwarf color cuts (Figure 19).

Subsequently, we sub-type the M-dwarfs according to equation 4. Figure 20 shows the histogram of M-dwarf subtypes in the BoRG fields as well as those objects in the

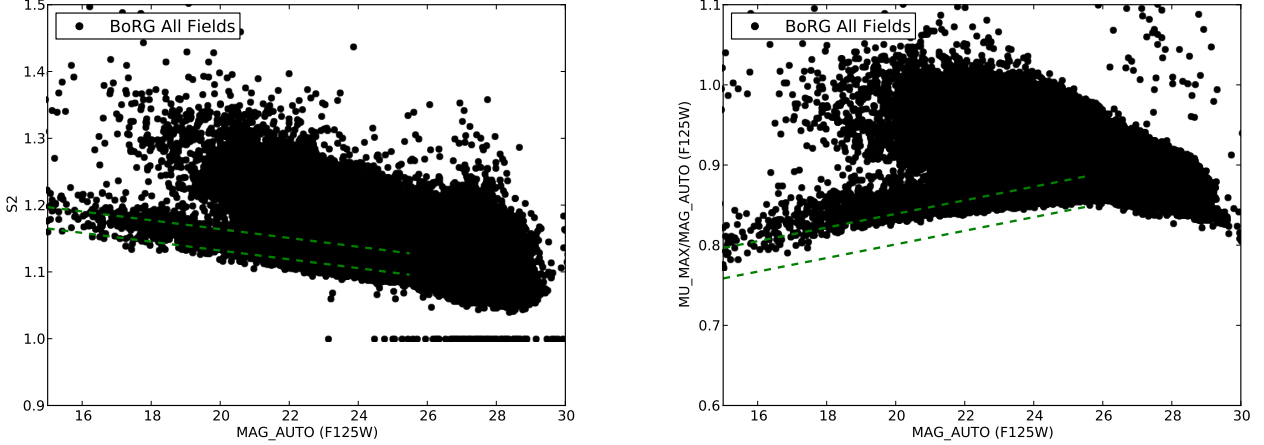


Figure 18. The two alternative morphological selections for star, for the BoRG data: the S_2 and the μ_{max}/mag_{auto} ratio.

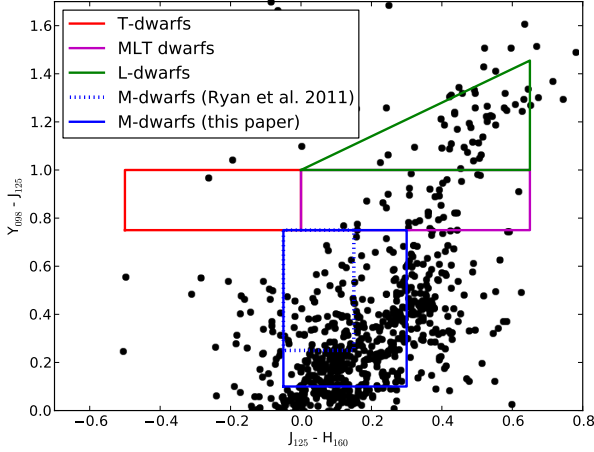


Figure 19. $J_{F125W} - H_{F160W}$ versus $G_{F098M} - J_{F125W}$ color diagram, similar to Figure 4 from Ryan et al. (2011), to distinguish between L, T, and M-dwarfs.

MLT box in Figure 19 for comparison. In effect this is an additional optical-near-infrared color criterion for M-dwarf selection as we will discard any star that could not be sub-typed. The dominant type in our M-dwarf sample is M0, specifically -1 to 1 type, not unexpectedly as these are the brightest and most numerous type of M-dwarf. There are almost as many later-type M-dwarfs (M4 and above) in the MLT color selection as in our exclusively M-dwarf box. However, as we note above, the later type classification is the most uncertain and in the MLT box, susceptible to L and T dwarf contamination.

There is still the possibility of contamination by Giants, sub-dwarfs and AGNs but we are confident that the morphological selection, luminosity limit and the color-color restriction select a very clean sample of Milky Way M-dwarfs.

5.1. Contamination by M-giants or M-type Sub-dwarfs

Bochanski et al. (2013) present a catalog of 404 M-giants from the UKIDSS survey DR8 (2400 deg^2 , $K < 17$), with these M-giants among the most distant

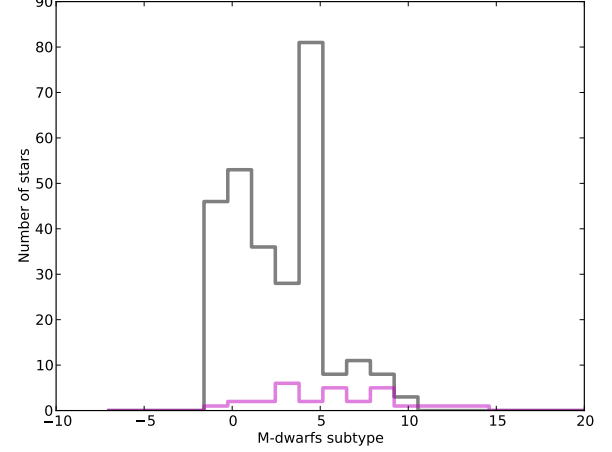


Figure 20. The histogram of M-dwarf types in our BoRG, inferred from equation 4. M0 and M1 are the most prevalent in the sample. As can be seen in the histogram, some of the stellar objects are not M-dwarfs but either other sub-stellar objects or possibly very distant (intergalactic?) M-giants.

stars belonging to the Milky Way. In principle, M-giants could be selected by our color selection. However, their on-sky density ($4.3 \times 10^{-5} \text{ M-giants/arcmin}^2$) makes it unlikely—not impossible—that even a single one is included in our selection. One could make a similar plausibility argument against very nearby M-type subdwarfs: the volume probed at close distances is comparatively small for a pencil beam survey.

Please note that beyond this point there are corrected versions of many of the figures available in the ERRATUM appended below.

6. DISCUSSION

Based on our bona-fide, morphologically and color selected M-dwarfs and the subsequent color sub-typing, we explore the North/South discrepancy, the Galactic thin disk scale-height as a function of subtype and whether or not we detect any additional Galactic component (Halo

or Thick disk).

6.1. The North-South Divide

Pirzkal et al. (2009) found a North-South discrepancy between the number of M-dwarfs in the PEARS fields. They find 51 and 63 M0-9 dwarfs in the GOODS North and South fields respectively. Accounting for the different field sizes (41.61 arcmin^2 and 59.50 arcmin^2 respectively) this is equivalent to 1.23 and 1.06 M-dwarfs/ arcmin^2 , an excess of 11% in the Northern field. Both GOODS fields are at similar Galactic Latitude and Pirzkal et. al. note that because the Sun is North of the Galactic plane, the Northern excess appears to be a contradiction. Widrow et al. (2012) and Yanny & Gardner (2013) find similar North-South discrepancies in the SDSS catalog of (dwarf) stars in the solar neighborhood.

One of our science goals with this study was to establish if this a real discrepancy or due to natural field variance. The BoRG fields are over many more lines of sight and dividing these in Galactic Northern and Southern Fields: 134.5 and 72.1 square arcminute respectively. We count the M-dwarfs in those fields above 20° Galactic Longitude to avoid two Southern fields that sample more along the Galactic Plane.

We find on average 1.157 ± 0.088 M-dwarfs of all types (M0-9) per arcmin^2 in the Northern fields and 1.293 ± 0.127 per arcmin^2 in the Southern Galactic fields (Table 8), which agrees with the previously observed discrepancy. The Northern over density is the most pronounced in the early (M0-4) type M-dwarfs. Taking into consideration that for these early-types the statistics are more secure, and early-types dominate the grism sample of Pirzkal et al. (2009) (or the SDSS catalog), our counts corroborate the previously found North-South discrepancy. The Northern overdensity is most pronounced in the earliest types, gradually diminishing and reversing for late-type M-dwarfs (Table 8).

Table 8

Average number of M-dwarfs per square arcminute in Southern and Northern Galactic fields ($|l| > 20^\circ$). M-dwarf numbers refer to those objects in the blue box in Figure 19. The last two columns are the ratio of M-dwarfs in Northern and Southern fields and the signal-to-noise of the noise.

	M-dwarfs	North	South	North /South	S/N
M-dwarfs	1.157 ± 0.088	1.293 ± 0.127	0.89	8.02	
M0-4	0.859 ± 0.076	0.779 ± 0.099	1.10	6.45	
M5-10	0.210 ± 0.038	0.465 ± 0.076	0.45	4.11	
M0	0.304 ± 0.045	0.176 ± 0.047	1.73	3.27	
M1	0.156 ± 0.032	0.151 ± 0.043	1.03	2.81	
M2	0.115 ± 0.028	0.088 ± 0.033	1.31	2.23	
M3	0.088 ± 0.024	0.075 ± 0.031	1.17	2.03	
M4	0.196 ± 0.036	0.289 ± 0.060	0.68	3.58	
M5	0.095 ± 0.025	0.364 ± 0.068	0.26	3.07	
M6	0.007 ± 0.007	0.025 ± 0.018	0.27	0.82	
M7	0.041 ± 0.017	0.025 ± 0.018	1.62	1.22	
M8	0.041 ± 0.017	0.013 ± 0.013	3.23	0.93	
M9	0.020 ± 0.012	0.038 ± 0.022	0.54	1.22	
M10	0.007 ± 0.007	0.000 ± 0.000	0.00	0.00	

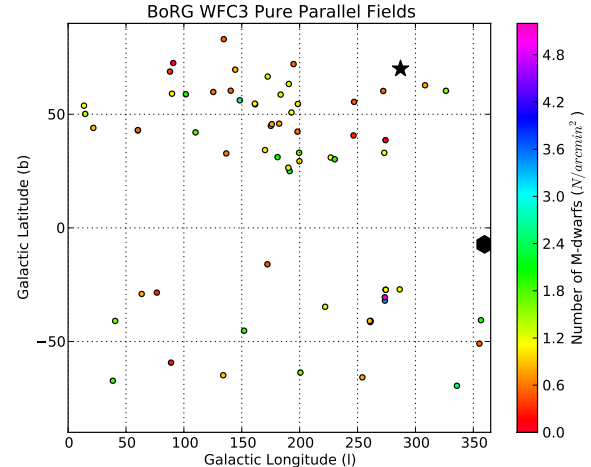


Figure 21. The distribution of BoRG fields with the number of M-dwarfs indicated. One field, borg_1230+0750 (star) stands out with 22 M-dwarfs ($\sim 20 \text{ stars}/\text{arcmin}^2$). We discard borg_1815-3244 (black circle) for its low latitudes and line-of-sight through the plane of the disk and close of the center of the bulge.

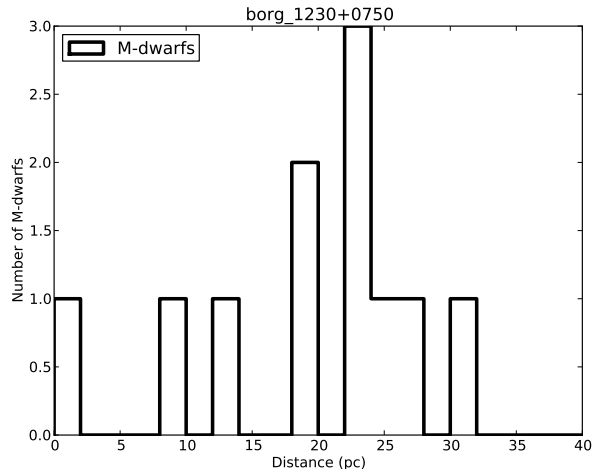


Figure 22. The distribution of M-dwarf distances in borg_1230+0750 , with a concentration at 20-25 kpc.

6.2. A Local Over-density of M-dwarfs

A single field, borg_1230+0750 stands out from the other BoRG fields with a local density of $21.4 \text{ M-dwarfs}/\text{arcmin}^2$. Such over-densities of faint Galactic stars are a possible contaminant for identifications of over-densities of high-redshift clusters (e.g., Trenti et al. 2012).

The Galactic position of this over-density ($l = 287.119670593^\circ, b = 70.0322203957^\circ$) argues against a spiral arm or disk substructure to be the origin of this over-density. However, its position is exactly on the Sagittarius stellar stream (Majewski et al. 2003; Belokurov et al. 2006). Figure 22 shows the histogram of photometric inferred distances for the M-dwarfs in borg_1230+0750 . The distance of the over-density of M-dwarfs at 20-25 kpc. is also in line with these M-dwarfs

belonging to the Sagittarius stream (Newberg et al. 2002; Belokurov et al. 2014) at this Galactic longitude.

The relative ease with which this stellar stream was identified in the BoRG data, shows that the future EUCLID mission will identify virtually *all* streams in the Milky Way halo from the dwarf stars alone.

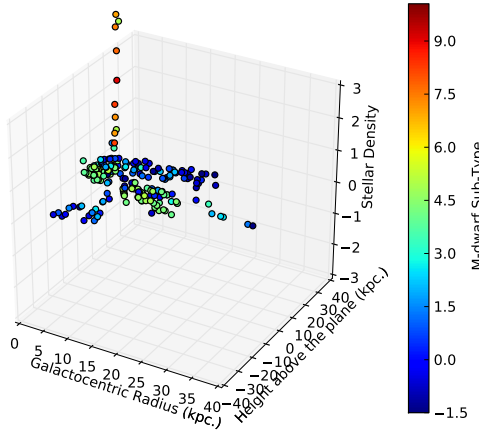


Figure 23. The computed volume for each M-dwarf as a function of Galactocentric radius, height above the plane. M-dwarf types as inferred from their optical-nir color.

Table 9

Local dwarf density from Figure 8 in Reid et al. (2008) and Cruz et al. (2007).

Subtype	Number within 20 pc. Reid et al. 2008	Cruz et al. 2007
0	35	
1	50	
2	140	
3	90	
4	350	
5	400	
6	190	
7	170	21
8	45	21
9	60	11
10	42	3

6.3.

In the original catalog of M-dwarfs presented, there is an issue with the conversion from celestial coordinates to Galactic ones, done with PYEPEM a wrapper around a trusted and vetted library *ephemis*. In the this updated astro-ph entry, we present the corrected coordinates (using ASTROPY) and distances based on AB magnitudes. We have amended the tables and Figures beyond this point accordingly.

6.4. Thin Disk Scale Height.

Previous studies based on small numbers of fields have already given us several estimates of the scale-height of

the thin disk of the Milky Way in substellar objects (Table 1). The consensus appears to be a scale-height between 300 and 400 pc for the thin disk. For M-dwarfs, Jurić et al. (2008) find a thin disk of $z_0 = 300$ pc. and a thick disk with $z_0 = 900$ pc. from SDSS data.

To estimate the distances to each M-dwarf, we compute the distance modulus from the inferred sub-type (and hence absolute magnitude) and the apparent magnitude in F125W. We compute the Galactic radius and height above the plane for all M-dwarfs, based on their Galactic longitude, latitude and the above distance, assuming the position of the Sun is 27 pc. above the plane, and at a Galactocentric radius of 8.5 kpc from the Galactic center. To compute the density at each M-dwarf's position, we compute the physical area at the inferred distance of the BoRG survey field in which the dwarf was found and a binwidth of 1pc.

We discard one field (borg_1815-3244) for two reasons: it is at low Galactic Latitude with a line-of-sight straight through the Galactic bulge (Figure 22), and secondly, there is only F600LP information available which makes subtyping of M-dwarfs more uncertain. This field contains 67 M-dwarf candidates but these are not used for the following analysis.

Figure 23 shows the distribution of radius and height above the disk for the 274 stars in the BoRG survey with their corresponding number density and type. The fainter late-sub-type M-dwarfs are in a localized thin disk and the bright early-sub-type (e.g., M0) correspond closer to the thick disk component.

We assume that the Galactic disk has the following parametric shape:

$$\rho(R, z) = \rho_0 \exp(-R/h) \operatorname{sech}^2\left(\frac{z}{z_0}\right), \quad (5)$$

where $\rho(R, z)$ is the dwarf number density in a point in the disk, ρ_0 is the central number density, R is galactocentric radius, h is the scale-length, z is height above the plane, and z_0 is the scale-height of the disk.

To collapse Figure 23, we weight the volume densities with the exponential part of this equation since we aim to infer the vertical structure first, i.e., we assume a single scale-length and calculate $\exp(-R/h)$ as a weight for each dwarf volume density. In Figure 25, the volume densities have all been scaled this way, assuming the scale-length (h) of the thin disk from Jurić et al. (2008) of 2.6 kpc. They found a scale-length for the thick disk of $h=2.9$ kpc. Alternatively, Bensby et al. (2011) found a thin-disk scale-length of $h=3.8$ kpc and $h=2.0$ for the thick disk, corroborated by Cheng et al. (2012) and the trend of stellar population and scale-length in Bovy et al. (2012). We use the Bensby et al. thin disk scale-length for dwarfs found in below 500 pc and the thick disk one for those more than 500 pc out of the plane. The implicit assumption in this renormalization is that the scale-height does not change with radius, which is observed in external galaxies seen edge-on (Comerón et al. 2011a,b,c, Streich et al *in preparation*).

Figure 25 shows more clearly how the later-type M-dwarfs (M4-8) in the BoRG fields are concentrated in the thin disk and the earlier types (M0-3) probe both thin and thick disks. It also shows that there may be several disk components in early types with different scale-

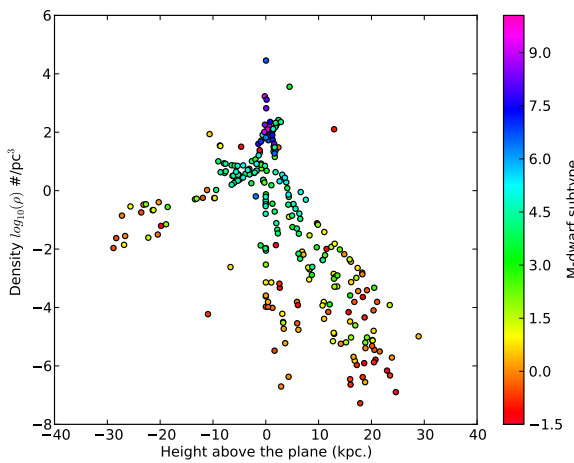


Figure 24. The volume density of M-dwarfs as a function as height above the plane of the Milky Way disk. The volume densities were normalized with a scale-length of 2.6 kpc. Points are color-coded by the M-dwarf sub-type.

heights above and below the plane of the disk. This would explain the North-South differential noted earlier by Pirzkal et al. (2009).

First we perform a naive fit on the vertical distribution of M-dwarfs as a function of sub-type: we fit the $\text{sech}^2(z/z_0)$ to their densities for each sub-type disregarding the different sampling or the existence more than a single disk component. Fit parameters, ρ_0 and z_0 are listed for each M-dwarf type in Table 10. The fit to the M4 dwarfs distribution is not a physical solution. Figure 25 shows the best fits to the densities and Figures 26 and 27, the central density and scale-height as a function of type.

The central densities in Figure 26 are not scaled by the central volume density of dwarfs. For comparison, we plot the volume densities computed from the local number of M-dwarfs compiled in Reid et al. (2008), their Figure 7, which is based on the numbers reported in Reid et al. (2004, 2007) and Cruz et al. (2007) for the latest M-dwarf types (M7-10). Table 9 lists the local densities as a function of M-dwarf type. We only note that both stay relatively constant with M-dwarf subtype.

Figure 27 shows the dependence of scale-height, z_0 with M-dwarf subtype. The progressive decline in scale-height with subtype is in part due to the different heights sampled. Early types are a mix of thin and thick disk while later types were only found in the thin disk.

Bovy et al. (2012) argue that the different metallicity (and hence age) populations of the Milky Way all have their own distinct and unique scale-length and -height. They find that older populations are more concentrated (shorter scale-length) but the most vertically distributed (greatest scale-height). Similar results were found by Bensby et al. (2011) (using a thin/thick disk terminology) and Cheng et al. (2012). The trend between scale-height and M-dwarf subtype in Figure 27 fits with this general picture that there are not distinct thick and thin disks but a gradual transition in scales with stellar population. Because the majority of our fields are high Galactic latitude, we lack the statistics to perform

a double fit (vertical and radial). We note however, that our use of the Bensby et al. (2011) thick- and thin-disk scale-lengths improved the vertical fits substantially over a single scale-length solution.

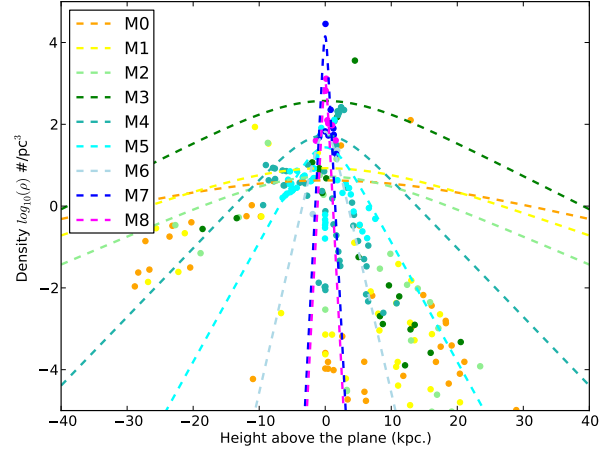


Figure 25. The volume density of M-dwarfs as a function as height above the plane of the Milky Way disk. Points are grayscaled by the M-dwarf sub-type with best fits shown for each M-dwarf type.

Table 10
The vertical profile fits to the full sample of identified M-dwarfs.

M-type (\circ)	ρ_0 (#/ pc^3)	z_0 (kpc)
0	4.25	22.85 ± 32.92
1	8.44	15.50 ± 14.33
2	5.29	12.62 ± 9.22
3	373.12	10.69 ± 14.41
4	53.93	-5.17 ± 2.74
5	27.27	2.97 ± 1.39
6	65.78	1.24 ± 0.42
7	14185.51	0.28 ± 0.41
8	1066.36	0.28 ± 0.12

There are several “spurs” of stars in the height-density plot of Figure 25. To investigate if these correspond to specific areas in the Milky Way, we replot the height-density plot for all M-dwarfs, coded with the Galactic position in Figure 28. Substructures become visible as a function of Galactic Longitude. For example, the upturn in M-dwarfs at 0 to -10 kpc above the plane is due to a few fields near $l \geq 310^\circ$ and $b = -40^\circ$. The Longitude position strongly suggests the Milky Way Bulge as the origin of the additional M-dwarfs but the Latitude is quite low for much of the effect of the Galactic bulge.

To characterize the different scale-heights implied by the spurs in Figure 28, we selected Galactic longitude or latitude sections for a sech^2 fit, summarized in Tables 11 and 12. The sech^2 fits to these cuts show an expected variety of z_0 values. Given the vertical extent that the observations probe, contributions from stellar halo components are likely included (similar to the Sagittarius

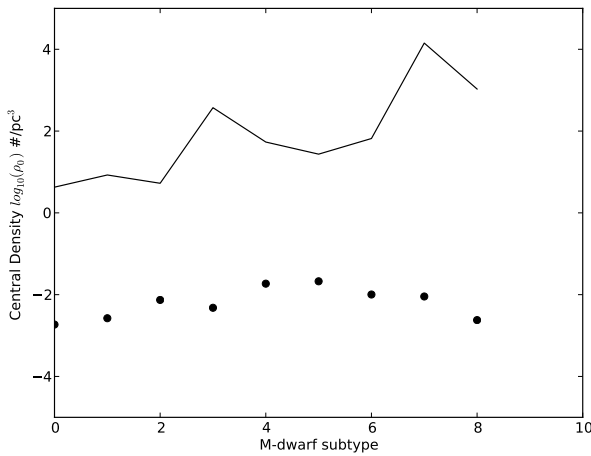


Figure 26. The central density of the best fit as a function of the M-dwarf type. The black circles are the values from Reid et al. (2008).

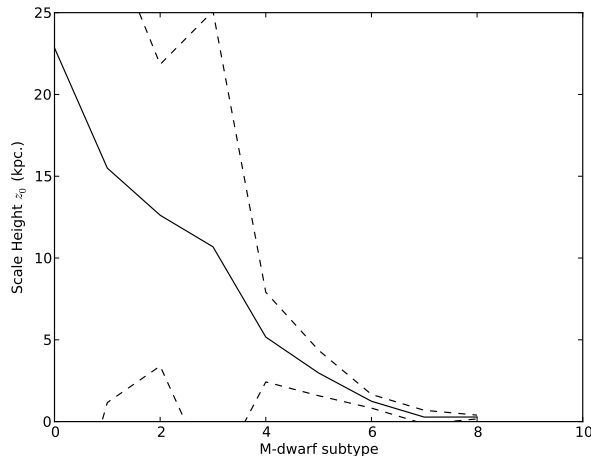


Figure 27. The scale-height of the best fit as a function of the M-dwarf type. Dashed lines are the uncertainty in the fit.

stream in §6.2). For example, the spur of stars at 20 kpc at $l = -75^\circ$ and $b = -75^\circ$ (yellow and red points in Figure 28 left and right panel respectively) is at a higher density than one would expect from the different Latitude observations at $l = 120^\circ$ (green point in Figure 28, left panel). However, that spur is the result of a single field and this may be simple cosmic variance in our counts. To reliably detect halo substructure or even typical scales, using M-dwarfs, one needs to image a much greater area of sky continuously (i.e., with EUCLID).

6.5. L and T Dwarfs

We do find a number of stellar objects in the L and T color selection criteria from Ryan et al. (2011). There is one object, brighter than 24 mag in $F125W$ in these fields that fall into the T-dwarf box. This is not the sole T-dwarf identified by Ryan et al. (2011) which is a 25.08 mag object. Table ?? lists the properties of the single $m < 24$ T-dwarf stars in BoRG. The color-color selection

Table 11
The fits to selected Galactic Latitude cuts.

b ($^\circ$)	ρ_0 (#/pc 3)	z_0 (kpc)
-75.00	140.03	0.77 ± 0.00
-55.00	60.60	2.14 ± 0.07
10.00	451455.50	0.02 ± 0.01
35.00	2394.64	0.19 ± 0.00
52.00	172.83	1.48 ± 0.27
60.00	25.13	1.98 ± 0.01

Table 12
The fits to selected Galactic Longitude cuts.

l ($^\circ$)	ρ_0 (#/pc 3)	z_0 (kpc)
310.00	6.45	6.68 ± 0.38
235.00	716.35	0.28 ± 0.00
75.00	12.64	32.24 ± 77.73
85.00	1921.33	0.54 ± 0.00
120.00	3875.14	0.13 ± 0.01
140.00	12.58	3.84 ± 3.12

also identifies 30 L-dwarfs in the BoRG survey. Table ?? lists their properties. Neither T nor L dwarfs have a reasonably well-calibrated relation between optical-near infrared color and sub-type (see e.g., Birmingham et al. 2013) to allow for a distance estimate similar to the M-dwarfs, nor do we have the statistics in hand to infer a scale-height for these objects.

Wilkins et al. (2014) reiterate that L and T-dwarfs pose a risk of contaminating high redshift ($z \sim 7$) color-selected samples and show how some dwarf spectra may even masquerade as objects with emission lines. They generated their color selections similar to Ryan et al. (2011) and the boxes in Figure 12 do generally agree with the derived colors. Wilkins et al. (2014) claim HST morphological information is insufficient to cull L- and T-dwarfs from a high-redshift galaxy sample. We have shown that dwarfs can be unequivocally identified by their stellar morphology using simple tools such as SEXTRACTOR down to 24. AB mag in *undithered* WFC3 data and a reliably star/galaxy separation is not only crucial for high-redshift studies but very likely possible down to much lower luminosities. The second issue is the surface density of these later dwarf types. For the first time, we can give an indication for random high-latitude, space-based observations based on the number of L-dwarfs found (Table ??). Figure 28 shows the surface density of L-dwarfs selected by our morphology and color criteria. It shows a WFC3 exposure has < 1 L-dwarf that can be selected against morphologically. Extrapolating to lower luminosities (including improved star/galaxy separation), the contamination problem may not be as dire as predicted. For example, Wilkins et al. (2014) assume that the local brown dwarf density (0.015 stars/pc 3) holds throughout all the Milky Way components (thin ad thick disks and halo). However, the spatial density drops exponentially with height above the plane. If L- and T-dwarfs follow a similar scale-height as the M-

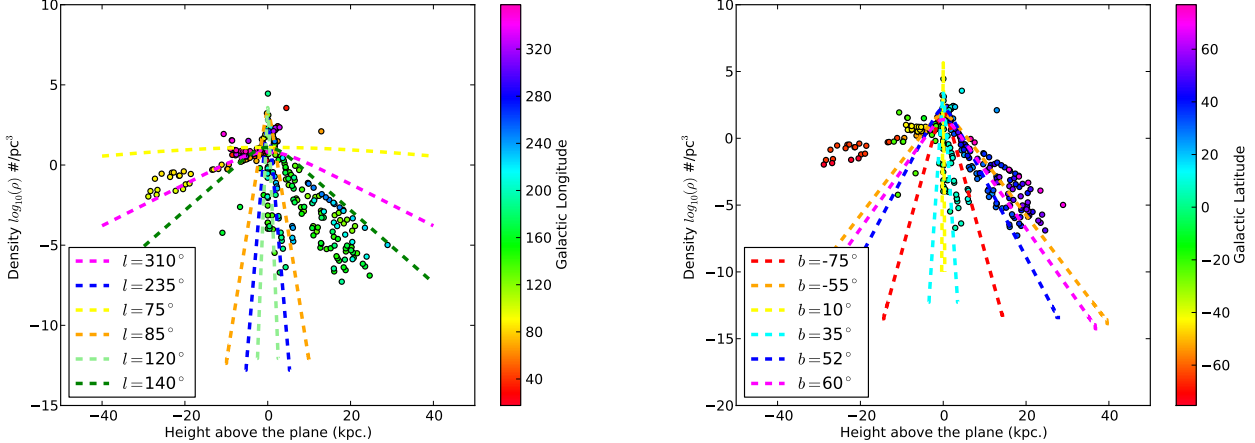


Figure 28. The volume density of M-dwarfs as a function as height above the plane of the Milky Way disk. Points are color-coded by the dwarf's Galactic Longitude (left) and Latitude (right panel).

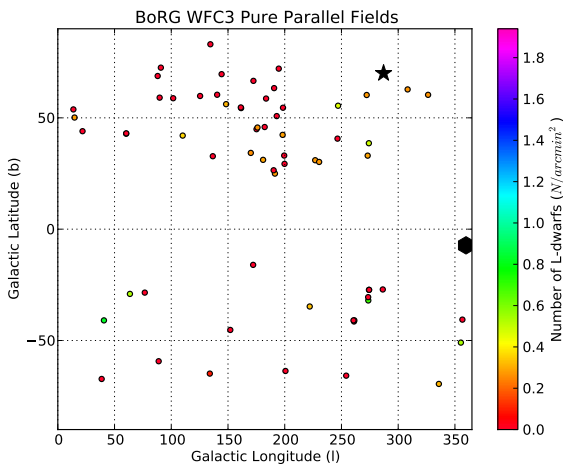


Figure 29. The distribution of BoRG fields with the number of L-dwarfs indicated. Other symbols identical to Figure 22.

dwarfs examined here ($z_0 \sim 300$ pc), then contaminating dwarf stars at 1-2 kpc distance will be very rare, even before morphological selection.

7. CONCLUSIONS

- Stars can be selected best using SExtractor's half-light radius (r_{50}), corroborating previous identifications (Figures 8 and 17).
- M-dwarfs can be reliably sub-typed using a near-infrared and optical color (Figure 14).
- Relatively more early-type M-dwarfs are identified in Northern fields as opposed to Southern Galactic ones. This confirms the dichotomy Pirzkal et al. (2009) noted (Table 8).
- We report an over-density in one of our fields, borg_1230+0750, consistent with the M-dwarf members of the Sagittarius stream at a distance of 20-25 kpc. (Figure 22).

- A naive, single-component fit of the vertical distribution of M-dwarfs shows a steady decline of scale-height, z_0 , with M-dwarf sub-type (Figure 27).
- The grouping of spurs of stars at different Galactic coordinates strongly hints at substructure in the Milky Way disk/halo of M-dwarfs (Figure 28).

8. FUTURE WORK

Future work with WFC3 (pure-parallel) programs on Milky Way Dwarfs will use the ever-increasing number of sight-lines available to build a comprehensive catalog of M,L and T dwarfs belonging to the thin and thick disks and stellar halo of our Milky Way. New pure-parallel observational programs with HST/WFC3 are needed to expand the number of sight-lines and improve statistics. At lower Galactic latitudes, this could easily be achieved with lower integration times than the BoRG or HIPPIES programs. Once such a proposed program is completed fully, the total tally of M-dwarfs should give a first idea of the size and shape of the Milky Way disks, thin and thick, and depending on the total statistics, the Galactic Halo.

In parallel, spectroscopic identification of Milky Way dwarf stars by the HST-3D near-infrared grism spectra (e.g., Brammer et al. 2012). The ongoing imaging and grism campaigns on the CANDELS fields (Koekemoer et al. 2011; Grogin et al. 2011) will improve the calibration of the photometric identifications of Galactic Dwarfs in the pure-parallel surveys as well as add additional statistics to the star counts.

The general technique of morphologically identifying stars in space-based imaging, identifying dwarfs from near-infrared colors and subsequently sub-type these using an optical-near-infrared color will be perfectly suited for the EUCLID mission (Laureijs et al. 2011). The wide-band optical filter can be used to morphologically identify the stars and the three near-infrared filters to hone in on the Galactic dwarfs. Finally, the optical-nir color and complementary grism spectroscopy can then be used to subtype these dwarfs. With the wide survey area to faint point source sensitivity (all-sky 24 mag, 26 mag in deep fields) the EUCLID mission will yield an accu-

rate measure of the shape and size of our Milky Way in sub-solar dwarfs as well as an accurate census of Halo substructure similar to the Sagittarius stream. Limiting factors may be the PSF in the near-infrared, leading to confusion issues and the width of the optical filter complicating subtyping. However, the two independent-angle grism spectra of all the objects in the field should unequivocally identify the Galactic dwarf stars.

Milky Way dwarfs are unlikely to be the focus of James Webb Space Telescope observations but they will certainly feature in them. The ubiquity of M-dwarfs in the BoRG fields points to their possible use as fine guidance for JWST image and NIRspec imaging/MOS registration.

The authors would like to thank N. Reid and K. Cruz for their help with the local density of M-dwarfs and R. Benjamin for useful discussions on Galactic substructures. The lead author thanks the European Space Agency for the Fellowship program and its support. We acknowledge the support of HST Archival grant number AR-12134, General Observer Grants GO-11700, GO-12572, and GO-12905 and the European Space Agency for support of this work. MT was partially supported by the European Commission through the Marie Curie Career Integration Fellowship PCIG12-GA-2012-333749" This work is based in part on observations taken by the CANDELS Multi-Cycle Treasury Program with the NASA/ESA HST, which is operated by the Association of Universities for Research in Astronomy, Inc., under NASA contract NAS5-26555. This research has made use of the NASA/IPAC Extragalactic Database (NED) which is operated by the Jet Propulsion Laboratory, California Institute of Technology, under contract with the National Aeronautics and Space Administration. This research has made use of NASA's Astrophysics Data System.

REFERENCES

- Astropy Collaboration, Robitaille, T. P., Tollerud, E. J., et al. 2013, *A&A*, 558, A33
- Bahcall, J. N. 1986, *ARA&A*, 24, 577
- Beckwith, S. V. W., Stiavelli, M., Koekemoer, A. M., et al. 2006, *AJ*, 132, 1729
- Belokurov, V., Zucker, D. B., Evans, N. W., et al. 2006, *ApJ*, 642, L137
- Belokurov, V., Koposov, S. E., Evans, N. W., et al. 2014, *MNRAS*, 437, 116
- Bensby, T., Alves-Brito, A., Oey, M. S., Yong, D., & Meléndez, J. 2011, *ApJ*, 735, L46
- Bertin, E., & Arnouts, S. 1996, *A&AS*, 117, 393, provided by the NASA Astrophysics Data System
- Bochanski, J. J., Willman, B., West, A. A., Strader, J., & Chomiuk, L. 2013, ArXiv e-prints/1310.7565, arXiv:1310.7565
- Bovy, J., Rix, H.-W., Liu, C., et al. 2012, *ApJ*, 753, 148
- Bradley, L. D., Trenti, M., Oesch, P. A., et al. 2012, *ApJ*, 760, 108
- Brammer, G. B., van Dokkum, P. G., Franx, M., et al. 2012, *ApJS*, 200, 13
- Burningham, B., Cardoso, C. V., Smith, L., et al. 2013, *MNRAS*, 433, 457
- Caballero, J. A., Burgasser, A. J., & Klement, R. 2008, *A&A*, 488, 181
- Casertano, S., de Mello, D., Dickinson, M., et al. 2000, *AJ*, 120, 2747
- Cheng, J. Y., Rockosi, C. M., Morrison, H. L., et al. 2012, *ApJ*, 752, 51
- Comerón, S., Knapen, J. H., Sheth, K., et al. 2011a, *ApJ*, 729, 18
- Comerón, S., Elmegreen, B. G., Knapen, J. H., et al. 2011b, *ApJ*, 738, L17
- . 2011c, *ApJ*, 741, 28
- Cruz, K. L., Reid, I. N., Kirkpatrick, J. D., et al. 2007, *AJ*, 133, 439
- Dressel, L., Wong, M. H., & Pavlovsky, C. 2010, in Wide Field Camera 3 Instrument Handbook, Version 3.0
- Fruchter, A. S., & Hook, R. N. 2002, *PASP*, 114, 144
- Giavalisco, M., Ferguson, H. C., Koekemoer, A. M., et al. 2004, *ApJ*, 600, L93
- Gilmore, G. 1984, *MNRAS*, 207, 223
- Gilmore, G., & Reid, N. 1983, *MNRAS*, 202, 1025
- Gilmore, G., Wyse, R. F. G., & Kuijken, K. 1989, *ARA&A*, 27, 555
- Grogan, N. A., Kocevski, D. D., Faber, S. M., et al. 2011, *ApJS*, 197, 35
- Hawley, S. L., Covey, K. R., Knapp, G. R., et al. 2002, *AJ*, 123, 3409
- Holwerda, B. W. 2005, astro-ph/0512139, astro-ph/0512139
- Holwerda, B. W., González, R. A., Allen, R. J., & van der Kruit, P. C. 2005, *AJ*, 129, 1396
- Holwerda, B. W., Trenti, M., Clarkson, W., et al. 2014, *ApJ*, 788, 77
- Hunter, J. D. 2007, Computing In Science & Engineering, 9, 90
- Jones, E., Oliphant, T., Peterson, P., & Others. 2001, SciPy: Open source scientific tools for Python
- Jurić, M., Ivezić, Ž., Brooks, A., et al. 2008, *ApJ*, 673, 864
- Kapteyn, J. C. 1922, *ApJ*, 55, 302
- Kilic, M., Mendez, R. A., von Hippel, T., & Winget, D. E. 2005, *ApJ*, 633, 1126
- King, I., Gilmore, G., & van der Kruit, P. C., eds. 1990, The Milky Way As Galaxy
- Koekemoer, A. M., Faber, S. M., Ferguson, H. C., et al. 2011, *ApJS*, 197, 36
- Laureijs, R., Amiaux, J., Arduini, S., et al. 2011, ArXiv e-prints, arXiv:1110.3193
- Leauthaud, A., Massey, R., Kneib, J., et al. 2007, *ApJS*, 172, 219
- Majewski, S. R. 1993, *ARA&A*, 31, 575
- Majewski, S. R., Skrutskie, M. F., Weinberg, M. D., & Ostheimer, J. C. 2003, *ApJ*, 599, 1082
- Newberg, H. J., Yanny, B., Rockosi, C., et al. 2002, *ApJ*, 569, 245
- Pirzkal, N., Xu, C., Malhotra, S., et al. 2004, *ApJS*, 154, 501
- Pirzkal, N., Sahu, K. C., Burgasser, A., et al. 2005, *ApJ*, 622, 319
- Pirzkal, N., Burgasser, A. J., Malhotra, S., et al. 2009, *ApJ*, 695, 1591
- Reid, I. N., Cruz, K. L., & Allen, P. R. 2007, *AJ*, 133, 2825
- Reid, I. N., Cruz, K. L., Kirkpatrick, J. D., et al. 2008, *AJ*, 136, 1290
- Reid, I. N., Cruz, K. L., Allen, P., et al. 2004, *AJ*, 128, 463
- Ryan, R. E., Thorman, P. A., Yan, H., et al. 2011, *ApJ*, 739, 83
- Ryan, Jr., R. E., Hathi, N. P., Cohen, S. H., & Windhorst, R. A. 2005, *ApJ*, 631, L159
- Ryan, Jr., R. E., & Reid, I. N. 2015, ArXiv e-prints, arXiv:1510.05019
- Siegel, M. H., Majewski, S. R., Reid, I. N., & Thompson, I. B. 2002, *ApJ*, 578, 151
- Stanway, E. R., Bremer, M. N., Lehnert, M. D., & Eldridge, J. J. 2008, *MNRAS*, 384, 348
- Steidel, C. C., Giavalisco, M., Dickinson, M., & Adelberger, K. L. 1996, *AJ*, 112, 352
- Trenti, M., & Stiavelli, M. 2008, *ApJ*, 676, 767
- Trenti, M., Bradley, L. D., Stiavelli, M., et al. 2011, *ApJ*, 727, L39
- . 2012, *ApJ*, 746, 55
- van Dokkum, P. G. 2001, *PASP*, 113, 1420
- Widrow, L. M., Gardner, S., Yanny, B., Dodelson, S., & Chen, H.-Y. 2012, *ApJ*, 750, L41
- Wilkins, S. M., Stanway, E. R., & Bremer, M. N. 2014, *MNRAS*, 439, 1038
- Windhorst, R. A., Cohen, S. H., Hathi, N. P., et al. 2011, *ApJS*, 193, 27
- Yan, H., Yan, L., Zamojski, M. A., et al. 2010, ArXiv e-prints, arXiv:1010.2261
- Yanny, B., & Gardner, S. 2013, ArXiv e-prints, arXiv:1309.2300
- Zheng, Z., Flynn, C., Gould, A., Bahcall, J. N., & Salim, S. 2001, *ApJ*, 555, 393

ERRATUM: “Milky Way Red Dwarfs in the BoRG Survey; Galactic scale-height and the distribution of dwarfs stars in WFC3 imaging” (2014, ApJ, 788, 77)

ABSTRACT

In the catalog of M-dwarfs presented in Holwerda et al. (2014), there is an issue with the conversion from celestial coordinates to Galactic ones, done with PYEPEM a wrapper around a trusted and vetted library *ephemis*. Here we present the corrected coordinates (using ASTROPY) and distances based on AB magnitudes. We have amended the tables and Figures accordingly. The relation between vertical scale-height (z_0) and M-dwarf subtype found in H14 is no longer present. We find a scale-height of 600 pc for all types, in part due to the presence of a second Galactic structural component.

9. MAPPING THE M-DWARF DISTRIBUTION

We re-computed the Galactic coordinates for the BoRG fields using the ASTROPY package (Astropy Collaboration et al. 2013) and the number of M-dwarfs in each, shown in the new Figure 22. To estimate the distances to each M-dwarf, we compute the distance modulus from the inferred sub-type (and hence absolute magnitude) and the apparent magnitude in J_{F125W} from Hawley et al. (2002), converted from Vega magnitudes to AB. We compute the Galactic radius and height above the plane for all M-dwarfs, based on their Galactic longitude, latitude and the inferred photometric distances, assuming the position of the Sun 27 pc. above the plane and 8.5 kpc from the Galactic center.

The net difference with H14 is that the vertical distribution observed for these M-dwarfs is much closer to the exponential drop-off one would expect for fields out of the plane of the Galaxy.

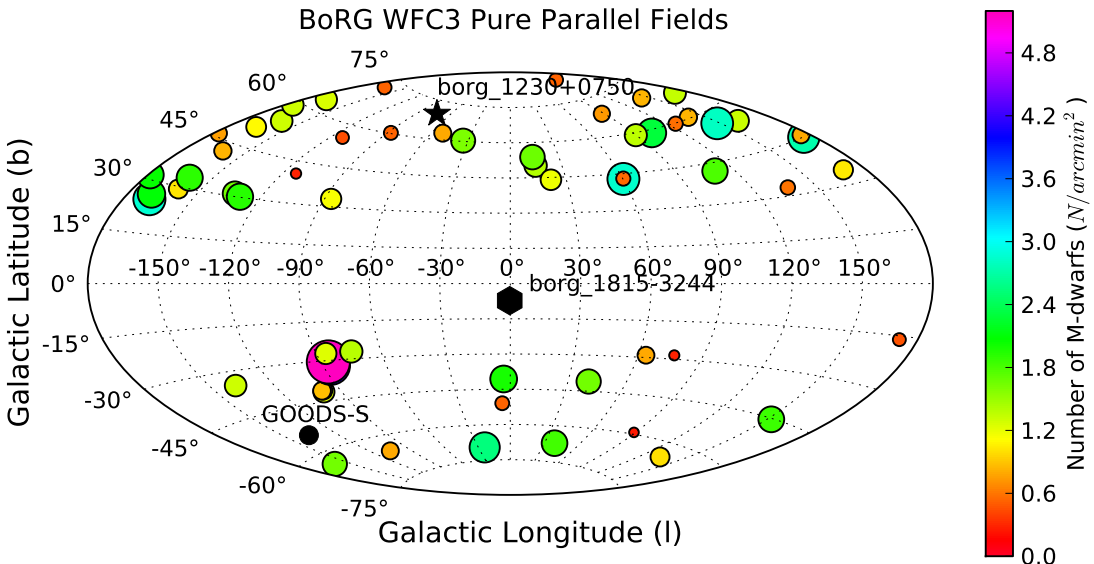


Figure 22. The Aitoff projection of the distribution of BoRG fields with the surface density of M-dwarfs of all types indicated. One field, borg_1230+0750 (star) stands out with 22 M-dwarfs (~ 20 stars/arcmin 2). We discard borg_1815-3244 (black circle) for its low latitudes and line-of-sight through the plane of the disk and close of the center of the bulge.

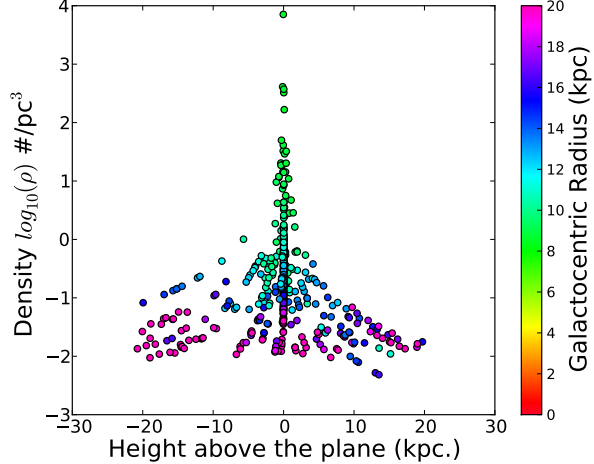


Figure 24. The volume density of M-dwarfs as a function as height above the plane of the Milky Way disk. The volume densities were normalized with a scale-length of 2.6 kpc and a depth of 1pc at each star's position. Points are color-coded by the inferred Galactic radius. The majority of M-dwarfs are found close to the plane of the disk.

Figure 24 shows the vertical distribution of M-dwarfs color-coded by their Galactocentric radius. There is a clear disk component with all the M-dwarfs are $\sim 6 - 10$ kpc from the center of the Milky Way and another component which shows a gradient with radius and is well above the plane of the disk. We now know this component to be the Halo part of the vertical distribution (van Vledder et al *accepted*) but it is sometimes treated as the thick disk by other authors (e.g., Ryan & Reid 2015). This second component is much clearer in the corrected Galactic positions compared to H14. The majority of stars close to the plane of the disk are ~ 8 kpc from the center of the Galaxy. This is because the majority of BoRG fields are pointing out of the disk at an angle away from the Galactic Center (to avoid confusion with Galactic Objects) and thus probe the vertical extent of the disk close to the position of the Sun.

We assume there is no need to correct the densities in this part of the disk for the exponential decline with radius. Figure 24 does show a radial dependence of the outer parts of the vertical distribution on the radius. Our assumption is that the scale-height does not change significantly with radius, which is observed in external galaxies seen edge-on (Comerón et al. 2011a,b,c, Streich et al *in preparation*).

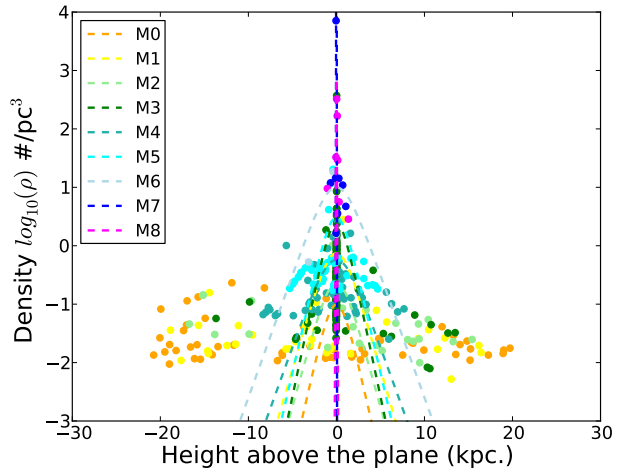


Figure 25. The volume density of M-dwarfs as a function as height above the plane of the Milky Way disk. Points and fits are color-coded by the M-dwarf sub-type.

We assume that the Galactic disk has the following parametric shape:

$$\rho(R, z) = \rho_0 \exp(-R/h) \operatorname{sech}^2\left(\frac{z}{2 \times z_0}\right), \quad (6)$$

where $\rho(R, z)$ is the dwarf number density in a point in the disk, ρ_0 is the central number density, R is Galactocentric

radius, h is the scale-length, z is height above the plane, and z_0 is the exponential scale-height of the disk. Figure 25 shows how the later-type M-dwarfs (M4-8) in the BoRG fields are concentrated in the thin disk and the earlier types (M0-3) probe both thin disk and the other component. We fit the sech^2 distribution to each photometric subtype, as well as early-, late- and all-types of M-dwarfs, summarized in the new Table 10 and the new Figures 26 and 27.

Figures 26 and 27 are significantly different from the versions in H14 in two ways: the relation between vertical scale-height (z_0) and M-dwarf subtype found in H14 is no longer present in Figure 27. Secondly, the densities inferred are much closer to the local (< 20 pc of the Sun) Reid et al. (2004) and Cruz et al. (2007) values (Figure 26). We note there is an offset of ~ 0.1 dex between our central density and the one implied by Reid et al. The likely culprit is the additional numbers of M-dwarfs in the secondary component well above the plane of the disk, i.e., we are including the density of Halo stars in our disk fit. A 0.1 dex offset suggest of order 10% of the stars in are, in fact, Halo stars (see also van Vledder et al. accepted).

The values in Figure 27 and Table 10 are still too high to be consistent with previous work on the vertical scale of stars in the thin disk. The vertical sech^2 profile does not describe the density distribution well above $\sim 500\text{pc}$ and this new distributions highlights the need to include another component well above and in addition to the disk.

Table 10

The vertical profile fits to the full sample of identified M-dwarfs. Values are scaled so to be compatible with exponential fits to the Galactic profiles ($\rho_0/4$ and $z_0/2$).

M-type (\circ)	ρ_0 (#/pc 3)	z_0 (kpc)
0	0.02	0.67 ± 0.73
1	0.19	0.84 ± 0.89
2	0.06	0.80 ± 1.31
3	0.60	0.61 ± 12.36
4	0.14	1.04 ± 0.67
5	0.77	0.67 ± 0.74
6	2.49	1.03 ± 5.42
7
8	181.04	-0.01 ± 0.02

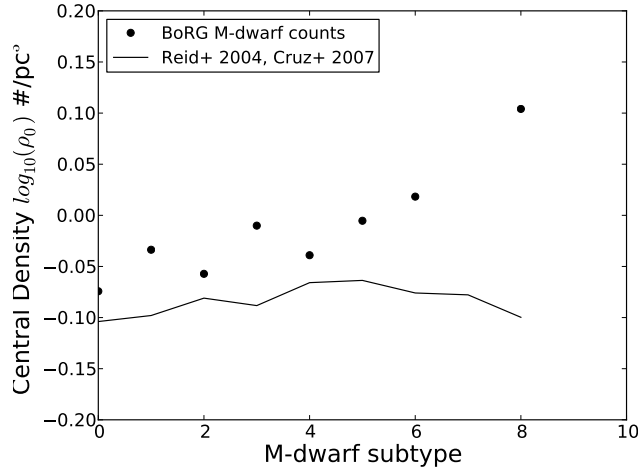


Figure 26. The in-plane central density – the number of M-dwarfs belonging to the disk at the center of the Milky Way – for the best fit to the vertical distribution of M-dwarfs as a function of the M-dwarf subtype. The black circles are the values from Reid et al. (2008) for the immediate Solar neighborhood (< 20 pc), renormalized to the center of the Milky Way.

For completeness, we include Figure 28 which shows the surface density of L-dwarfs selected by our morphology and color criteria.

10. CONCLUSIONS

The majority of conclusions for Holwerda et al. (2014) remain the same, only the last two change:

- The secondary component visible in the vertical distribution of M-dwarfs is likely the Halo and not the thick disk of the Milky Way (Figures 24 and 25).

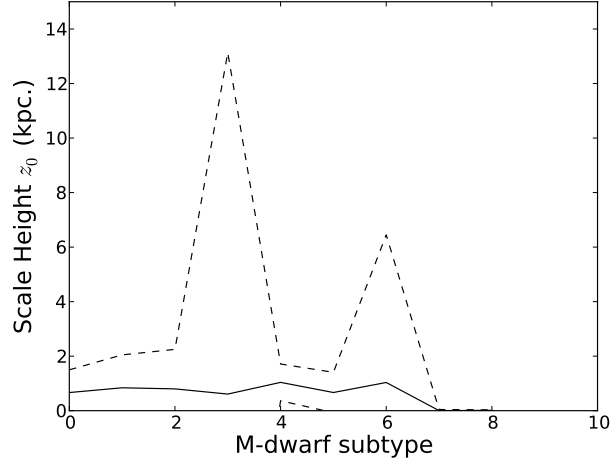


Figure 27. The scale-height ($z_0/2$) of the best vertical fit as a function of the M-dwarf subtype. Dashed lines are the uncertainty in the fit. A constant value of 600 pc would be consistent with most of these fits. This is $\sim 10\times$ greater than expected from previous work.

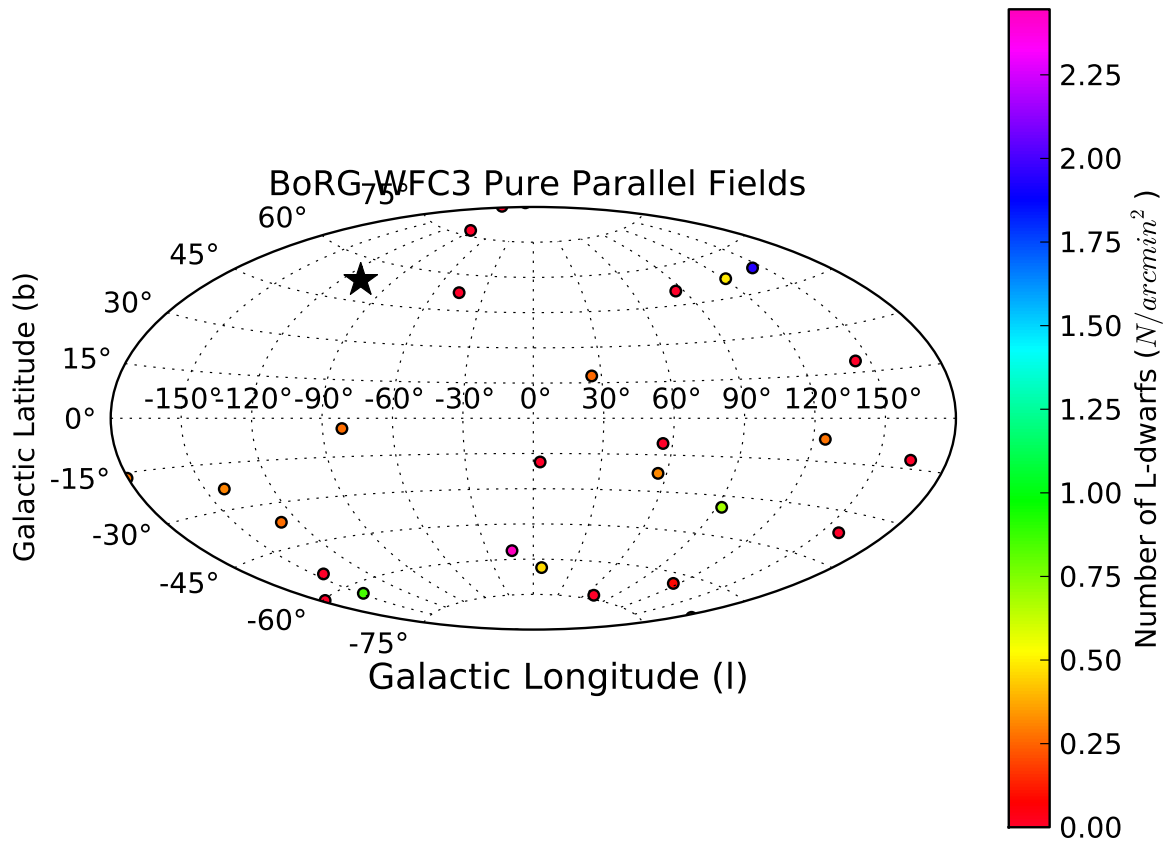


Figure 28. The distribution of BoRG fields with the number of L-dwarfs indicated. Other symbols identical to Figure 22.

- A naive, single-component fit of the vertical distribution of M-dwarfs shows no dependence on M-dwarf subtype and a scale-height for all M-dwarf subtypes that is still too high to be consistent with previous measures of the scale-height: $z_0 \sim 600$ pc, (Figure 27), a result of the second structural component.

The authors would like to thank the referee, K. Cruz for her help with the erratum. This research made use of Astropy, a community-developed core Python package for Astronomy (Astropy Collaboration et al. 2013). This research made use of matplotlib, a Python library for publication quality graphics (Hunter 2007). PyRAF is a product of the Space Telescope Science Institute, which is operated by AURA for NASA. This research made use of SciPy (Jones et al. 2001).

Table 10

The M-dwarfs found in the BoRG13 data with photometry, corrected Galactic coordinates and positions

Field	RA	DEC	J2000	m_{F098W}			m_{F125W}			m_{F160W}			m_{F125W}			m_{F098W}			m_{F125W}			m_{F160W}				
				α	δ	\circ	α	δ	\circ	α	δ	\circ	α	δ	\circ	α	δ	\circ	α	δ	\circ	α	δ	\circ		
Volume	Area	arcmin 2																								
borg	0110-0224.551	-2.418265	133.918256	-64.593095	23.82	± 0.04	23.46	± 0.02	23.28	± 0.03	25.17	± 0.09	2.04	± 0.32	15.59	13.10	± 1.22	9.47	14.06	100.63	10.88	10.88	10.88	10.88		
borg	0110-0224.719	17.503556	-2.415663	133.921454	-64.590220	24.33	± 0.05	23.97	± 0.03	23.87	± 0.04	25.83	± 0.14	14.71	± 1.81	10.62	14.74	126.76	10.88	10.88	10.88	10.88				
borg	0110-0224.820	17.553100	-2.4111389	133.921421	-64.5881654	19.68	± 0.00	19.51	± 0.00	19.45	± 0.00	22.77	± 0.01	7.30	± 0.04	1.30	± 0.46	16.29	18.10	± 2.55	13.54	16.18	191.93	10.88	10.88	
borg	0110-0224.916	17.553100	-2.4007883	134.033565	-64.5876102	24.08	± 0.09	23.90	± 0.04	25.39	± 0.13	24.40	± 0.05	1.43	± 0.27	16.37	18.79	± 45.62	13.53	16.48	206.91	10.88	10.88	10.88		
borg	0110-0224.916	17.553100	-2.4007883	134.044244	-64.5860685	24.08	± 0.09	23.71	± 0.06	23.44	± 0.04	25.76	± 0.05	2.51	± 0.60	15.78	14.33	± 2.02	10.33	14.59	120.39	10.88	10.88	10.88		
borg	0110-0224.916	17.553100	-2.4007883	134.054731	-64.5862858	24.22	± 0.13	23.91	± 0.04	23.78	± 0.05	24.41	± 0.04	2.82	± 0.14	14.34	17.37	± 0.58	5.33	11.63	31.85	10.88	10.88	10.88		
borg	0110-0224.916	17.553100	-2.381891	133.938981	-64.5877116	22.47	± 0.01	22.44	± 0.02	23.51	± 0.02	23.71	± 0.02	23.50	± 0.02	23.71	± 0.02	3.26	± 0.10	12.68	13.05	14.04	1.94	11.37	3.38	
borg	0110-0224.916	17.553100	-2.381891	133.937294	-64.5854348	24.25	± 0.05	23.57	± 0.02	23.49	± 0.02	23.68	± 0.07	14.57	18.19	± 0.45	5.92	11.98	39.28	10.88	10.88	10.88	10.88			
borg	0110-0224.916	17.553100	-2.381891	133.943112	-64.5830879	22.33	± 0.04	22.18	± 0.01	21.90	± 0.01	23.49	± 0.02	23.49	± 0.02	23.49	± 0.02	23.49	± 0.02	14.57	18.19	± 0.45	5.92	11.98	39.28	
borg	0110-0224.916	17.553100	-2.381891	133.953995	-64.5824003	24.35	± 0.08	23.81	± 0.02	23.54	± 0.03	24.10	± 0.21	4.00	± 0.73	14.58	18.23	± 4.25	5.95	12.00	39.68	10.88	10.88	10.88		
borg	0110-0224.916	17.553100	-2.381891	133.954212	-64.5817676	21.52	± 0.01	21.20	± 0.00	20.94	± 0.00	23.00	± 0.02	2.32	± 0.07	13.33	14.64	± 0.18	3.36	10.17	12.60	10.88	10.88	10.88		
borg	0110-0224.916	17.553100	-2.381891	133.954212	-64.5817676	23.38	± 0.04	23.19	± 0.04	22.97	± 0.07	25.36	± 0.91	3.59	± 3.10	13.96	16.19	± 6.41	2.93	12.85	7.76	10.88	10.88	10.88		
borg	0110-0224.916	17.553100	-2.381891	133.954212	-64.5817676	23.75	± 0.06	23.47	± 0.05	23.51	± 0.06	25.90	± 0.94	4.44	± 3.18	14.24	17.06	± 7.26	3.34	13.47	10.12	10.12	10.12	10.88		
borg	0110-0224.916	17.553100	-2.381891	133.954212	-64.5817676	22.73	± 0.03	22.28	± 0.02	22.13	± 0.02	22.52	± 0.91	3.82	± 3.06	13.05	14.04	± 3.97	1.94	11.37	3.38	10.88	10.88	10.88		
borg	0110-0224.916	17.553100	-2.381891	133.954212	-64.5817676	22.98	± 0.02	22.84	± 0.02	22.82	± 0.02	25.38	± 0.90	4.84	± 3.06	12.51	18.18	± 3.06	3.03	9.80	2.03	3.71	3.71	10.88		
borg	0110-0224.916	17.553100	-2.381891	133.954212	-64.5817676	23.17	± 0.04	23.00	± 0.03	22.88	± 0.03	25.27	± 0.91	3.92	± 3.10	13.77	18.68	± 5.54	2.69	12.50	5.65	3.77	3.77	10.88		
borg	0110-0224.916	17.553100	-2.381891	133.954212	-64.5817676	23.99	± 0.07	23.74	± 0.06	23.46	± 0.05	25.85	± 0.93	3.39	± 3.16	15.61	13.26	± 13.80	6.25	17.83	35.66	10.88	10.88	10.88		
borg	0110-0224.916	17.553100	-2.381891	133.954212	-64.5817676	23.73	± 0.05	23.48	± 0.04	23.38	± 0.05	24.77	± 0.92	4.01	± 3.14	14.25	17.08	± 6.91	3.35	13.48	10.17	10.17	10.17	10.88		
borg	0110-0224.916	17.553100	-2.381891	133.954212	-64.5817676	22.11	± 0.02	21.73	± 0.01	21.45	± 0.01	23.84	± 0.89	3.38	± 3.02	13.60	15.24	± 4.52	2.49	12.19	5.58	3.77	3.77	10.88		
borg	0110-0224.916	17.553100	-2.381891	133.954212	-64.5817676	23.83	± 0.03	23.71	± 0.03	23.44	± 0.04	26.00	± 0.92	4.20	± 3.11	14.48	17.88	± 7.69	1.76	12.44	10.12	10.12	10.12	10.88		
borg	0110-0224.916	17.553100	-2.381891	133.954212	-64.5817676	22.73	± 0.03	22.58	± 0.02	22.13	± 0.02	22.52	± 0.91	3.82	± 3.06	13.05	14.04	± 3.97	1.94	11.37	3.38	3.77	3.77	10.88		
borg	0110-0224.916	17.553100	-2.381891	133.954212	-64.5817676	23.17	± 0.04	23.00	± 0.03	22.88	± 0.03	23.71	± 0.04	23.49	± 0.03	23.49	± 0.03	23.49	± 0.03	14.57	18.68	± 5.54	2.69	12.50	5.65	
borg	0110-0224.916	17.553100	-2.381891	133.954212	-64.5817676	23.99	± 0.07	23.74	± 0.06	23.46	± 0.05	25.85	± 0.93	3.94	± 3.12	14.69	18.69	± 8.90	3.35	13.48	10.17	10.17	10.17	10.88		
borg	0110-0224.916	17.553100	-2.381891	133.954212	-64.5817676	23.09	± 0.03	22.83	± 0.02	22.56	± 0.02	23.07	± 0.03	26.01	± 0.91	4.26	± 3.07	14.00	17.88	± 8.90	3.35	13.48	10.17	10.17	10.17	10.88
borg	0110-0224.916	17.553100	-2.381891	133.954212	-64.5817676	23.98	± 0.04	23.73	± 0.03	23.56	± 0.03	25.60	± 0.91	4.26	± 3.07	14.00	17.88	± 8.90	3.35	13.48	10.17	10.17	10.17	10.88		
borg	0110-0224.916	17.553100	-2.381891	133.954212	-64.5817676	23.09	± 0.02	22.83	± 0.01	22.56	± 0.01	23.07	± 0.02	26.01	± 0.91	4.26	± 3.07	14.00	17.88	± 8.90	3.35	13.48	10.17	10.17	10.17	10.88
borg	0110-0224.916	17.553100	-2.381891	133.954212	-64.5817676	23.98	± 0.05	23.73	± 0.04	23.56	± 0.05	25.60	± 0.91	4.26	± 3.07	14.00	17.88	± 8.90	3.35	13.48	10.17	10.17	10.17	10.88		
borg	0110-0224.916	17.553100	-2.381891	133.954212	-64.5817676	23.09	± 0.03	22.83	± 0.02	22.56	± 0.02	23.07	± 0.03	26.01	± 0.91	4.26	± 3.07	14.00	17.88	± 8.90	3.35	13.48	10.17	10.17	10.17	10.88
borg	0110-0224.916	17.553100	-2.381891	133.954212	-64.5817676	23.98	± 0.07	23.73	± 0.06	23.56	± 0.05	25.60	± 0.91	4.26	± 3.07	14.00	17.88	± 8.90	3.35	13.48	10.17	10.17	10.17	10.88		
borg	0110-0224.916	17.553100	-2.381891	133.954212	-64.5817676	23.09	± 0.05	22.83	± 0.04	22.56	± 0.04	23.07	± 0.05	26.01	± 0.91	4.26	± 3.07	14.00	17.88	± 8.90	3.35	13.48	10.17	10.17	10.17	10.88
borg	0110-0224.916	17.553100	-2.381891	133.954212	-64.5817676	23.98	± 0.03	23.73	± 0.02	23.56	± 0.03	25.60	± 0.91	4.26	± 3.07	14.00	17.88	± 8.90	3.35	13.48	10.17	10.17	10.17	10.88		
borg	0110-0224.916	17.553100	-2.381891	133.954212	-64.5817676	23.09	± 0.01	22.83	± 0.00	22.56	± 0.01	23.07	± 0.02	26.01	± 0.91	4.26	± 3.07	14.00	17.88	± 8.90	3.35	13.48	10.17	10.17	10.17	10.88
borg	0110-0224.916	17.553100	-2.381891	133.954212	-64.5817676	23.98	± 0.05	23.73	± 0.04	23.56	± 0.05	25.60	± 0.91	4.26	± 3.07	14.00	17.88	± 8.90	3.35	13.48	10.17	10.17	10.17	10.88		
borg	0110-0224.916	17.553100	-2.381891	133.954212	-64.5817676	23.09	± 0.03	22.83	± 0.02	22.56	± 0.02	23.07	± 0.03	26.01	± 0.91	4.26	± 3.07	14.00	17.88	± 8.90	3.35	13.48	10.17	10.17	10.17	10.88
borg	0110-0224.916	17.553100	-2.381891	133.954212	-64.5817676	23.98	± 0.07	23.73	± 0.06	23.56	± 0.05	25.60	± 0.91	4.26	± 3.07	14.00	17.88	± 8.90	3.35	13.48	10.17	10.17	10.17	10.88		
borg	0110-0224.916	17.553100	-2.381891	133.954212	-64.5817676	23.09	± 0.05	22.83	± 0.04	22.56	± 0.04	23.07	± 0.05	26.01	± 0.91	4.26	± 3.07	14.00	17.88	± 8.90	3.35	13.48	10.17	10.17	10.17	10.88
borg	0110-0224.916	17.553100	-2.381891	133.954212	-64.5817676	23.98	± 0.03	23.73	± 0.02	23.56	± 0.03	25.60	± 0.91	4.26	± 3.07	14.00	17.88	± 8.90	3.35	13.48	10.17	10.17	10.17	10.88		
borg	0110-0224.916	17.553100	-2.381891	133.954212	-64.5817676	23.09	± 0.01	22.83	± 0.00	22.56	± 0.01	23.07	± 0.02	26.01	± 0.91	4.26	± 3.07	14.00	17.88	± 8.90	3.35	13.48	10.17	10.17	10.17	10.88
borg	0110-0224.916	17.553100	-2.381891	133.954212																						

Table 10
Table 10 – *continued*

Field	RA J2000	DEC J2000	<i>l</i>	<i>b</i>	<i>m</i> _{F098W}	<i>m</i> _{F125W}	<i>m</i> _{F606W}	<i>m</i> _{F125W}	<i>m</i> _{F606W}	M-type	M-m mag	Dist. kpc.	Radius kpc.	Volume kpc ²	Area arcmin ²
borg_0751+2917.46	117.702830	29.265557	191.372718	24.945643	20.53 ± 0.00	20.06 ± 0.00	19.91 ± 0.00	23.47 ± 0.04	7.79 ± 0.15	8.03	0.40 ± 0.01	-0.05	8.87	0.03	3.47
borg_-0751+2917.153	117.715195	29.272066	191.369734	24.961181	20.45 ± 0.00	20.10 ± 0.00	20.12 ± 0.00	23.77 ± 0.06	8.68 ± 0.19	7.78	0.36 ± 0.03	-0.04	8.83	0.02	3.47
borg_-0751+2917.271	117.695308	29.275292	191.360309	24.945472	20.92 ± 0.00	20.68 ± 0.00	20.43 ± 0.00	23.93 ± 0.03	3.87 ± 0.09	11.45	1.95 ± 0.08	-0.36	10.27	0.71	3.47
borg_-0751+2917.354	117.717431	29.277303	191.364861	24.964436	21.34 ± 0.00	20.93 ± 0.00	20.77 ± 0.00	24.78 ± 0.13	9.30 ± 0.45	8.61	0.53 ± 0.02	-0.08	8.98	0.05	3.47
borg_-0751+2917.464	117.698929	29.278551	191.357935	24.949517	23.40 ± 0.02	23.08 ± 0.01	23.01 ± 0.02	25.27 ± 0.14	3.67 ± 0.48	13.85	5.88 ± 1.56	-1.13	13.83	6.46	3.47
borg_-0751+2917.509	117.709001	29.280669	191.358778	24.955522	21.71 ± 0.01	21.56 ± 0.01	21.38 ± 0.01	26.96 ± 0.27	14.56 ± 0.40	11.67	3.47	3.47	
borg_-0751+2917.550	117.698802	29.281850	191.354548	24.950449	22.19 ± 0.01	21.86 ± 0.01	20.77 ± 0.28	11.90 ± 0.95	9.65	0.85 ± 0.07	-0.14	9.27	0.14	3.47	
borg_-0751+2917.1102	117.723347	29.281890	191.351388	24.973935	19.94 ± 0.00	19.66 ± 0.00	19.52 ± 0.00	21.48 ± 0.01	2.38 ± 0.03	11.79	2.28 ± 0.06	-0.42	10.57	0.97	3.47
borg_-0751+2917.1165	117.684941	29.289420	191.342313	24.941372	20.80 ± 0.01	20.69 ± 0.00	20.60 ± 0.01	20.59 ± 0.00	-4.12 ± 0.02	11.80	3.47	3.47	
borg_-0751+2917.1188	117.691430	29.285805	191.345168	24.946478	21.08 ± 0.00	21.73 ± 0.00	20.56 ± 0.00	23.81 ± 0.06	6.67 ± 0.21	8.92	0.61 ± 0.11	-0.09	9.05	0.07	3.47
borg_-0756+3043.50	118.698218	30.701126	190.223301	26.443911	23.87 ± 0.03	23.70 ± 0.03	23.47 ± 0.03	25.18 ± 0.10	1.18 ± 0.36	16.11	16.67 ± 2.13	-2.93	23.43	49.69	3.32
borg_-0756+3043.329	118.976165	30.715315	190.216272	26.442662	21.65 ± 0.01	21.47 ± 0.01	21.25 ± 0.01	22.61 ± 0.02	0.11 ± 0.06	14.13	6.69 ± 0.38	-1.16	14.49	7.99	3.32
borg_-0756+3043.330	118.987214	30.714753	190.220020	26.451567	23.38 ± 0.04	23.10 ± 0.03	23.00 ± 0.03	23.74 ± 0.03	-0.60 ± 0.14	12.21	3.32	3.32	
borg_-0756+3043.420	118.981397	30.718316	190.218316	26.455398	23.67 ± 0.03	23.51 ± 0.03	23.27 ± 0.04	24.71 ± 0.07	0.30 ± 0.25	16.17	17.11 ± 2.22	-3.01	23.82	52.31	3.32
borg_-0756+3043.458	118.982586	30.722844	190.210168	26.450168	20.92 ± 0.00	20.73 ± 0.04	20.57 ± 0.04	24.05 ± 0.04	-2.98 ± 0.17	12.19	3.32	3.32	
borg_-0756+3043.523	118.998415	30.724658	190.212647	26.463702	24.02 ± 0.04	23.61 ± 0.03	23.35 ± 0.03	25.60 ± 0.16	2.95 ± 0.57	15.48	12.50 ± 4.16	-2.19	19.69	27.94	3.32
borg_-0756+3043.550	119.006638	30.719813	190.220243	26.469261	23.96 ± 0.04	23.75 ± 0.04	23.65 ± 0.05	24.30 ± 0.05	-1.92 ± 0.22	12.86	3.32	3.32	
borg_-0808+3946.171	122.092545	39.748276	190.934209	31.129392	24.07 ± 0.05	23.97 ± 0.05	23.96 ± 0.07	24.95 ± 0.10	-0.44 ± 0.36	16.63	11.14 ± 2.96	-0.32	26.60	82.05	3.41
borg_-0808+3946.252	122.093443	39.751983	190.931138	31.135304	22.77 ± 0.02	22.42 ± 0.02	22.21 ± 0.02	25.42 ± 0.17	6.41 ± 0.57	11.35	1.86 ± 0.36	-0.00	10.09	0.64	3.41
borg_-0808+3946.306	122.072045	39.751872	190.732844	26.455398	23.67 ± 0.03	23.51 ± 0.03	23.27 ± 0.04	24.52 ± 0.07	-1.13 ± 0.28	16.40	19.04 ± 2.54	-0.28	24.80	66.57	3.41
borg_-0808+3946.456	122.070245	39.751872	190.721007	26.450168	24.09 ± 0.05	23.73 ± 0.04	23.47 ± 0.04	25.03 ± 0.11	0.63 ± 0.38	16.12	17.44 ± 2.43	-0.24	28.84	51.48	3.41
borg_-0808+3946.624	122.096390	39.765203	190.915453	31.135158	23.05 ± 0.02	22.72 ± 0.02	22.56 ± 0.02	23.50 ± 0.03	-1.11 ± 0.12	15.38	11.91 ± 1.05	-0.16	18.69	26.03	3.41
borg_-0808+3946.824	122.083062	39.771358	190.906115	31.126633	23.88 ± 0.04	23.63 ± 0.03	23.53 ± 0.04	24.75 ± 0.07	0.02 ± 0.26	16.29	18.12 ± 2.08	-0.26	24.01	60.25	3.41
borg_-0808+3946.715	122.095042	39.768585	190.915585	31.135138	17.79 ± 0.00	17.59 ± 0.00	17.46 ± 0.00	20.08 ± 0.01	8.07 ± 0.02	5.56	0.13 ± 0.02	0.02	8.61	0.00	3.41
borg_-0819+4911.137	124.335305	49.174426	170.110184	34.248170	23.89 ± 0.04	23.75 ± 0.04	23.57 ± 0.04	25.38 ± 0.06	1.75 ± 0.53	15.88	15.01 ± 2.10	0.61	20.91	46.77	3.85
borg_-0819+4911.213	124.808368	49.174256	170.105588	34.230505	23.89 ± 0.07	23.67 ± 0.04	23.58 ± 0.07	24.68 ± 0.09	-0.37 ± 0.32	16.33	18.46 ± 2.38	-3.20	23.77	70.76	3.85
borg_-0819+4911.739	124.816577	49.185192	170.082124	34.235148	23.17 ± 0.02	22.97 ± 0.02	22.56 ± 0.02	23.50 ± 0.03	1.62 ± 0.30	15.18	10.85 ± 1.26	1.89	17.43	24.43	3.85
borg_-0819+4911.958	124.813802	49.193857	170.082124	34.235148	23.73 ± 0.04	23.46 ± 0.03	23.30 ± 0.05	24.46 ± 0.07	0.32 ± 0.27	16.17	16.12 ± 1.98	2.92	22.36	58.37	3.85
borg_-0820+2332.116	125.019422	39.745656	29.324725	23.14 ± 0.03	22.74 ± 0.03	22.49 ± 0.03	22.49 ± 0.13	4.59 ± 0.44	12.41	3.03 ± 0.83	-1.00	11.14	1.94	3.93	
borg_-0820+2332.354	125.03777	39.533128	29.346125	24.22 ± 0.08	23.82 ± 0.08	23.66 ± 0.15	25.79 ± 0.18	2.91 ± 0.66	15.69	13.73 ± 4.96	-4.63	20.47	39.91	3.93	
borg_-0820+2332.680	125.015773	39.535305	29.332020	23.79 ± 0.04	23.56 ± 0.04	23.32 ± 0.04	23.58 ± 0.07	25.24 ± 0.12	15.93	1.93 ± 0.42	-0.43	20.47	39.91	3.93	
borg_-0820+2332.706	125.025405	39.535305	29.332020	23.79 ± 0.04	23.51 ± 0.03	22.51 ± 0.03	24.79 ± 0.09	3.17 ± 0.31	16.69	8.35 ± 0.88	-5.02	24.06	68.09	3.67	
borg_-0820+2332.728	128.835467	49.267868	199.547766	33.070920	22.98 ± 0.02	22.78 ± 0.02	22.60 ± 0.02	24.09 ± 0.05	0.68 ± 0.19	15.17	10.80 ± 1.13	-3.59	17.55	23.02	3.67
borg_-0820+2332.744	128.835467	49.267868	199.547766	33.070920	22.98 ± 0.02	22.78 ± 0.02	22.60 ± 0.02	24.08 ± 0.05	-1.88 ± 0.19	12.63	13.03 ± 4.96	-4.63	20.47	39.91	3.93
borg_-0820+2332.758	128.835467	49.267868	199.547766	33.070920	22.98 ± 0.02	22.78 ± 0.02	22.60 ± 0.02	24.08 ± 0.05	-1.88 ± 0.19	12.63	13.73 ± 4.96	-4.63	20.47	39.91	3.93
borg_-0820+2332.858	128.835467	49.267868	199.547766	33.070920	22.98 ± 0.02	22.78 ± 0.02	22.60 ± 0.02	24.08 ± 0.05	-1.88 ± 0.19	12.63	13.73 ± 4.96	-4.63	20.47	39.91	3.93
borg_-0820+2332.878	128.835467	49.267868	199.547766	33.070920	22.98 ± 0.02	22.78 ± 0.02	22.60 ± 0.02	24.08 ± 0.05	-1.88 ± 0.19	12.63	13.73 ± 4.96	-4.63	20.47	39.91	3.93
borg_-0825+2456.115	128.835467	49.267868	199.547766	33.070920	22.98 ± 0.02	22.78 ± 0.02	22.60 ± 0.02	24.08 ± 0.05	-1.88 ± 0.19	12.63	13.73 ± 4.96	-4.63	20.47	39.91	3.93
borg_-0825+2456.413	128.810038	49.267868	199.547766	33.070920	22.98 ± 0.02	22.78 ± 0.02	22.60 ± 0.02	24.08 ± 0.05	-1.88 ± 0.19	12.63	13.73 ± 4.96	-4.63	20.47	39.91	3.93
borg_-0825+2456.561	128.802913	49.267868	199.547766	33.070920	22.98 ± 0.02	22.78 ± 0.02	22.60 ± 0.02	24.08 ± 0.05	-1.88 ± 0.19	12.63	13.73 ± 4.96	-4.63	20.47	39.91	3.93
borg_-0825+2456.732	128.802913	49.267868	199.547766	33.070920	22.98 ± 0.02	22.78 ± 0.02	22.60 ± 0.02	24.08 ± 0.05	-1.88 ± 0.19	12.63	13.73 ± 4.96	-4.63	20.47	39.91	3.93
borg_-0906+0255.172	136.407801	22.640780	30.956620	23.82 ± 0.04	23.49 ± 0.04	23.36 ± 0.03	24.06 ± 0.04	1.84 ± 0.16	12.61	11.03	-0.47 ± 0.26	-0.26	22.26	53.62	
borg_-0906+0255.404	136.394485	22.640780	30.956620	23.82 ± 0.04	23.49 ± 0.04	23.36 ± 0.03	24.06 ± 0.04	1.84 ± 0.16	12.61	11.03	-0.47 ± 0.26	-0.26	22.26	53.62	
borg_-0906+0255.506	136.393392	22.640780	30.956620	23.82 ± 0.04	23.49 ± 0.04	23.36 ± 0.03	24.06 ± 0.04	1.84 ± 0.16	12.61	11.03	-0.47 ± 0.26	-0.26	22.26	53.62	
borg_-0906+0255.552	136.392213	22.640780	30.956620	23.82 ± 0.04	23.49 ± 0.04	23.36 ± 0.03	24.06 ± 0.04	1.84 ± 0.16	12.61	11.03	-0.47 ± 0.26	-0.26	22.26	53.62	
borg_-0906+0255.577	136.393625	22.640780	30.956620	23.82 ± 0.04	23.49 ± 0.04	23.36 ± 0.03	24.06 ± 0.04	1.84 ± 0.16	12.61	11.03	-0.47 ± 0.26	-0.26	22.26	53.62	
borg_-0906+0255.602	136.393625	22.640780	30.956620	23.82 ± 0.04	23.49 ± 0.04	23.36 ± 0.03	24.06 ± 0.04	1.84 ± 0.16	12.61	11.03	-0.47 ± 0.26	-0.26	22.26	53.62	
borg_-0906+0255.657	136.393625	22.640780	30.956620	23.82 ± 0.04	23.49 ± 0.04	23.36 ± 0.03	24.06 ± 0.04	1.84 ± 0.16	12.61	11.03	-0.47 ± 0.26	-0.26	22.26	53.62	
borg_-0906+0255.709	136.393625	22.6													

Table 10
Table 10 – *continued*

Table 10
Table 10 – *continued*

Field	RA J2000	DEC J2000	<i>l</i>	<i>b</i>	<i>m</i> _{F098W}	<i>m</i> _{F125W}	<i>m</i> _{F606W}	<i>m</i> _{F606W}	Type	M-m mag	Dist kpc.	Radius kpc.	Height kpc.	Volume kpc ²	Area arcmin ²
borg_1230+0750.4286	187.471959	7.820086	287.128967	70.0227773	22.49 ± 0.02	22.38 ± 0.03	22.28 ± 0.02	22.99 ± 0.02	-1.71 ± 0.11	120.49	0.52	
borg_-1230+0750.3901	187.447223	7.825443	287.055567	70.026957	23.52 ± 0.05	23.11 ± 0.10	22.83 ± 0.07	25.29 ± 0.14	3.62 ± 0.56	13.88	5.98 ± 1.93	-5.69	10.54	0.99	
borg_-1230+0750.4108	187.461291	7.827180	287.032062	70.0232062	24.15 ± 0.07	23.88 ± 0.05	23.81 ± 0.08	25.51 ± 0.15	1.75 ± 0.55	16.01	15.92 ± 2.61	-15.19	13.94	7.04	
borg_-1230+0750.4516	187.450540	7.827297	287.063559	70.029562	22.98 ± 0.03	22.82 ± 0.02	22.71 ± 0.03	23.71 ± 0.15	-0.73 ± 0.15	15.48	12.45 ± 1.26	-11.88	12.75	4.31	
borg_-1230+0750.5771	187.4787632	7.831401	287.139635	70.040361	24.14 ± 0.08	23.94 ± 0.06	23.89 ± 0.08	25.06 ± 0.16	0.02 ± 0.57	16.60	20.80 ± 3.55	-19.94	15.63	12.13	
borg_-1230+0750.7878	187.4842833	7.834039	287.153652	70.044287	24.13 ± 0.07	23.51 ± 0.04	23.36 ± 0.06	24.89 ± 0.09	0.93 ± 0.34	15.90	15.12 ± 2.05	-1.44	13.66	6.34	
borg_-1230+0751.644	190.541474	125.4283032	59.796557	70.0427912	24.09 ± 0.05	23.88 ± 0.06	23.68 ± 0.11	26.25 ± 0.99	4.28 ± 3.38	14.65	8.50 ± 8.76	6.96	12.78	3.48	
borg_-1242+5716.751	190.541474	125.4283032	59.8004040	70.0427912	24.27 ± 0.05	23.82 ± 0.07	23.78 ± 0.05	26.35 ± 0.93	4.80 ± 3.15	13.49	4.99 ± 4.86	4.09	11.01	4.67	
borg_-1245+3356.46	191.189394	33.921404	134.472249	83.056624	23.87 ± 0.03	23.73 ± 0.03	23.45 ± 0.04	24.68 ± 0.07	-0.54 ± 0.25	16.39	18.96 ± 2.22	13.56	10.79	3.75	
borg_-1246+2806.0	191.194944	33.921404	134.472249	83.037709	24.54 ± 0.07	23.97 ± 0.05	23.90 ± 0.07	24.86 ± 0.08	-0.78 ± 0.32	16.74	21.22 ± 2.94	15.18	10.95	3.75	
borg_-1301+0000.433	195.319541	-0.010028	308.312641	62.758786	24.18 ± 0.24	23.97 ± 0.11	23.86 ± 0.11	24.61 ± 0.98	4.50 ± 3.36	14.74	8.87 ± 9.20	-6.93	12.56	3.69	
borg_-1301+0000.856	195.317724	0.005917	308.311551	62.774829	24.13 ± 0.06	23.89 ± 0.06	23.78 ± 0.09	26.33 ± 0.96	4.49 ± 3.27	14.66	8.55 ± 8.81	-6.68	12.41	14.55	
borg_-1301+0000.922	195.318490	0.003289	308.312758	62.772147	23.62 ± 0.04	23.13 ± 0.03	23.08 ± 0.04	25.62 ± 0.92	4.69 ± 3.11	12.80	3.62 ± 3.49	-2.82	10.16	2.61	
borg_-1337+028.119	204.215604	-0.477434	326.357132	60.3232307	23.20 ± 0.06	23.06 ± 0.06	22.98 ± 0.03	25.51 ± 0.91	4.54 ± 3.08	13.52	3.52 ± 3.60	-1.92	10.24	2.47	
borg_-1337+028.242	204.190280	-0.474743	326.311337	60.3123078	23.02 ± 0.02	22.88 ± 0.02	22.85 ± 0.03	25.39 ± 0.91	4.74 ± 3.08	12.55	3.23 ± 3.11	-1.77	10.10	2.08	
borg_-1337+028.357	204.209496	-0.472242	326.3439407	60.318829	23.46 ± 0.03	23.26 ± 0.04	23.22 ± 0.05	25.76 ± 0.93	4.69 ± 3.16	12.93	3.86 ± 3.73	-2.11	10.41	2.98	
borg_-1337+028.816	204.215639	-0.4630774	326.367430	60.325255	24.10 ± 0.03	23.97 ± 0.04	23.73 ± 0.04	26.27 ± 0.92	4.02 ± 3.14	14.74	8.88 ± 8.67	-4.89	15.74	3.70	
borg_-1337+028.945	204.184943	326.311198	60.3382325	23.87 ± 0.03	23.73 ± 0.03	23.69 ± 0.04	26.22 ± 0.92	4.70 ± 3.13	13.40	4.78 ± 4.61	-6.62	10.86	4.55		
borg_-1337+028.1417	204.213879	-0.452933	326.371489	60.335337	23.81 ± 0.04	23.36 ± 0.03	23.32 ± 0.04	25.86 ± 0.91	4.69 ± 3.10	13.03	4.04 ± 3.89	-2.21	10.50	3.25	
borg_-1408+5503.460	211.965695	55.052371	101.703844	58.8112182	24.07 ± 0.03	23.68 ± 0.03	23.43 ± 0.03	25.73 ± 0.14	3.16 ± 0.48	15.55	12.91 ± 3.53	12.67	15.18	31.21	
borg_-1408+5503.545	212.001432	55.054457	101.673271	58.8001521	24.12 ± 0.11	23.87 ± 0.02	23.79 ± 0.06	24.43 ± 0.05	-0.18 ± 0.23	12.11	3.55 ± 3.60	-1.92	10.24	3.48	
borg_-1408+5503.557	211.951370	55.0595894	101.702555	58.815135	23.12 ± 0.02	23.00 ± 0.02	22.97 ± 0.02	23.99 ± 0.03	-0.41 ± 0.13	15.66	13.55 ± 1.11	13.30	15.52	3.40	
borg_-1408+5503.737	211.957353	55.059124	101.718628	58.810550	23.44 ± 0.03	23.24 ± 0.04	23.22 ± 0.13	24.11 ± 0.04	-0.83 ± 2.19	15.90	15.12 ± 3.68	14.84	16.33	42.83	
borg_-1408+5503.752	211.957353	55.0595552	101.707565	58.7857366	23.21 ± 0.02	22.91 ± 0.02	22.64 ± 0.02	24.81 ± 0.07	0.70 ± 0.29	16.09	16.51 ± 2.09	17.05	15.02	3.48	
borg_-1408+5503.922	212.010126	55.068508	101.6801266	58.785757	23.70 ± 0.03	23.66 ± 0.03	23.57 ± 0.03	24.91 ± 0.07	0.10 ± 0.26	16.43	19.31 ± 2.10	18.93	18.50	69.82	
borg_-1408+5503.977	211.965695	55.066386	101.719076	58.801926	23.94 ± 0.03	23.77 ± 0.03	23.70 ± 0.02	24.51 ± 0.07	0.61 ± 0.32	15.20	10.96 ± 1.21	10.75	14.17	22.47	
borg_-1408+5503.978	211.966709	55.0664490	101.715862	58.803087	23.72 ± 0.03	23.33 ± 0.02	23.09 ± 0.02	25.21 ± 0.09	0.61 ± 0.32	15.20	10.96 ± 1.21	10.75	14.17	3.48	
borg_-1408+5503.980	211.966709	55.0664490	101.715862	58.803087	23.79 ± 0.10	23.63 ± 0.05	23.54 ± 0.06	24.36 ± 0.08	0.80 ± 0.27	18.18	3.07 ± 0.60	3.10	10.08	3.64	
borg_-1437+5043.801	219.242275	50.7075248	89.735364	59.0805183	20.45 ± 0.00	19.91 ± 0.00	19.91 ± 0.00	24.36 ± 0.02	5.20 ± 0.15	12.44	8.30 ± 8.10	2.14	13.16	3.55	
borg_-1437+5043.83	219.246895	50.705228	89.744911	59.0805193	22.92 ± 0.04	22.77 ± 0.02	22.54 ± 0.02	25.41 ± 0.05	5.20 ± 0.15	12.44	8.39 ± 8.87	1.04	11.06	3.05	
borg_-1437+5043.833	219.264083	50.7232983	89.741888	59.050379	23.02 ± 0.02	22.66 ± 0.02	22.57 ± 0.02	26.20 ± 0.31	8.24 ± 1.07	10.63	1.34 ± 0.19	1.36	9.19	3.64	
borg_-1437+5043.912	219.227427	50.7357012	89.7893159	59.0521489	21.19 ± 0.05	20.98 ± 0.01	20.85 ± 0.01	21.89 ± 0.13	0.74 ± 0.23	14.70	6.68 ± 0.05	0.71	8.85	3.48	
borg_-1437+5043.915	219.249669	50.731502	89.7656159	59.0521489	22.23 ± 0.13	21.88 ± 0.02	21.79 ± 0.02	25.13 ± 0.13	7.22 ± 0.45	10.08	1.04 ± 0.10	0.71	9.03	3.64	
borg_-1437+5043.918	219.249669	50.731502	89.7886791	59.0521489	23.79 ± 0.10	23.63 ± 0.05	23.54 ± 0.06	26.06 ± 0.94	4.47 ± 3.20	14.40	7.59 ± 7.80	1.95	13.36	3.55	
borg_-1437+5043.919	219.242422	50.731502	89.7886791	59.0521489	24.22 ± 0.04	23.82 ± 0.04	23.60 ± 0.05	26.12 ± 0.92	4.01 ± 3.14	14.59	8.30 ± 8.10	2.14	13.16	3.55	
borg_-1437+5043.920	219.246895	50.731502	89.7886791	59.0521489	22.77 ± 0.01	22.24 ± 0.02	21.94 ± 0.02	24.46 ± 0.90	3.77 ± 3.04	13.01	3.99 ± 3.87	1.04	11.06	3.05	
borg_-1437+5043.925	219.247209	50.731502	89.7886791	59.0521489	24.20 ± 0.04	23.93 ± 0.04	23.76 ± 0.07	24.68 ± 0.08	0.72 ± 0.31	14.70	8.72 ± 8.51	2.25	14.09	3.55	
borg_-1437+5043.938	219.249669	50.731502	89.7886791	59.0521489	23.60 ± 0.02	23.26 ± 0.03	23.05 ± 0.03	25.57 ± 0.91	4.07 ± 3.08	14.03	6.38 ± 6.21	1.65	12.59	3.55	
borg_-1437+5043.940	219.249669	50.731502	89.7886791	59.0521489	21.19 ± 0.05	18.83 ± 0.00	18.33 ± 0.01	21.82 ± 0.01	1.82 ± 0.06	8.40	0.18 ± 0.06	0.63	8.63	3.37	
borg_-1437+5043.945	219.249669	50.731502	89.7886791	59.0521489	22.79 ± 0.04	22.38 ± 0.04	22.87 ± 0.03	23.89 ± 0.04	0.20 ± 0.37	16.53	20.23 ± 0.12	7.53	23.05	3.37	
borg_-1437+5043.950	219.249669	50.731502	89.7886791	59.0521489	22.68 ± 0.05	22.39 ± 0.05	22.45 ± 0.05	23.61 ± 0.05	0.62 ± 0.13	12.08	10.40 ± 0.48	1.04	17.32	3.37	
borg_-1437+5043.955	219.249669	50.731502	89.7886791	59.0521489	22.77 ± 0.04	22.39 ± 0.04	22.46 ± 0.05	23.99 ± 0.06	0.89 ± 0.20	16.59	20.77 ± 504.30	7.74	23.44	6.737	
borg_-1437+5043.960	219.249669	50.731502	89.7886791	59.0521489	20.83 ± 0.01	20.51 ± 0.02	20.22 ± 0.00	23.30 ± 0.02	4.33 ± 0.07	11.28	1.80 ± 0.07	1.92	9.82	3.50	
borg_-1437+5043.965	219.249669	50.731502	89.7886791	59.0521489	23.37 ± 0.02	23.37 ± 0.02	23.37 ± 0.03	24.43 ± 0.08	10.05 ± 0.28	8.04	0.41 ± 0.02	0.38	8.80	3.50	
borg_-1437+5043.970	219.249669	50.731502	89.7886791	59.0521489	24.51 ± 0.07	23.83 ± 0.06	23.54 ± 0.08	24.88 ± 0.08	-0.20 ± 0.34	16.49	19.84 ± 3.09	17.25	23.04	3.37	
borg_-1437+5043.975	219.249669	50.731502	89.7886791	59.0521489	22.45 ± 0.01	22.45 ± 0.02	23.15 ± 0.02	24.17 ± 0.02	-1.41 ± 0.09	15.11	16.53 ± 0.72	9.17	20.93	3.50	
borg_-1437+5043.980	219.249669	50.731502	89.7886791	59.0521489	23.39 ± 0.05	22.97 ± 0.02	22.71 ± 0.02	23.61 ± 0.04	-1.62 ± 0.13	12.08	10.40 ± 0.48	1.04	17.32	3.37	
borg_-1437+5043.985	219.249669	50.731502	89.7886791	59.0521489	24.10 ± 0.04	23.93 ± 0.03	23.76 ± 0.07	24.68 ± 0.08	0.71 ± 0.30	16.59	20.77 ± 504.30	7.74	23.44	3.55	
borg_-1437+5043.990	219.249669	50.731502	89.7886791	59.0521489	20.83 ± 0.02	20.51 ± 0.02	20.22 ± 0.02	23.30 ± 0.02	4.33 ± 0.07	14.76	12.33 ± 18.88	1.88	21.88	3.27	
borg_-1437+5043.995	219.249669	50.731502	89.7886791	59.0521489	23.35 ± 0.02	23.35 ± 0.02	23.3								

Table 10
Table 10 – *continued*

Field	RA J2000	DEC J2000	<i>l</i>	<i>b</i>	<i>m</i> <i>F</i> 098W mag	<i>m</i> <i>F</i> 125W mag	<i>m</i> <i>F</i> 125W mag	<i>m</i> <i>F</i> 125W mag	<i>m</i> <i>F</i> 606W mag	<i>m</i> <i>F</i> 606W mag	M-type	Radius mag.	Height kpc.	Volume kpc. ²	Area arcmin ²	
borg_1815-3244.336	273.630284	-32.751479	359.743625	-7.275362	20.91 ± 0.03	20.81 ± 0.02	20.76 ± 0.03	22.81 ± 0.91	3.01 ± 3.09	12.68	3.43 ± 2.97	0.01	11.90	2.07	3.27	
borg_1815-3244.355	273.628645	-32.751255	359.743177	-7.274039	21.66 ± 0.07	21.55 ± 0.05	21.54 ± 0.07	23.58 ± 0.95	3.12 ± 3.21	13.42	4.83 ± 4.21	0.01	13.30	4.12	3.27	
borg_1815-3244.361	273.628142	-32.751044	359.741201	-7.263841	22.64 ± 0.14	22.23 ± 0.12	22.26 ± 0.30	24.30 ± 1.18	3.24 ± 4.04	14.10	6.62 ± 6.98	-0.00	15.07	7.73	3.27	
borg_1815-3244.372	273.628252	-32.750901	359.742948	-7.272835	23.26 ± 0.22	22.98 ± 0.14	23.02 ± 0.19	25.07 ± 1.07	3.30 ± 3.65	14.85	9.34 ± 9.88	-0.01	17.77	15.38	3.27	
borg_1815-3244.375	273.617257	-32.750999	359.733923	-7.265437	21.01 ± 0.04	20.80 ± 0.03	20.68 ± 0.03	22.73 ± 0.91	2.77 ± 3.10	12.67	3.42 ± 2.96	0.01	11.89	2.06	3.27	
borg_1815-3244.396	273.617470	-32.756665	359.733036	-7.265440	21.70 ± 0.07	21.39 ± 0.04	21.37 ± 0.05	23.42 ± 0.93	3.13 ± 3.16	13.26	4.48 ± 3.89	0.01	12.94	3.53	3.27	
borg_1815-3244.458	273.626748	-32.756685	359.743942	-7.267359	20.71 ± 0.05	20.50 ± 0.03	20.54 ± 0.03	21.56 ± 0.91	2.96 ± 3.09	12.43	3.06 ± 2.64	0.01	11.53	1.65	3.27	
borg_1815-3244.461	273.628250	-32.752559	359.741787	-7.263259	22.52 ± 0.14	21.84 ± 0.06	21.54 ± 0.06	23.59 ± 0.94	2.15 ± 3.20	13.97	6.22 ± 4.40	-0.00	14.67	6.81	3.27	
borg_1815-3244.480	273.629148	-32.750093	359.744416	-7.273872	21.93 ± 0.16	21.81 ± 0.09	21.77 ± 0.10	23.82 ± 0.98	3.04 ± 3.34	13.68	5.45 ± 4.80	0.01	13.90	5.23	3.27	
borg_1815-3244.526	273.617555	-32.746224	359.742024	-7.265043	20.61 ± 0.03	20.30 ± 0.02	20.35 ± 0.02	22.30 ± 0.96	2.90 ± 3.26	12.31	4.20 ± 2.50	0.01	11.37	1.48	3.27	
borg_1815-3244.528	273.616130	-32.749712	359.733628	-7.264000	21.48 ± 0.06	21.37 ± 0.05	21.30 ± 0.08	23.36 ± 0.96	2.98 ± 3.26	13.24	4.44 ± 3.87	0.01	12.91	3.48	3.27	
borg_1815-3244.564	273.617578	-32.745033	359.743855	-7.264981	20.45 ± 0.03	20.33 ± 0.02	20.19 ± 0.02	22.24 ± 0.90	2.70 ± 3.06	12.20	2.75 ± 2.38	0.01	11.23	1.34	3.27	
borg_1815-3244.578	273.622935	-32.743985	359.744569	-7.272640	20.95 ± 0.04	20.67 ± 0.02	20.55 ± 0.03	22.59 ± 0.91	2.75 ± 3.07	12.54	3.22 ± 2.78	0.01	11.70	1.83	3.27	
borg_1815-3244.580	273.633930	-32.747840	359.750460	-7.280455	21.20 ± 0.06	21.07 ± 0.04	20.97 ± 0.05	23.01 ± 0.93	2.80 ± 3.16	12.94	3.88 ± 3.37	0.01	12.35	2.65	3.27	
borg_1815-3244.749	273.618595	-32.747212	359.748381	-7.264674	22.94 ± 0.21	22.83 ± 0.14	22.59 ± 0.15	24.64 ± 1.03	2.37 ± 3.52	14.96	8.82 ± 8.77	-0.02	18.24	16.98	3.27	
borg_1815-3244.778	273.615220	-32.747408	359.741326	-7.262251	21.12 ± 0.05	20.83 ± 0.03	20.79 ± 0.04	22.83 ± 0.91	3.01 ± 3.10	12.70	3.47 ± 3.00	0.01	11.94	2.12	3.27	
borg_1815-3244.779	273.612860	-32.747524	359.740945	-7.260422	21.29 ± 0.05	21.19 ± 0.04	21.13 ± 0.04	22.47 ± 0.99	3.17 ± 0.92	14.31	13.06 ± 13.06	0.01	12.56	2.95	3.27	
borg_1815-3244.847	273.619900	-32.746520	359.743963	-7.263325	21.36 ± 0.05	21.15 ± 0.03	21.14 ± 0.04	23.19 ± 0.92	3.13 ± 3.13	13.02	4.02 ± 3.49	0.01	12.49	2.85	3.27	
borg_1815-3244.879	273.614545	-32.746668	359.742080	-7.262082	20.66 ± 0.04	20.51 ± 0.03	20.41 ± 0.04	22.46 ± 0.91	2.84 ± 3.10	12.38	2.99 ± 2.59	0.01	11.47	1.57	3.27	
borg_1815-3244.937	273.618053	-32.748076	359.741663	-7.260019	19.85 ± 0.02	19.59 ± 0.14	19.60 ± 0.03	21.65 ± 0.91	2.80 ± 3.13	11.46	3.96 ± 3.75	0.01	12.35	2.65	3.27	
borg_1815-3244.938	273.616544	-32.744054	359.741552	-7.263555	21.19 ± 0.05	20.88 ± 0.03	20.89 ± 0.02	19.92 ± 0.02	21.96 ± 0.92	2.91 ± 3.05	12.75	3.55 ± 3.07	0.01	12.02	2.21	3.27
borg_1815-3244.986	273.630717	-32.740905	359.746033	-7.273184	20.70 ± 0.05	20.50 ± 0.03	20.79 ± 0.04	22.42 ± 0.12	24.47 ± 0.99	3.12 ± 3.38	12.36 ± 2.03	0.02	10.84	0.98	3.27	
borg_1815-3244.106	273.638961	-32.744611	359.751747	-7.278635	22.70 ± 0.14	22.44 ± 0.09	22.42 ± 0.12	22.42 ± 0.12	24.47 ± 0.99	3.12 ± 3.38	12.40 ± 1.40	3.09 ± 5.55	0.01	15.70	9.29	3.27
borg_1815-3244.136	273.619078	-32.749000	359.743966	-7.263712	22.32 ± 0.11	22.08 ± 0.11	22.19 ± 0.12	23.23 ± 0.18	25.23 ± 1.08	3.07 ± 3.69	15.09 ± 15.09	10.40 ± 11.03	-0.02	19.06	3.27	3.27
borg_1815-3244.144	273.641255	-32.744188	359.754455	-7.280114	23.40 ± 0.22	23.22 ± 0.16	23.19 ± 0.20	23.22 ± 0.18	24.14 ± 0.97	2.54 ± 3.29	14.15	6.77 ± 5.73	0.01	15.21	8.06	3.27
borg_1815-3244.145	273.618053	-32.743677	359.743889	-7.250889	23.22 ± 0.55	23.05 ± 0.43	23.02 ± 1.34	23.02 ± 1.34	25.07 ± 2.22	3.09 ± 2.22	14.92	6.63 ± 4.09	-0.02	18.05	16.33	3.27
borg_1815-3244.147	273.614129	-32.744072	359.750887	-7.277480	21.07 ± 0.07	20.84 ± 0.06	20.78 ± 0.09	22.83 ± 0.97	2.96 ± 3.29	12.71	3.49 ± 3.05	0.01	11.96	2.14	3.27	
borg_1815-3244.148	273.615765	-32.744361	359.754847	-7.273184	21.61 ± 0.20	21.44 ± 0.09	21.41 ± 0.19	23.46 ± 1.07	3.07 ± 3.63	13.31	4.60 ± 4.82	0.01	13.06	3.73	3.27	
borg_1815-3244.149	273.638961	-32.744117	359.742051	-7.256717	22.70 ± 0.12	22.00 ± 0.07	21.90 ± 0.10	22.95 ± 0.92	2.95 ± 3.11	13.80	5.75 ± 5.04	0.00	14.20	5.82	3.27	
borg_1815-3244.174	273.619079	-32.744203	359.742913	-7.257965	22.30 ± 0.12	21.93 ± 0.07	21.90 ± 0.11	23.36 ± 0.93	3.08 ± 3.31	13.80	4.34 ± 3.37	0.01	12.36	3.26	3.27	
borg_1815-3244.179	273.615199	-32.744222	359.750756	-7.273224	22.53 ± 0.12	22.28 ± 0.08	22.10 ± 0.09	24.14 ± 0.97	2.54 ± 3.29	14.15	6.77 ± 5.94	-0.00	15.21	8.06	3.27	
borg_1815-3244.184	273.618053	-32.743677	359.751362	-7.282655	22.40 ± 0.29	22.27 ± 0.08	22.16 ± 0.10	22.16 ± 0.10	22.41 ± 0.98	2.80 ± 3.32	14.14	5.92 ± 5.92	-0.00	15.18	7.98	3.27
borg_1815-3244.185	273.614032	-32.743818	359.751698	-7.270809	21.64 ± 0.08	21.40 ± 0.08	21.30 ± 0.06	23.35 ± 0.12	2.82 ± 3.20	13.27	4.52 ± 3.94	0.01	12.98	3.60	3.27	
borg_1815-3244.187	273.621815	-32.743229	359.746755	-7.265222	21.84 ± 0.07	21.72 ± 0.05	21.52 ± 0.05	21.52 ± 0.05	23.57 ± 0.93	2.50 ± 3.17	13.85	5.89 ± 5.13	0.00	14.34	6.11	3.27
borg_1815-3244.192	273.619079	-32.742882	359.747246	-7.263701	21.79 ± 0.19	21.08 ± 0.03	20.91 ± 0.04	22.95 ± 0.92	2.58 ± 3.11	12.95	3.84 ± 3.37	0.01	13.06	3.73	3.27	
borg_1815-3244.193	273.619389	-32.742690	359.754891	-7.277747	21.70 ± 0.08	21.29 ± 0.14	21.29 ± 0.14	23.99 ± 0.93	2.90 ± 3.17	13.19	4.34 ± 3.37	0.01	12.80	3.32	3.27	
borg_1815-3244.194	273.614129	-32.742656	359.752828	-7.272532	23.03 ± 0.19	22.58 ± 0.10	22.59 ± 0.13	24.64 ± 1.01	2.31 ± 3.43	14.45	7.76 ± 8.14	-0.00	16.20	10.60	3.27	
borg_1815-3244.196	273.619191	-32.743019	359.746809	-7.263170	21.25 ± 0.08	21.15 ± 0.07	21.09 ± 0.14	23.14 ± 1.02	2.98 ± 3.47	13.02	4.01 ± 3.52	0.01	12.48	2.83	3.27	
borg_1815-3244.197	273.642913	-32.743342	359.754693	-7.274824	22.78 ± 0.25	22.60 ± 0.23	22.54 ± 0.28	24.58 ± 1.15	2.95 ± 3.39	14.47	7.83 ± 8.42	-0.01	16.26	10.79	3.27	
borg_1815-3244.198	273.633432	-32.743198	359.750495	-7.274787	22.25 ± 0.10	22.00 ± 0.07	21.93 ± 0.08	23.98 ± 0.96	2.92 ± 3.20	13.87	5.96 ± 5.21	0.00	14.41	6.25	3.27	
borg_1815-3244.199	273.619079	-32.742910	359.743322	-7.264884	21.69 ± 0.27	21.56 ± 0.05	21.54 ± 0.07	23.58 ± 0.95	3.10 ± 3.22	13.43	4.84 ± 4.22	0.01	13.30	4.13	3.27	
borg_1815-3244.200	273.619389	-32.742614	359.754891	-7.272564	22.36 ± 0.15	22.13 ± 0.05	21.31 ± 0.06	23.36 ± 0.94	3.08 ± 3.19	13.21	4.38 ± 3.81	0.01	12.80	3.32	3.27	
borg_1815-3244.201	273.614043	-32.742556	359.750708	-7.272537	23.02 ± 0.17	22.91 ± 0.12	22.94 ± 0.17	24.99 ± 1.04	3.27 ± 3.57	14.78	9.04 ± 9.53	-0.01	17.47	14.40	3.27	
borg_1815-3244.202	273.614053	-32.742413	359.750505	-7.274439	21.74 ± 0.08	20.76 ± 0.02	20.63 ± 0.03	21.81 ± 0.07	2.72 ± 3.08	12.63	3.36 ± 3.22	0.01	11.83	1.98	3.27	
borg_1815-3244.203	273.614053	-32.742413	359.750505	-7.274439	21.74 ± 0.09	21.74 ± 0.06	21.60 ± 0.06	23.65 ± 0.94	2.69 ± 3.20	13.61	5.27 ± 4.60	0.00	13.73	4.90	3.27	
borg_1815-3244.204	273.614053	-32.742413	359.750505	-7.274439	22.25 ± 0.10	21.95 ± 0.07	21.91 ± 0.09	23.96 ± 0.96	2.98 ± 3.22	13.53	5.96 ± 5.21	0.00	13.55	4.66	3.27	
borg_1815-3244.205	273.614053	-32.742413	359.750505	-7.274439	21.17 ± 0.18	21.15 ± 0.05	21.16 ± 0.07	21.86 ± 0.90	2.91 ± 3.04	12.95	4.84 ± 4.22	0.01	13.3			

Table 10

Table 10 – *continued*

Field	RA J2000	DEC J2000	<i>l</i>	<i>b</i>	<i>m</i> _{F098W} mag	<i>m</i> _{F125W} mag	<i>m</i> _{F125W} mag	<i>m</i> _{F125W} mag	<i>m</i> _{F606W} mag	<i>M</i> -type	Radius mag	Height kpc	Volume kpc ²	Area arcmin ²	
borg_1815-3244.2391	273.648867	-32.735169	359.762826	-7.283023	21.31 ± 0.05	21.18 ± 0.04	21.15 ± 0.05	23.20 ± 0.92	3.07 ± 3.14	13.05	4.08 ± 3.54	0.01	12.54	2.93	
borg_-1815-3244.2411	273.649471	-32.737717	359.763467	-7.282363	22.05 ± 0.09	21.84 ± 0.06	21.70 ± 0.07	23.75 ± 0.95	2.70 ± 3.21	13.71	5.51 ± 4.81	0.01	13.97	5.35	
borg_-1815-3244.2414	273.647984	-7.282254	21.14 ± 0.05	21.03 ± 0.04	21.07 ± 0.04	2.80 ± 0.92	2.80 ± 3.12	13.01	3.99 ± 3.46	0.01	12.46	2.81	3.27		
borg_-1815-3244.2423	273.635752	-32.738100	359.757523	-7.273221	19.97 ± 0.02	19.84 ± 0.01	19.85 ± 0.01	21.89 ± 0.89	3.20 ± 3.03	11.71	2.90 ± 1.89	0.01	10.68	0.85	
borg_-1815-3244.2510	273.612674	-32.737335	359.748959	-7.255861	21.78 ± 0.11	21.57 ± 0.07	21.59 ± 0.10	23.63 ± 0.98	3.21 ± 3.35	13.44	4.88 ± 5.10	0.01	13.35	4.20	
borg_-1815-3244.2514	273.620024	-32.737249	359.755832	-7.267814	22.67 ± 0.14	22.54 ± 0.10	22.35 ± 0.11	24.39 ± 0.99	2.53 ± 3.38	14.41	7.61 ± 6.72	-0.01	16.05	10.20	
borg_-1815-3244.2532	273.654481	-32.737288	359.765823	-7.267632	22.06 ± 0.09	21.92 ± 0.08	23.96 ± 0.96	3.29 ± 3.25	5.62 ± 5.85	14.08	5.57	0.01	14.08	5.57	
borg_-1815-3244.2552	273.636462	-32.737052	359.766190	-7.275632	23.40 ± 0.27	23.05 ± 0.15	23.06 ± 0.20	25.11 ± 1.08	3.19 ± 3.70	14.92	6.95 ± 10.23	-0.01	18.07	16.40	
borg_-1815-3244.2582	273.610632	-32.737762	359.746434	-7.251145	20.30 ± 0.04	20.14 ± 0.02	20.06 ± 0.02	22.11 ± 0.90	2.90 ± 3.06	12.01	2.52 ± 2.18	0.01	11.00	1.12	
borg_-1815-3244.2637	273.64026	-32.737038	359.761930	-7.275882	21.81 ± 0.09	21.44 ± 0.10	21.44 ± 0.13	24.87 ± 1.01	3.16 ± 3.45	13.31	4.59 ± 4.81	0.01	13.05	3.71	
borg_-1815-3244.2768	273.632934	-32.736612	359.757942	-7.270430	20.61 ± 0.03	20.43 ± 0.02	20.35 ± 0.02	22.39 ± 0.90	2.88 ± 3.06	12.30	2.88 ± 2.49	0.01	11.36	1.47	
borg_-1815-3244.2782	273.603581	-32.734630	359.748700	-7.286654	22.58 ± 0.15	22.33 ± 0.12	22.09 ± 0.12	24.14 ± 1.00	2.38 ± 3.42	14.46	7.79 ± 6.92	-0.00	16.23	10.69	
borg_-1815-3244.2784	273.634771	-32.735157	359.766625	-7.275446	22.99 ± 0.25	22.81 ± 0.15	22.83 ± 0.20	24.87 ± 1.08	3.24 ± 3.69	14.68	8.62 ± 9.13	-0.01	17.05	13.08	
borg_-1815-3244.2743	273.608398	-32.737052	359.748416	-7.270528	22.36 ± 0.12	22.14 ± 0.08	21.96 ± 0.09	24.00 ± 0.97	2.55 ± 3.29	14.01	6.34 ± 5.57	0.00	14.79	7.09	
borg_-1815-3244.2748	273.634156	-32.738691	359.754174	-7.271747	20.77 ± 0.05	20.63 ± 0.04	20.58 ± 0.04	20.51 ± 0.05	22.56 ± 0.93	2.94 ± 3.17	12.45	3.09 ± 2.69	0.01	11.64	1.76
borg_-1815-3244.2762	273.630111	-32.734714	359.756699	-7.268301	20.95 ± 0.09	20.58 ± 0.04	20.51 ± 0.05	22.46 ± 1.12	3.16 ± 3.24	12.50	3.16 ± 2.74	0.01	11.00	1.12	
borg_-1815-3244.2766	273.632934	-32.736612	359.757942	-7.270430	20.61 ± 0.03	20.43 ± 0.02	20.35 ± 0.02	22.39 ± 0.90	2.88 ± 3.06	12.30	2.88 ± 2.49	0.01	11.36	1.47	
borg_-1815-3244.2781	273.634771	-32.735157	359.764590	-7.276113	21.79 ± 0.05	21.53 ± 0.01	19.54 ± 0.01	21.58 ± 0.89	3.20 ± 3.03	11.40	1.90 ± 1.64	0.01	11.76	1.90	
borg_-1815-3244.2816	273.645790	-32.736138	359.764136	-7.281129	22.18 ± 0.10	21.99 ± 0.07	21.92 ± 0.08	23.96 ± 0.96	2.93 ± 3.27	13.86	5.91 ± 5.17	0.01	14.36	6.15	
borg_-1815-3244.2817	273.640775	-32.735143	359.761449	-7.276054	22.36 ± 0.12	22.14 ± 0.08	21.96 ± 0.09	24.00 ± 0.97	2.55 ± 3.29	14.01	6.34 ± 5.57	0.00	14.79	7.09	
borg_-1815-3244.2853	273.614091	-32.738020	359.751048	-7.256120	22.12 ± 0.11	21.81 ± 0.06	21.63 ± 0.08	23.74 ± 0.95	3.24 ± 3.24	13.68	4.55 ± 4.77	0.00	13.91	5.24	
borg_-1815-3244.2858	273.655578	-32.735300	359.758585	-7.258578	23.85 ± 0.35	23.41 ± 0.19	23.41 ± 0.24	25.46 ± 1.12	3.18 ± 3.85	15.28	3.16 ± 12.12	-0.02	19.77	22.73	
borg_-1815-3244.2968	273.628313	-32.735382	359.750355	-7.265134	20.85 ± 0.03	20.71 ± 0.02	20.61 ± 0.03	22.65 ± 1.12	3.18 ± 3.85	12.45	3.09 ± 2.69	0.01	11.57	1.68	
borg_-1815-3244.2974	273.629211	-32.735472	359.754944	-7.267128	21.46 ± 0.04	21.29 ± 0.03	21.19 ± 0.04	23.24 ± 0.91	2.84 ± 3.10	13.16	4.28 ± 3.71	0.01	11.76	1.90	
borg_-1815-3244.2978	273.615959	-32.735439	359.751616	-7.268925	21.79 ± 0.08	21.59 ± 0.05	21.42 ± 0.06	22.54 ± 0.91	2.47 ± 0.94	13.46	4.92 ± 4.29	0.01	13.38	4.26	
borg_-1815-3244.3048	273.618591	-32.735430	359.755266	-7.266026	20.74 ± 0.03	20.57 ± 0.02	20.46 ± 0.03	22.51 ± 0.91	2.78 ± 3.08	12.44	4.08 ± 4.44	0.01	11.56	1.67	
borg_-1815-3244.3091	273.614091	-32.738020	359.751048	-7.256761	20.38 ± 0.02	20.23 ± 0.02	20.17 ± 0.02	22.22 ± 0.90	2.98 ± 3.05	12.10	2.63 ± 2.27	0.02	11.10	1.21	
borg_-1815-3244.3095	273.615957	-32.735300	359.755749	-7.258994	23.56 ± 0.29	23.43 ± 0.21	23.30 ± 0.24	25.34 ± 1.12	3.18 ± 3.87	15.30	11.51 ± 12.34	-0.02	19.92	23.33	
borg_-1815-3244.3097	273.615957	-32.735300	359.754911	-7.250300	20.88 ± 0.03	20.71 ± 0.02	20.72 ± 0.03	22.76 ± 0.91	3.18 ± 3.09	12.58	3.28 ± 2.84	0.01	11.76	1.90	
borg_-1815-3244.3104	273.629211	-32.735405	359.751115	-7.250144	21.42 ± 0.05	21.19 ± 0.04	21.19 ± 0.05	23.24 ± 0.92	2.87 ± 3.14	13.16	4.26 ± 3.70	0.01	12.73	3.22	
borg_-1815-3244.3108	273.618591	-32.735439	359.751650	-7.250526	20.74 ± 0.03	20.57 ± 0.02	20.46 ± 0.03	22.51 ± 0.91	2.78 ± 3.08	12.44	4.08 ± 4.44	0.01	11.56	1.67	
borg_-1815-3244.3121	273.626957	-32.735459	359.756849	-7.266026	20.45 ± 0.04	20.25 ± 0.02	20.17 ± 0.03	22.43 ± 0.91	2.75 ± 3.08	12.12	4.65 ± 4.77	0.00	13.91	5.24	
borg_-1815-3244.3236	273.624743	-32.735300	359.758966	-7.265761	20.76 ± 0.03	20.56 ± 0.02	20.38 ± 0.02	22.43 ± 0.92	2.59 ± 3.07	12.43	3.06 ± 2.64	0.01	11.53	1.64	
borg_-1815-3244.3238	273.624741	-32.735300	359.745258	-7.244741	20.76 ± 0.03	20.56 ± 0.02	20.38 ± 0.02	22.43 ± 0.92	2.59 ± 3.07	12.43	3.06 ± 2.64	0.01	11.53	1.64	
borg_-1815-3244.3298	273.624754	-32.735300	359.745154	-7.264251	21.70 ± 0.11	21.29 ± 0.06	21.23 ± 0.07	23.28 ± 0.95	2.99 ± 3.23	13.16	4.28 ± 3.73	0.01	12.74	3.23	
borg_-1815-3244.3308	273.624589	-32.735300	359.745323	-7.258877	22.32 ± 1.64	23.64 ± 0.22	23.59 ± 0.28	25.63 ± 1.16	4.54 ± 4.00	15.51	12.66 ± 13.60	-0.02	21.05	28.22	
borg_-1815-3244.3309	273.624589	-32.735300	359.745323	-7.250514	21.42 ± 0.06	21.29 ± 0.05	21.26 ± 0.05	23.31 ± 0.93	3.07 ± 3.16	13.16	4.29 ± 3.73	0.01	12.76	3.22	
borg_-1815-3244.3319	273.625420	-32.735158	359.751312	-7.258502	19.10 ± 0.02	18.74 ± 0.01	18.74 ± 0.02	20.98 ± 0.90	2.75 ± 3.08	12.12	3.16 ± 3.44	0.01	9.81	0.31	
borg_-1815-3244.3328	273.625353	-32.735300	359.751677	-7.263447	19.47 ± 0.05	19.09 ± 0.02	18.94 ± 0.02	20.98 ± 0.90	2.64 ± 3.06	10.96	1.56 ± 1.34	0.02	10.04	0.43	
borg_-1815-3244.3344	273.624567	-32.735300	359.754528	-7.244741	22.63 ± 0.13	22.63 ± 0.08	22.25 ± 0.10	24.33 ± 0.98	2.79 ± 3.33	14.23	3.01 ± 6.17	-0.02	15.46	8.67	
borg_-1815-3244.3348	273.624567	-32.735300	359.754516	-7.244741	19.77 ± 0.06	19.62 ± 0.05	19.43 ± 0.03	21.48 ± 0.91	2.53 ± 3.09	11.49	1.99 ± 1.73	0.02	10.47	0.70	
borg_-1815-3244.3349	273.624567	-32.735300	359.756058	-7.277942	13.77 ± 0.00	13.59 ± 0.00	13.42 ± 0.00	15.47 ± 0.88	2.60 ± 2.99	5.46	0.12 ± 0.11	0.03	8.62	0.00	
borg_-1815-3244.3409	273.624589	-32.735300	359.756082	-7.284047	22.57 ± 0.18	22.49 ± 0.14	22.45 ± 0.12	24.53 ± 0.92	2.87 ± 3.48	14.44	7.74 ± 6.85	-0.00	16.18	10.56	
borg_-1815-3244.3427	273.625392	-32.735300	359.753991	-7.255802	21.39 ± 0.06	21.12 ± 0.04	21.13 ± 0.05	23.17 ± 0.93	3.20 ± 3.15	12.99	3.96 ± 3.44	0.01	13.08	3.76	
borg_-1815-3244.3449	273.624567	-32.735300	359.753833	-7.287693	18.86 ± 0.02	18.43 ± 0.02	18.42 ± 0.02	20.47 ± 0.90	3.14 ± 3.04	10.30	1.56 ± 1.34	0.02	14.02	4.45	
borg_-1815-3244.3454	273.624549	-32.735300	359.762419	-7.269571	18.80 ± 0.01	18.66 ± 0.01	18.67 ± 0.01	20.71 ± 0.89	3.21 ± 3.01	10.53	1.27 ± 1.10	0.02	10.39	0.64	
borg_-1815-3244.3456	273.624567	-32.735300	359.762424	-7.262226	21.99 ± 0.15	22.97 ± 0.15	22.86 ± 0.18	24.90 ± 1.05	2.77 ± 3.61	14.84	9.31 ± 8.33	-0.01	17.73	15.26	
borg_-1815-3244.3457	273.624567	-32.735300	359.762424	-7.275021	20.53 ± 0.30	20.37 ± 0.02	20.28 ± 0.02	22.33 ± 0.90	2.86 ± 3.06	12.24	2.81 ± 2.42	0.02	11.29	1.39	
borg_-1815-3244.3458	273.624567	-32.735300	359.762424	-7.275021	21.18 ± 0.15	21.15 ± 0.05	21.32 ± 0.05	23.37 ± 0.93	2.72 ± 3.17	13.32	4.62 ± 4.02	0.01	13.08	3.27	
borg_-1815-3244.3466	273.624567	-32.735300	359.762424	-7.284771	20.82 ±										

Table 10
Table 10 – *continued*

Field	RA J2000	DEC J2000	<i>l</i>	<i>b</i>	<i>m</i> <i>F</i> 098W mag	<i>m</i> <i>F</i> 125W mag	<i>m</i> <i>F</i> 125W mag	<i>m</i> <i>F</i> 606W mag	<i>m</i> <i>F</i> 606W mag	M-type	M-mag	M-m mag	Dist kpc.	Radius kpc. mag	Height kpc.	Volume kpc. mag	Area arcmin ²
borg_1815-3244.4016	272.630301	-32.731098	359.761828	-7.265908	21.31 ± 0.07	21.17 ± 0.05	21.04 ± 0.05	23.09 ± 0.93	2.74 ± 3.17	13.04	4.05 ± 3.53	0.01	12.52	2.90	3.27	3.27	
borg_1815-3244.4042	273.615880	-32.731286	359.755379	-7.255253	20.27 ± 0.03	20.05 ± 0.02	19.96 ± 0.03	22.01 ± 0.90	2.87 ± 3.07	11.92	2.42 ± 2.09	0.02	10.90	1.03	3.27	3.27	
borg_1815-3244.4083	273.617450	-32.731099	359.755764	-7.256336	21.50 ± 0.06	21.38 ± 0.05	21.32 ± 0.06	23.37 ± 0.94	2.97 ± 3.19	13.25	4.47 ± 3.89	0.01	12.93	3.52	3.27	3.27	
borg_1815-3244.4172	273.637173	-32.723422	359.755167	-7.267865	21.79 ± 0.05	21.61 ± 0.05	21.57 ± 0.06	23.62 ± 0.94	3.05 ± 3.20	13.48	4.96 ± 4.32	0.01	13.42	4.34	3.27	3.27	
borg_1815-3244.4178	273.611336	-32.724876	359.759321	-7.248936	21.43 ± 0.05	21.23 ± 0.04	21.12 ± 0.04	23.17 ± 0.92	2.81 ± 3.13	13.10	4.16 ± 3.61	0.01	12.63	3.05	3.27	3.27	
borg_1815-3244.4196	273.620784	-32.726365	359.764249	-7.261592	17.27 ± 0.00	17.15 ± 0.00	16.95 ± 0.00	19.00 ± 0.88	2.51 ± 2.99	9.02	0.64 ± 0.55	0.02	9.13	0.07	3.27	3.27	
borg_1815-3244.4206	273.637663	-32.719363	359.771189	-7.268108	21.89 ± 0.05	21.66 ± 0.05	21.61 ± 0.05	23.71 ± 0.95	3.04 ± 3.24	13.57	5.17 ± 4.52	0.01	13.63	4.72	3.27	3.27	
borg_1815-3244.4221	273.632322	-32.725612	359.767522	-7.264865	20.82 ± 0.05	20.61 ± 0.03	20.48 ± 0.04	22.53 ± 0.92	2.74 ± 3.11	12.48	3.13 ± 2.71	0.01	11.61	1.73	3.27	3.27	
borg_1815-3244.4303	273.637545	-32.724386	359.770673	-7.268188	22.28 ± 0.11	22.07 ± 0.07	22.03 ± 0.09	24.07 ± 0.97	3.03 ± 3.30	13.94	6.13 ± 5.37	0.01	14.58	6.62	3.27	3.27	
borg_1815-3244.4409	273.639094	-32.723456	359.771248	-7.268600	22.00 ± 0.18	22.67 ± 0.11	22.54 ± 0.13	24.59 ± 1.00	2.74 ± 3.44	8.09 ± 7.16	-0.01	16.52	11.53	3.27	3.27		
borg_1815-3244.4405	273.614862	-32.724818	359.761351	-7.251490	22.68 ± 0.11	22.43 ± 0.11	22.30 ± 0.13	24.35 ± 1.01	2.71 ± 3.44	12.76	6.44	-0.00	15.70	9.28	3.27	3.27	
borg_1815-3244.4477	273.621356	-32.726734	359.762199	-7.257218	21.10 ± 0.09	20.66 ± 0.05	20.52 ± 0.06	22.57 ± 0.93	2.70 ± 3.18	12.63	3.20 ± 2.79	0.01	11.68	1.81	3.27	3.27	
borg_1815-3244.4503	273.622206	-32.726772	359.762946	-7.257636	20.53 ± 0.03	20.42 ± 0.04	20.33 ± 0.05	22.37 ± 0.93	2.85 ± 3.15	12.29	2.87 ± 2.49	0.02	11.35	1.45	3.27	3.27	
borg_1815-3244.4524	273.630925	-32.727121	359.757688	-7.248396	22.74 ± 0.15	22.52 ± 0.13	22.56 ± 0.13	24.56 ± 1.01	3.03 ± 3.44	14.42	6.76 ± 6.78	-0.01	16.11	10.36	3.27	3.27	
borg_1815-3244.4609	273.645904	-32.727456	359.771225	-7.265841	21.56 ± 0.08	21.38 ± 0.05	21.11 ± 0.05	23.15 ± 0.93	2.25 ± 3.17	13.51	5.03 ± 5.54	0.01	13.49	4.45	3.27	3.27	
borg_1815-3244.4616	273.617945	-32.727770	359.759331	-7.255157	21.89 ± 0.08	21.78 ± 0.06	21.75 ± 0.07	23.79 ± 0.95	3.05 ± 3.23	13.65	5.38 ± 4.69	0.01	13.83	5.09	3.27	3.27	
borg_1815-3244.4649	273.676368	-32.726661	359.763162	-7.264934	23.31 ± 0.29	23.03 ± 0.15	23.06 ± 0.21	25.11 ± 1.08	1.27 ± 1.17	14.90	9.56 ± 10.13	-0.01	17.98	16.11	3.27	3.27	
borg_1815-3244.4697	273.631772	-32.726282	359.763143	-7.260280	21.06 ± 0.11	20.91 ± 0.04	20.86 ± 0.05	22.91 ± 0.93	3.01 ± 3.15	12.78	3.60 ± 3.13	0.01	12.07	2.28	3.27	3.27	
borg_1815-3244.4782	273.640872	-32.726828	359.769804	-7.271800	23.10 ± 0.20	22.84 ± 0.13	22.71 ± 0.15	24.76 ± 1.03	2.72 ± 3.52	14.71	8.77 ± 7.81	-0.01	17.20	13.55	3.27	3.27	
borg_1815-3244.4792	273.619481	-32.726856	359.761552	-7.255677	20.55 ± 0.03	20.15 ± 0.01	20.18 ± 0.01	22.23 ± 1.23	3.27 ± 4.18	12.02	2.54 ± 2.62	0.02	11.02	1.13	3.27	3.27	
borg_1815-3244.4742	273.633199	-32.727286	359.771201	-7.263331	23.04 ± 0.16	23.05 ± 0.21	25.09 ± 0.18	23.02 ± 1.08	3.19 ± 3.72	14.91	6.61 ± 10.19	-0.01	18.03	16.26	3.27	3.27	
borg_1815-3244.4772	273.616197	-32.727713	359.775934	-7.263229	22.06 ± 0.11	21.57 ± 0.06	21.32 ± 0.06	23.36 ± 0.94	2.32 ± 3.20	13.70	5.49 ± 4.79	0.01	13.94	5.30	3.27	3.27	
borg_1815-3244.4773	273.625573	-32.727288	359.763277	-7.260662	21.06 ± 0.05	20.61 ± 0.02	20.46 ± 0.03	22.50 ± 0.91	2.66 ± 3.08	12.48	3.13 ± 2.70	0.01	11.60	1.72	3.27	3.27	
borg_1815-3244.4778	273.624591	-32.727288	359.762988	-7.263220	21.56 ± 0.07	21.58 ± 0.05	21.55 ± 0.06	22.17 ± 0.90	2.93 ± 3.06	12.07	2.59 ± 2.24	0.02	10.40	0.65	3.27	3.27	
borg_1815-3244.4802	273.637504	-32.728331	359.761944	-7.270222	19.66 ± 0.02	19.54 ± 0.02	19.47 ± 0.02	21.52 ± 0.90	2.92 ± 3.06	11.41	1.92 ± 1.65	0.02	10.40	0.65	3.27	3.27	
borg_1815-3244.4846	273.633199	-32.727286	359.761930	-7.263331	20.95 ± 0.06	20.79 ± 0.04	20.76 ± 0.05	22.81 ± 0.93	3.06 ± 3.17	12.66	3.41 ± 2.96	0.01	11.88	2.05	3.27	3.27	
borg_1815-3244.4772	273.616197	-32.727713	359.775934	-7.263229	22.06 ± 0.11	21.57 ± 0.06	21.35 ± 0.04	23.13 ± 0.92	2.95 ± 3.12	13.02	4.02 ± 3.48	0.01	12.49	2.85	3.27	3.27	
borg_1815-3244.4774	273.621502	-32.727288	359.763277	-7.260662	21.62 ± 0.15	22.62 ± 0.08	22.20 ± 0.10	24.24 ± 0.98	2.96 ± 3.33	14.13	6.69 ± 5.88	0.01	15.14	7.89	3.27	3.27	
borg_1815-3244.4822	273.640874	-32.727288	359.763143	-7.264701	19.53 ± 0.02	19.41 ± 0.01	19.27 ± 0.01	21.32 ± 0.90	2.70 ± 3.03	11.28	1.80 ± 1.55	0.02	10.29	0.57	3.27	3.27	
borg_1815-3244.4845	273.640902	-32.727288	359.763277	-7.263090	20.20 ± 0.02	20.13 ± 0.02	20.13 ± 0.02	22.17 ± 0.90	2.93 ± 3.06	12.07	2.59 ± 2.24	0.02	11.07	1.18	3.27	3.27	
borg_1815-3244.4850	273.616698	-32.728331	359.766688	-7.270222	22.47 ± 0.12	22.35 ± 0.09	22.37 ± 0.12	24.42 ± 1.00	3.22 ± 3.41	14.22	7.00 ± 7.33	-0.01	15.44	8.62	3.27	3.27	
borg_1815-3244.4846	273.639338	-32.727286	359.761930	-7.264570	20.95 ± 0.06	20.79 ± 0.04	20.76 ± 0.05	22.81 ± 0.93	3.06 ± 3.21	13.52	5.06 ± 4.41	0.01	13.52	4.61	3.27	3.27	
borg_1815-3244.4871	273.640581	-32.728181	359.767481	-7.272212	21.57 ± 0.06	21.15 ± 0.03	21.09 ± 0.04	23.13 ± 0.92	2.95 ± 3.12	13.02	4.69 ± 4.26	-0.03	20.71	26.67	3.27	3.27	
borg_1815-3244.4935	273.646702	-32.727288	359.765904	-7.249553	23.72 ± 0.27	23.58 ± 0.20	23.61 ± 0.27	25.66 ± 1.15	3.28 ± 3.95	15.45	12.30 ± 13.16	0.01	13.90	3.30	3.27	3.27	
borg_1815-3244.4987	273.640290	-32.730400	359.772766	-7.267682	20.08 ± 0.02	19.93 ± 0.01	19.85 ± 0.02	21.90 ± 0.90	2.88 ± 3.04	11.80	2.29 ± 1.98	0.02	10.78	0.93	3.27	3.27	
borg_1815-3244.5052	273.618209	-32.729440	359.771201	-7.263209	21.91 ± 0.08	21.71 ± 0.06	21.71 ± 0.07	23.76 ± 0.95	2.94 ± 3.23	13.65	5.38 ± 4.69	0.01	13.83	5.09	3.27	3.27	
borg_1815-3244.5099	273.616698	-32.729329	359.765803	-7.265763	22.47 ± 0.45	23.73 ± 0.24	23.52 ± 0.26	25.56 ± 1.14	2.45 ± 3.95	15.86	4.95 ± 3.59	-0.04	23.24	38.90	3.27	3.27	
borg_1815-3244.5089	273.626903	-32.729673	359.767213	-7.264537	22.65 ± 0.65	22.51 ± 0.10	22.42 ± 0.12	24.47 ± 1.00	2.87 ± 3.24	13.52	7.52 ± 6.64	-0.01	15.96	9.98	3.27	3.27	
borg_1815-3244.5114	273.609840	-32.728703	359.765904	-7.249553	23.72 ± 0.27	23.58 ± 0.20	23.61 ± 0.27	25.66 ± 1.15	3.28 ± 3.95	15.45	12.30 ± 13.16	0.01	13.90	3.30	3.27	3.27	
borg_1815-3244.5187	273.646702	-32.727002	359.772988	-7.264259	20.08 ± 0.02	19.93 ± 0.01	19.85 ± 0.02	21.90 ± 0.90	2.78 ± 3.06	12.19	2.75 ± 2.37	0.02	11.23	1.33	3.27	3.27	
borg_1815-3244.5310	273.615241	-32.730123	359.756765	-7.254236	20.44 ± 0.03	20.32 ± 0.02	20.21 ± 0.02	22.26 ± 0.90	2.78 ± 3.06	13.14	4.25 ± 3.70	0.02	12.72	3.18	3.27	3.27	
borg_1815-3244.5552	273.625288	-32.730288	359.755344	-7.282327	23.55 ± 0.34	23.30 ± 0.16	23.19 ± 0.16	25.06 ± 1.08	2.56 ± 3.72	15.08	10.28 ± 9.28	-0.01	18.70	18.61	3.27	3.27	
borg_1815-3244.5563	273.618784	-32.727288	359.765806	-7.253207	21.89 ± 0.06	21.87 ± 0.06	21.89 ± 0.06	23.92 ± 0.95	2.78 ± 3.24	13.85	5.00 ± 5.16	0.01	14.35	6.13	3.27	3.27	
borg_1815-3244.5571	273.639889	-32.721402	359.771481	-7.263839	22.54 ± 0.16	21.75 ± 0.05	21.62 ± 0.06	23.67 ± 0.94	2.74 ± 3.20	13.62	5.29 ± 4.62	0.01	13.75	4.94	3.27	3.27	
borg_1815-3244.5581	273.626903	-32.724579	359.765507	-7.259683	20.90 ± 0.03	20.79 ± 0.03	20.54 ± 0.03	23.34 ± 0.94	2.81 ± 3.18	13.18	4.50 ± 3.92	0.01	12.96	3.57	3.27	3.27	
borg_1815-3244.5587	273.634981	-32.721669	359.779868	-7.263054	21.87 ± 0.10	21.											

Table 10

Table 10 – *continued*

Field	RA J2000	DEC J2000	<i>l</i>	<i>b</i>	<i>m</i> _{F098W} mag	<i>m</i> _{F125W} mag	<i>m</i> _{F125W} mag	<i>m</i> _{F606W} mag	<i>M</i> type	<i>M</i> - <i>m</i> mag	Dist. kpc.	Radius kpc.	Height kpc.	Volume kpc ²	Area arcmin ²	
borg	1815-3244,6368	-32.71619638	359.775141	-7.260667	22.63 ± 0.13	22.41 ± 0.09	22.37 ± 0.11	24.42 ± 0.99	3.04 ± 3.37	14.28	7.18 ± 6.32	-0.00	15.63	9.09	3.27	
borg	1815-3244,6357	-32.7181826	359.771201	-7.257217	17.82 ± 0.00	17.65 ± 0.00	17.59 ± 0.00	19.64 ± 0.88	2.96 ± 3.00	9.52	0.80 ± 0.69	0.02	9.30	0.11	3.27	
borg	1815-3244,6162	-32.71776768	359.772080	-7.256660	20.63 ± 0.03	20.19 ± 0.01	20.07 ± 0.02	22.11 ± 0.90	2.74 ± 3.04	12.06	2.58 ± 2.23	0.02	11.06	1.18	3.27	
borg	1815-3244,6159	-32.71719052	359.772865	-7.260878	19.87 ± 0.02	19.74 ± 0.01	19.75 ± 0.02	21.79 ± 0.89	3.20 ± 3.04	11.61	2.10 ± 1.81	0.02	10.58	0.78	3.27	
borg	1815-3244,6502	-32.716892	359.773463	-7.257332	20.65 ± 0.04	20.35 ± 0.02	20.32 ± 0.03	22.37 ± 0.91	3.06 ± 3.09	12.22	2.78 ± 2.41	0.02	11.26	1.36	3.27	
borg	1815-3244,6520	-32.71812825	359.7769266	-7.253985	22.08 ± 0.10	21.98 ± 0.09	21.88 ± 0.10	23.93 ± 0.98	2.84 ± 3.33	13.85	5.88 ± 5.17	0.00	14.33	6.09	3.27	
borg	1815-3244,6557	-32.71812829	359.772547	-7.253975	20.56 ± 0.03	20.14 ± 0.02	20.00 ± 0.02	22.04 ± 0.90	2.69 ± 3.04	12.01	2.52 ± 2.18	0.02	11.00	1.12	3.27	
borg	1815-3244,6582	-32.7181436	359.772465	-7.253772	21.93 ± 0.08	21.78 ± 0.05	21.78 ± 0.07	23.83 ± 0.95	3.17 ± 3.23	13.65	5.37 ± 4.68	0.01	13.83	5.08	3.27	
borg	2057-4412,119	314.337373	-44.219836	356.566670	-40.6321829	24.10 ± 0.04	23.88 ± 0.05	23.82 ± 0.07	26.34 ± 0.94	4.58 ± 3.20	13.55	5.14 ± 5.28	-0.28	12.40	4.97	3.50
borg	2057-4412,222	314.321363	-44.213636	356.574849	-40.631217	22.12 ± 0.01	21.46 ± 0.01	21.46 ± 0.02	23.07 ± 0.92	3.80 ± 3.02	12.30	3.10 ± 2.33	-0.16	10.92	1.92	3.50
borg	2057-4412,345	314.333151	-44.210865	356.578475	-40.618773	24.00 ± 0.04	23.79 ± 0.04	23.70 ± 0.06	26.23 ± 0.94	4.50 ± 3.18	13.46	4.91 ± 5.04	-0.27	12.23	4.55	3.50
borg	2057-4412,389	314.315098	-44.209357	356.580395	-40.605825	23.33 ± 0.03	23.13 ± 0.03	22.91 ± 0.04	25.43 ± 0.91	4.04 ± 3.10	13.90	6.02 ± 5.86	-0.33	13.07	6.83	3.50
borg	2132+1104,471	314.313670	-44.206425	356.584247	-40.604789	23.33 ± 0.03	23.08 ± 0.03	22.90 ± 0.03	25.42 ± 0.91	4.17 ± 3.09	13.85	5.89 ± 5.73	-0.32	12.97	6.53	3.50
borg	2132+1104,500	314.330535	-44.205433	356.585511	-40.620101	23.19 ± 0.02	22.90 ± 0.02	22.94 ± 0.03	25.46 ± 0.91	4.91 ± 3.09	12.57	3.27 ± 3.15	-0.17	10.98	2.02	3.50
borg	2132+1104,638	314.321323	-44.199526	356.593369	-40.610248	24.16 ± 0.05	23.83 ± 0.04	23.80 ± 0.06	26.32 ± 0.94	4.68 ± 3.19	13.50	5.02 ± 5.15	-0.27	12.31	4.74	3.50
borg	2132+1104,649	323.066868	10.082622	63.582505	-29.067204	24.12 ± 0.05	23.77 ± 0.05	23.69 ± 0.08	26.21 ± 0.96	4.50 ± 3.25	13.44	4.88 ± 5.02	-0.27	12.77	4.83	3.76
borg	2132+1104,1021	323.071939	10.072133	63.579464	-29.077681	23.74 ± 0.04	23.44 ± 0.03	23.21 ± 0.05	25.94 ± 0.93	3.99 ± 3.15	14.22	6.97 ± 6.79	-0.27	14.59	9.84	3.76
borg	2132+1104,1052	323.056728	10.084320	63.580190	-29.059661	24.23 ± 0.05	23.91 ± 0.05	23.92 ± 0.08	26.44 ± 0.96	4.79 ± 3.26	13.58	5.21 ± 5.04	-0.39	13.05	5.49	3.76
borg	2153+4411,1007	328.809295	-44.164632	355.268307	-50.945752	24.19 ± 0.04	23.99 ± 0.04	23.96 ± 0.06	26.53 ± 0.93	4.85 ± 3.17	13.66	5.38 ± 5.20	-0.42	11.89	5.79	3.71
borg	2153+4411,1162	328.840576	-44.172033	355.250686	-50.906436	23.74 ± 0.03	23.53 ± 0.03	23.32 ± 0.04	25.39 ± 0.91	4.22 ± 3.10	14.30	7.25 ± 7.06	-0.57	13.07	10.50	3.71
borg	2153+4411,638	330.250556	-48.557744	356.485522	-28.485522	23.44 ± 0.03	23.05 ± 0.02	22.93 ± 0.02	25.39 ± 0.90	4.17 ± 3.04	13.82	5.80 ± 5.63	-0.57	13.60	6.24	3.44
borg	2153+4411,656	330.250556	-48.557744	356.485522	-28.485522	23.44 ± 0.03	23.05 ± 0.02	22.93 ± 0.02	25.39 ± 0.90	4.17 ± 3.04	13.82	5.80 ± 5.63	-0.57	13.60	6.24	3.44
borg	2153+4411,676	330.250556	-48.557744	356.485522	-28.485522	23.44 ± 0.03	23.05 ± 0.02	22.93 ± 0.02	25.39 ± 0.90	4.17 ± 3.04	13.82	5.80 ± 5.63	-0.57	13.60	6.24	3.44
borg	2153+4411,694	330.250556	-48.557744	356.485522	-28.485522	23.44 ± 0.03	23.05 ± 0.02	22.93 ± 0.02	25.39 ± 0.90	4.17 ± 3.04	13.82	5.80 ± 5.63	-0.57	13.60	6.24	3.44
borg	2153+4411,714	330.250556	-48.557744	356.485522	-28.485522	23.44 ± 0.03	23.05 ± 0.02	22.93 ± 0.02	25.39 ± 0.90	4.17 ± 3.04	13.82	5.80 ± 5.63	-0.57	13.60	6.24	3.44
borg	2153+4411,734	330.250556	-48.557744	356.485522	-28.485522	23.44 ± 0.03	23.05 ± 0.02	22.93 ± 0.02	25.39 ± 0.90	4.17 ± 3.04	13.82	5.80 ± 5.63	-0.57	13.60	6.24	3.44
borg	2153+4411,758	330.250556	-48.557744	356.485522	-28.485522	23.44 ± 0.03	23.05 ± 0.02	22.93 ± 0.02	25.39 ± 0.90	4.17 ± 3.04	13.82	5.80 ± 5.63	-0.57	13.60	6.24	3.44
borg	2153+4411,772	330.250556	-48.557744	356.485522	-28.485522	23.44 ± 0.03	23.05 ± 0.02	22.93 ± 0.02	25.39 ± 0.90	4.17 ± 3.04	13.82	5.80 ± 5.63	-0.57	13.60	6.24	3.44
borg	2153+4411,792	330.250556	-48.557744	356.485522	-28.485522	23.44 ± 0.03	23.05 ± 0.02	22.93 ± 0.02	25.39 ± 0.90	4.17 ± 3.04	13.82	5.80 ± 5.63	-0.57	13.60	6.24	3.44
borg	2153+4411,811	330.250556	-48.557744	356.485522	-28.485522	23.44 ± 0.03	23.05 ± 0.02	22.93 ± 0.02	25.39 ± 0.90	4.17 ± 3.04	13.82	5.80 ± 5.63	-0.57	13.60	6.24	3.44
borg	2153+4411,831	330.250556	-48.557744	356.485522	-28.485522	23.44 ± 0.03	23.05 ± 0.02	22.93 ± 0.02	25.39 ± 0.90	4.17 ± 3.04	13.82	5.80 ± 5.63	-0.57	13.60	6.24	3.44
borg	2153+4411,851	330.250556	-48.557744	356.485522	-28.485522	23.44 ± 0.03	23.05 ± 0.02	22.93 ± 0.02	25.39 ± 0.90	4.17 ± 3.04	13.82	5.80 ± 5.63	-0.57	13.60	6.24	3.44
borg	2153+4411,871	330.250556	-48.557744	356.485522	-28.485522	23.44 ± 0.03	23.05 ± 0.02	22.93 ± 0.02	25.39 ± 0.90	4.17 ± 3.04	13.82	5.80 ± 5.63	-0.57	13.60	6.24	3.44
borg	2153+4411,891	330.250556	-48.557744	356.485522	-28.485522	23.44 ± 0.03	23.05 ± 0.02	22.93 ± 0.02	25.39 ± 0.90	4.17 ± 3.04	13.82	5.80 ± 5.63	-0.57	13.60	6.24	3.44
borg	2153+4411,911	330.250556	-48.557744	356.485522	-28.485522	23.44 ± 0.03	23.05 ± 0.02	22.93 ± 0.02	25.39 ± 0.90	4.17 ± 3.04	13.82	5.80 ± 5.63	-0.57	13.60	6.24	3.44
borg	2153+4411,931	330.250556	-48.557744	356.485522	-28.485522	23.44 ± 0.03	23.05 ± 0.02	22.93 ± 0.02	25.39 ± 0.90	4.17 ± 3.04	13.82	5.80 ± 5.63	-0.57	13.60	6.24	3.44
borg	2153+4411,951	330.250556	-48.557744	356.485522	-28.485522	23.44 ± 0.03	23.05 ± 0.02	22.93 ± 0.02	25.39 ± 0.90	4.17 ± 3.04	13.82	5.80 ± 5.63	-0.57	13.60	6.24	3.44
borg	2153+4411,971	330.250556	-48.557744	356.485522	-28.485522	23.44 ± 0.03	23.05 ± 0.02	22.93 ± 0.02	25.39 ± 0.90	4.17 ± 3.04	13.82	5.80 ± 5.63	-0.57	13.60	6.24	3.44
borg	2153+4411,991	330.250556	-48.557744	356.485522	-28.485522	23.44 ± 0.03	23.05 ± 0.02	22.93 ± 0.02	25.39 ± 0.90	4.17 ± 3.04	13.82	5.80 ± 5.63	-0.57	13.60	6.24	3.44
borg	2153+4411,011	330.250556	-48.557744	356.485522	-28.485522	23.44 ± 0.03	23.05 ± 0.02	22.93 ± 0.02	25.39 ± 0.90	4.17 ± 3.04	13.82	5.80 ± 5.63	-0.57	13.60	6.24	3.44
borg	2153+4411,031	330.250556	-48.557744	356.485522	-28.485522	23.44 ± 0.03	23.05 ± 0.02	22.93 ± 0.02	25.39 ± 0.90	4.17 ± 3.04	13.82	5.80 ± 5.63	-0.57	13.60	6.24	3.44
borg	2153+4411,051	330.250556	-48.557744	356.485522	-28.485522	23.44 ± 0.03	23.05 ± 0.02	22.93 ± 0.02	25.39 ± 0.90	4.17 ± 3.04	13.82	5.80 ± 5.63	-0.57	13.60	6.24	3.44
borg	2153+4411,071	330.250556	-48.557744	356.485522	-28.485522	23.44 ± 0.03	23.05 ± 0.02	22.93 ± 0.02	25.39 ± 0.90	4.17 ± 3.04	13.82	5.80 ± 5.63	-0.57	13.60	6.24	3.44
borg	2153+4411,091	330.250556	-48.557744	356.485522	-28.485522	23.44 ± 0.03	23.05 ± 0.02	22.93 ± 0.02	25.39 ± 0.90	4.17 ± 3.04	13.82	5.80 ± 5.63	-0.57	13.60	6.24	3.44
borg	2153+4411,111	330.250556	-48.557744	356.485522	-28.485522	23.44 ± 0.03	23.05 ± 0.02	22.93 ± 0.02	25.39 ± 0.90	4.17 ± 3.04	13.82	5.80 ± 5.63	-0.57	13.60	6.24	3.44
borg	2153+4411,131	330.250556	-48.557744	356.485522	-28.485522	23.44 ± 0.03	23.05 ± 0.02	22.93 ± 0.02	25.39 ± 0.90	4.17 ± 3.04	13.82	5.80 ± 5.63	-0.57	13.60	6.24	3.44
borg	2153+4411,151	330.250556	-48.557744	356.485522	-28.485522	23.44 ± 0.03	23.05 ± 0.02	22.93 ± 0.02	25.39 ± 0.90	4.17 ± 3.04	13.82	5.80 ± 5.63	-0.57	13.60	6.24	3